

Magnetic mapping of archaeological iron

Bruce Bevan and Tatiana Smekalova



Figure 0: Heavy iron that affects a magnetic survey. Even though the two ships are distant, they probably cause the magnetic readings to drop by about 10 nT at this location. However, the change in the magnetic field is so gradual that it causes no difficulty for the analysis of the measurements.

This magnetic survey was done at the 9th century site of Avaldsnes, which is located on the island of Karmøy at the west coast of Norway. The total-field Overhauser magnetometer is a model GSM-19WG from Gem Systems. The magnetic sensor is in the white cylinder and magnetic readings are displayed on and recorded in the gray console.

Magnetic mapping of archaeological iron

by: Bruce W. Bevan (Geosight)

and: Tatiana N. Smekalova (V. I. Vernadsky Crimean Federal University)

date: 7 March 2026

Summary

Magnetic surveys have detected a wide variety of iron artifacts. Some of these artifacts are important for archaeology, such as an iron sword ([Figure 5](#)) or a cluster of cannon balls ([Figure 14](#)). Other objects cause unwanted magnetic anomalies; these could be buried pipes ([Figure 50](#)) or parts of a plow that were lost in a farmed field ([Figure 37](#)). A mouse click at the blue text above will take you to a magnetic map.

This report shows how several magnetic maps were analyzed, giving estimates of the depth, size, and location of the underground iron. This analysis also shows that a magnetic survey may help to identify objects that are rather flat or elongated. Some examples show the benefit of measuring the orientation of bipolar magnetic anomalies (the direction from a magnetic high to its companion low) along with the ratio of magnetic amplitudes (the high to the low). Measurements of the magnetic parameters of more than a dozen iron artifacts are included here. Unlike most other archaeological artifacts, iron objects typically have an induced magnetization that is stronger than their remanent magnetization.

Introduction

Iron artifacts are often easy to detect with a magnetic survey; this is sometimes good, but sometimes it is bad. At a modern site (less than 200 years old), iron would have been so inexpensive that it may have been discarded and it may now be spread randomly around the site. If the site was only occupied in ancient times, all of the buried iron could be important to find. Both conditions are discussed here: Iron as an important "signal" and iron as unwanted "noise".

The captions for the figures have been written to provide a summary of this report, starting with [Figure 1](#).

It can be valuable to detect shipwrecks by the iron that they contain. Iron industries can be good to locate, whether they are new or old. Old iron is usually very important; this may be an artifact, such as a sword or a cannon ball. If iron objects like these are most important to your work, you may skip to the series of figures in this report that have these illustrations (starting at [Figure 5](#)).

Unwanted iron may be buried water pipes, storage tanks for fuel, an iron roof, or a passing car or train. These unwanted features are discussed later in this report, starting with [Figure 40](#). Fields that have been farmed in modern times will have many buried iron objects that have been lost from plows or tractors; segments of wire fencing will also be common.

There is no certain method for distinguishing old and important iron from modern trash with a magnetic survey. However, the orientations of dipolar magnetic anomalies may sometimes help with this distinction; an orientation of an anomaly toward magnetic north could suggest old iron (an earthen feature or a fired-in-place artifact are also possible). Estimates of the depth of the objects can also help, for recent iron may be quite shallow.

Geological iron will also be discussed. While the detection of an iron meteorite would be welcome, other natural iron objects may cause confusion. Black sands (magnetite) may have accumulated at beaches or the edges of rivers and these can create strong anomalies.

The magnetic properties of iron

The magnetic properties of iron will be described next. A helpful approximation is that 1 kg of iron buried at a depth of 1 m will cause a magnetic anomaly of about 50 nT. This is true for both a total-field magnetometer (with perhaps a cesium sensor) and also for a typical fluxgate gradiometer. An iron mass of 1 kg, could be a cube with sides that are about 5 cm long. The following discussion of the magnetic properties of iron will get more technical as the text proceeds. While magnetic viscosity and self-demagnetization can be important to consider, you may delay that part of the study.

Iron and steel are usually the most magnetic artifacts that are detected by a magnetic survey; [Figure 1](#) approximates the magnetic equivalence of different quantities of modern steel, old iron, fired earth, and random brick.

There are many different types of iron and steel; these differ in their magnetic properties. These differences may be a result of composition, such as the fraction of carbon or silica that the metal contains. Types of iron also differ in their granularity: The size of crystals or magnetic domains in iron. Also, iron and steel can differ by the shearing forces that have resulted from hammering or the extrusion of the iron.

The terms "soft iron" and "steel" have often been applied to distinguish between forms of this metal by their physical properties of ductility (bendability) and strength or hardness. Since it is difficult to detect or quantify these differences, particularly when the metal is buried underground, the words iron and steel will usually be applied without distinction here. However, geophysical measurements on small samples can tell how easily iron may be magnetized as compared to how strongly that magnetization can remain unchanged.

Magnetic moment, Am^2

A fundamental parameter can quantify the magnetism in an object; this is called the object's magnetic moment, and it has the unit of ampere-meter-squared. This quantity is abbreviated as Am^2 . Since magnetic moment usually increases with the weight of an object, it can be further defined by dividing the moment by the mass of the object, giving a relative magnetic moment, in ampere-meter squared per kilogram, or Am^2/kg . Many archaeological

The magnetic properties of iron

artifacts of iron are rather small, and it may sometimes be convenient to multiply moment in Am^2/kg by 1000 to give a helpful quantity that has the even longer unit name of milliampere-meter-squared per kilogram, or mAm^2/kg .

The magnetic properties of 20 iron objects are plotted in [Figure 2](#); these values were determined by rotating a sample near the sensor of a magnetometer and noting the strongest and weakest anomaly. Some of these artifacts are made of iron and others could be a type of steel. Some of the earlier artifacts could be manufactured from cast iron.

[Figure 2](#) suggests that a relative magnetic moment of $100 \text{ mAm}^2/\text{kg}$ could be assumed if the antiquity of the iron is not known; with that assumption, the error in the estimated mass could be a factor of ten. However, if the feature was reasonably made in the 20th century or more recent (and therefore is perhaps steel), a relative moment of $500 \text{ mAm}^2/\text{kg}$ could be assumed. Also, if the feature is likely to be older, a moment of $50 \text{ mAm}^2/\text{kg}$ might allow the most accurate estimate of the mass of the iron.

Susceptibility

Susceptibility is a pure number, without a unit name; this parameter will indicate the induced magnetization of an object. This quantity will usually be followed by (SI) to indicate that it is a susceptibility with its value in the International System of units.

It would be convenient to measure the magnetic susceptibility of iron with one of the common hand-held magnetic susceptibility meters, but it is probably impossible to get a correct measurement from these instruments. If one of these meters is applied to this test, the operating frequency of the meter should be as low as possible (Clark 1980).

Susceptibility meters that are now available can measure to a maximum of 1 - 10 (SI), and the susceptibility of iron is usually greater than that. For example, Ravat (1996) found the magnetic susceptibility of steel drums (for storing industrial chemicals) to be 15 - 20 (SI).

Simple test equipment

The magnetic properties of iron artifacts can best be tested with the same magnetometer that you apply for magnetic mapping. As an alternative, simple equipment will allow fast, but less accurate, tests.

A magnetic compass, like that shown in the lower right side of [Figure 3](#), is all that is needed for testing iron objects. Place the compass on a non-metallic table. Now move an object to be tested to the right hand (eastern) side of the north pointer on the compass. See if the angle of the pointer changes slightly. Rotate the object by 180° , and see if the pointer is attracted or repelled by the object. Next, place the object on the left side of the north pointer on the compass and rotate it again. If any of these movements of the iron object cause a deflection of the pointer, that object is magnetic. For example, the steel bar at the upper right side of [Figure 3](#) has remanent magnetization and it deflects the north pointer (red) of the compass toward that bar, or away from the bar, as the bar is rotated. The iron

head of a hammer, at the lower left side of [Figure 3](#) has mostly induced magnetization. The freely-rotating magnet in the white gimbal "cage" at the upper left side of the figure is also valuable for finding the direction of magnetic fields.

Many smart phones have a magnetic sensor (Bevan and Smekalova 2025b, p. 36), although it is much inferior to your mapping magnetometer. Since most iron artifacts are very magnetic, the small magnetometer in a phone can reveal the magnetization of most artifacts. The Physics Toolbox Magnetometer (for Android) from vieyrasoftware.net will display a time graph of changes in the magnetic field. Before beginning your tests, locate the magnetic sensor by moving the point of a nail (or similar rod) over the phone.

The Q ratio

A simple magnetic test like the rotation mentioned above allows an estimate of the ratio of remanent to induced magnetization in a sample of iron; this is the Q ratio. If one has a sample of iron, in particular one that is rather compact (neither flat nor elongated like a bar or rod), the Q ratio is readily apparent when that sample is brought close to the sensor of a magnetometer, and then the sample is rotated. On first bringing the sample near the sensor, the readings will rise; then the readings will rise and fall in several cycles as the sample is rotated. The initial rise shows the effect of induced magnetization; then the rise and fall of the readings will reveal the remanent magnetization. [Figure 22](#) has an example.

Most objects of iron or steel have a magnetic Q ratio that is less than one. Ravat (1996) found this ratio to be in the range of 0.2 to 0.3. Another collection of parameters (Bevan 2002a) determined the following Q ratios: 19th century cannonball (0.02), 19th century cannonball fragment (0.6), 19th century cannon shell (Hotchkiss) (0.2), 40-gallon drum (0.25), 18th century iron (3 objects with ratios of 0.7, 0.9, and 0.6), medieval nail (0.92), an 18th century cannonball found at the Salgir Fort in Crimea ([Figure 22](#) = 0.1). While there are few measurements here, a modern steel object which is very hard (such as a ball bearing or the blade of a knife) could have a Q ratio of more than 1.

Elongated objects

The magnetic character of an elongated object of iron, such as a water pipe or a rifle barrel, may require a different parameter; it is called "pole strength" and it has the unit of Am (ampere-meter). This unit quantifies the magnetic moment per unit of length of an object that is long in comparison to its diameter. An excellent approximation of this type of feature is a pair of magnetic poles (not dipoles), that have opposite polarity at the opposite ends of the object. The polarity of the upper pole of a vertical bar of iron will usually be negative; this was true for an iron-filled well ([Figure 29](#)). If the feature is vertical and long, the depth of the lower magnetic pole cannot usually be determined (for it cannot be detected); however, the magnetic moment per unit of length is a valuable finding. Some examples of the strength of magnetic monopoles or monopole-pairs are as follows:

The magnetic properties of iron

The dug well at the Petersburg battlefield = 193 Am (Figure 29)

A vertical grounding rod at Valley Forge = 30 Am (Figure 52)

A corrugated steel culvert at Petersburg = 7 Am (Figure 51)

An iron rod; diameter 0.38 cm, length 53 cm = 0.174 Am (Figure 3)

Rusting

There are uncertainties about how the magnetic properties of iron change as iron becomes rust. One test of this change was made with the rusting of iron particles in a saline solution (Bevan 2004a, p. C-10). The object was a commercial hand warmer for field work in the winter. The magnetic moment of the iron dropped by 50% after the iron became rust (no metallic iron was visible, but perhaps some remained). Ravat (1996, p.1334) made careful tests of the rusting of steel drums during a two-year period; while the magnetic anomalies of some drums decreased, there was an increase or irregular change with other drums.

An archaeological excavation (Ziegler 2001, p. 207) found that rusted fragments of iron were non-magnetic. Magnetic surveys explored fortifications from World War 2 in France, and considered factors that affected the rusting of reinforcing iron. Salinity of the soil speeded this, while alkalinity slowed rusting (Everett +5, 2006, p. 292). Andrew Edwards, an archaeologist at Colonial Williamsburg (Virginia, USA), mentioned on 19 May 2010 that nails that were found in burned areas were not rusted.

Magnetic viscosity

The magnetic properties of some materials change with time; this is called magnetic viscosity, and it is like a slowly changing magnetic remanence. The magnetic viscosity of steel drums was investigated by Freed, Doheny and Bechtel (2009), and they include graphs that illustrate temporal change in the magnetic anomaly of drums; these plots will be applicable to other iron objects.

A simple test of magnetic viscosity was made with a pair of magnetometers, one had its sensor close to an iron object, and the other magnetometer was quite distant. Figure 4 shows how the magnetic anomaly of an object increased during several hours.

A better test of magnetic viscosity could be made with one's automobile. It could be parked for a period of a week before the start of measurements. While in that original location, magnetic measurements could begin with one magnetometer close to the car and a second magnetometer at a distance of more than 50 m. To start the test, the car would be moved back to its original location after it is turned around by 180°. Both magnetometers should have readings whose times are synchronized, and the reading at the distant magnetometer can be subtracted from the nearby instrument. The mass of iron in the car should create a strong, but slowly changing, anomaly.

Perhaps magnetic viscosity could aid the search for buried iron. A strong DC magnetic field could be applied to the Earth in the area of test, perhaps with an electrical

current around a large coil of wire. A magnetic map could be made shortly after the magnetic field was stopped, and further maps could be made at later times.

Self-demagnetization

The magnetic analysis of iron causes a difficulty that is usually not found with other archaeological artifacts. Iron is so magnetic that each separate part of an object can have a noticeable effect on other nearby parts of the same object. While one can assume that most other artifacts or features are magnetized only by the Earth's magnetic field, that is not true for iron. While iron objects are magnetized by the Earth's field, they are further magnetized by the different parts of the same object and by other nearby objects that are very magnetic. Therefore, an accurate analysis can require that the magnetic model of the object be broken into many small parts (perhaps called voxels), and the interaction between those separate parts must be quantified.

Demagnetization was discussed in an earlier report in this series (Bevan and Smekalova 2025b, p. 41-43), where its study may improve the accuracy of the analysis of ceramic objects, which are less magnetic than iron. Several references to demagnetization have a detailed explanation of this effect (Clark and Emerson 1999; Purss and Cull 2005; Hillan and Foss 2012a; Krahenbuhl and Li 2017; and Liu and Hu 2017).

Ravat (1996, p. 1326 and 1332) has pointed out that it may be easier to measure demagnetization than to calculate it. The mass of a buried feature is to be determined. Its shape can be estimated or assumed, but its size is not known. However, its magnetic moment can be determined from the analysis of a magnetic map. Next, find a reference feature with a similar shape that is not buried. Measure its relative magnetic moment. The mass of the buried feature is its magnetic moment divided by the relative magnetic moment of the reference feature.

Measuring magnetic parameters

The magnetic quantification of two samples of iron (seen in [Figure 3](#)) are summarized here. Procedures for measurements like these are described in several other publications, starting with Parasnis (1966, p. 326-327) and Breiner (1973, p. 33-34).

These measurements were made by rotating an iron object near a magnetometer's sensor, noting the magnetic high and low and also the field when the object was moved to a distance away. The line between the object and magnetic sensor is about that of the Earth's field, in inclination and declination. An illustration of this geometry is found in Bevan (2004b, Fig. C40).

The definitions of the parameters are below:

r = distance between the center of the sensor and the center of the sample, m

B_e = Earth's magnetic field when the sample is not near the sensor, nT

B_{hi} = highest magnetic field during rotation of the sample, nT

Blo = lowest magnetic field during rotation of the sample, nT

mr = remanent magnetization, Am^2

mr_m = mr / mass = remanent magnetization relative to mass, Am^2/kg

mi = induced magnetization, Am^2

mi_m = mi / mass = induced magnetization relative to mass, Am^2/kg

Q = mr / mi

mm = mr_m + mi_m = total magnetization relative to mass, Am^2/kg

k = magnetic susceptibility (SI)

The measurements and calculations are as follows:

cylindrical steel bar, length = 81 mm, diameter = 3 mm,

$V = 573 \text{ mm}^3 = 5.73 \times 10^{-7} \text{ m}^3$

mass = 4.3 g, density = 7.5 g/cm^3

r = 17 cm (mid-sample to mid-sensor)

A Scintrex MP-2 proton magnetometer gives rotated values:

Be = 49,262 nT; Bhi = 49,885 nT; Blo = 48,927 nT

Calculated values:

mr = 11.8 mAm^2 ; mi = 3.54 mAm^2

Q = 3.33; k = 157 (SI)

total moment = mr + mi = $11.8 + 3.54 = 15.34 \text{ mAm}^2$

mm = total moment relative to mass = $3567 \text{ mAm}^2/\text{kg}$

hammer head, missing claw part at rear, so rather compact

mass = 113 g; r = 20 cm, $V = 14.3 \text{ cm}^3$; density = 7.92 g/cm^3

Scintrex MP-2 proton magnetometer gives rotated values:

Be = 49,261 nT; Bhi = 49,315 nT; Blo = 49,281 nT

Calculated values:

mr = $0.68 (10^{-3}) \text{ Am}^2$; mi = $1.48 (10^{-3}) \text{ Am}^2$

Q = 0.46; k = 2.6 (SI)

total moment = mr + mi = 2.16 mAm^2

mm = total moment relative to mass = $19.1 \text{ mAm}^2/\text{kg}$

Notes about iron and magnetics

This report has examples from archaeological sites in the northern hemisphere, where magnetic highs will often be found over magnetic features. At equatorial locations or in the southern hemisphere, the polarity and shapes of anomalies will usually be different; for an introduction to this effect, see a report that compares the anomalies at different areas (Bevan 2025a).

The magnetic properties of iron

If a magnetic anomaly could be caused by either iron or by fired earth, perhaps an additional survey with an EM induction meter will reveal the high conductivity of iron as compared to the low conductivity of ceramic.

It may be important for a magnetic map to illustrate both the strong anomalies from iron along with the weak anomalies from earthen features. As shown in [Figure 13](#) and also [Figure 37](#), there may be benefit to having both contour lines and gray-level changes plotted in the same map.

The lateral gradient of the magnetic field can sometimes be so large near iron objects that good measurements are not possible with a magnetometer. This problem is found most with proton magnetometers; cesium or fluxgate magnetometers can operate at higher gradients.

A page on Wikipedia states that the magnetic susceptibility of pure iron is 200,000 (SI).

While the slag from iron furnaces can contain a large amount of iron, these topics are not discussed here.

Light is neither generated nor (significantly) absorbed by an optical lens; instead, a lens both increases and decreases brightness. The illumination from the lens will be brighter than usual near the middle of the lens, but it will also become darker than usual outside that bright spot, for some of the light has been refracted toward the central bright spot. The total amount of light is neither increased nor decreased by the lens. This is like a magnetic anomaly that has both a high and a low, but whose total or average anomaly is zero.

The Saint-Gaudens National Historic Site in the USA preserves the 19th century studio of a bronze sculptor. A magnetic survey detected about 1000 kg of buried iron in or near his burned studio (Bevan 2025b). It is possible that some of the magnetic features were iron armatures that supported the molds for metallic statues.

Several recent reports and books have important information on magnetic surveys and their analysis:

A publication called "Image Atlas" by Southern Geoscience Consultants is illustrated with more than 40 different maps that display the processing of magnetic data from one geological area in Australia, using different procedures. This is an excellent illustration and comparison, and it is freely-available at:

https://geoscience.nt.gov.au/gemis/ntgsjspui/bitstream/1/77007/2/GR215_2012_AS_Appendix1_Image_Atlas.pdf

A 320-page book titled "Exploration Magnetism, Theory and Practice" has details about many major topics in magnetic interpretation. While this book is too technical for individuals who have just begun to do magnetic surveys, it is freely-available in both PDF and ePUB formats from:

<https://www.publish.csiro.au/ebook/download/pdf/8049>

Also from Australia, introductions to topics in magnetism are available from the software company, Tensor Research. This series is also free. It is called the Magnetic

Mentor; topics that have already been discussed include the coloring of magnetic maps, and also the creation of the best monochrome maps. These tutorials are available at: www.tensor-research.com.au

A few publications that were not mentioned in an earlier volume of "Magnetic mapping" are noted here:

A recent article has compared different procedures for calculating the two-dimensional magnetic anomalies of polygonal prisms (Ghirotto +3, 2021); see also pyMag2DPoly at GitHub.

Two recent theses have discussed the application of magnetic surveys to archaeological exploration:

Investigation of magnetic anomalies in archaeological prospection, by Sandra Elisabeth Hahn, 2022, Ludwig Maximilians Universitat. Free at https://edoc.ub.uni-muenchen.de/33367/1/Hahn_Sandra.pdf

Investigating depth estimation to archaeological magnetic source bodies, by Jeremy G. Menzer, 2021, University of Arkansas, Fayetteville. Free at <https://scholarworks.uark.edu/etd/4327/>

The magnetic character of different objects and artifacts

The magnetic maps and parameters of many different iron objects will now be illustrated. Iron objects that are old or very important are discussed first. Later, the magnetic character of new or modern objects will be described. These modern objects will usually be unwanted in a magnetic map, but it is important to understand them so that they might be identified as unimportant.

A Roman sword in Egypt

The ancient town of Dimai is located in the Fayoum depression in the western desert of Egypt. An area of 8620 m² was mapped at that site with a magnetometer. The strongest anomaly is shown in [Figure 5](#). An archaeological excavation at this location revealed a Roman sword; see [Figure 6](#).

This magnetic anomaly is so distinct and localized that no further analysis is necessary. However, there may be a benefit to a study of the magnetic high with its unusual pair of lows: [Figure 7](#) is illustrated with three magnetic models that are quite different from each other, although each of their calculated patterns is similar to the measurements. The best model appears to be #1, which is calculated at the upper right side of the figure; the magnetic moment of this model of the sword is estimated to be about 2 Am². If it is assumed that the relative magnetic moment of iron is 0.1 Am²/kg, then the mass of this sword is estimated to be 20 kg, although this appears to be too high.

An unknown magnetic object that causes the extra magnetic low is modeled with a sphere; this has remanent magnetization and a moment of 0.4 Am². This object that may

cause this anomaly was not seen in the excavation.

The magnetic lows were examined further with a conversion of the magnetic measurements to a map of total gradient; this is plotted on the left side of [Figure 8](#). A map of total gradient may clarify the actual locations of objects that are confused within a cluster of nearby magnetic highs and lows; for another example, see Bevan and Smekalova (2021, Fig. 24). The map of the converted measurements shows two peaks along a north-south line; these may be caused by the two ends of the sword. The eastern and third peak in the total gradient may result from the unknown object that is suggested by the sphere in model #1.

An ancient iron bar from Denmark

The magnetic anomaly of an elongated and double-pointed iron bar was measured; the bar is illustrated in [Figure 9](#). That figure also shows how a line of magnetic measurements was made; the result is plotted in [Figure 10](#). Change in the total magnetic field is graphed there with a black curve, while the red and blue curves show changes in the direction of the magnetic field along the line of traverse.

These magnetic measurements provided two estimates of the magnetic moment of the bar; [Figure 11](#) shows one analysis, and [Figure 12](#) shows a similar finding. Since the mass of this iron is about 1.2 kg, the relative magnetic moment of this iron is estimated to be 20 mAm²/kg.

This test did not include a determination of both induced and remanent magnetization. Since the iron probably has a low Q ratio, the total magnetic moment of 20 mAm²/kg is probably caused mostly by induced magnetization; the remanent magnetization is smaller.

A medieval iron nail from Denmark

Description: A large-headed nail that is covered with a cream-colored layer that may be a combination of corrosion and the surrounding soil, from the Moesgaard Museum in Denmark.

Size and weight: length = 4.5 cm, shank diameter = 0.6 cm, head diameter = 1.9 cm. Mass: 11.99 g, density = 5240 kg/m³, less than typical iron because of rust and attached soil.

Magnetic measurements: The nail was rotated while its center was along the line (in inclination and declination) of the Earth's magnetic field (51,370 nT) with a mid-sample to mid-sensor distance of 23.2 cm. The nail was rotated to find the magnetic high and low (the high was toward the point of the nail).

Result: Remanent magnetic moment = 1.12 mAm², induced moment = 1.22 mAm², Q ratio = 0.92. Total relative magnetic moment (remanent plus induced) = 0.03 Am² / kg.

Iron pillars in India

Several iron pillars were manufactured and erected in India more than 1000 years ago (Swain 2021). These have a mass of about 800 kg and a length of about 8 m. They are

about 98% wrought iron. Should any of these be buried and lost, it is likely that they could be readily located with a magnetic survey.

Cannon balls in an old fort

An earthen fort that was constructed in Crimea in the 1770s was readily detected with a magnetic survey. This was because one of its powder magazines still contained hundreds of iron cannon balls; there is no trace of this fort at the ground surface. See the magnetic map in [Figure 13](#). A summary of this study is next, and further details about the site and survey continue later.

Historical records describe this fort. Also, visible artifacts suggest several possible locations for the fort. Fortunately, an excellent map reveals the shape of the fort and the buildings within it ([Figure 19](#)). Two powder magazines are shown on that map, but only one of them could be the magazine that was found to have cannon balls. With this information and the known orientation of the fort, its location could be determined; see [Figure 20](#).

The excavation of a 5-m square at the strong magnetic anomaly revealed more than 500 cannon balls in several clusters. The magnetic properties of two balls were measured; with this information and the known locations of the balls and the shapes of the clusters, the magnetic anomaly of those cannonballs could be calculated. The pattern of the calculated anomaly was similar to the measured anomaly in the large-area magnetic map. This indicates that the cannon balls were the cause of the anomaly. Many details about this survey and its analysis are described next, beginning again with [Figure 13](#).

The strong anomaly in [Figure 13](#) is enlarged as [Figure 14](#), and this reveals a complex pattern of magnetic highs and lows. The general pattern of the anomalies in this figure can be revealed or clarified by pairing each magnetic high with its likely magnetic low. This pairing is not always possible and it may not be accurate, but this process can aid one's understanding of the anomalies. See the result in [Figure 15](#).

There are about five magnetic highs in [Figure 15](#), and it appears that a magnetic low is associated with each high. The orientation of each anomaly pair is indicated with an arrow that extends from the magnetic high to the low. These directions are close to the current direction of magnetic north. This suggests that there may be about five separate objects in the area, and all of them may be magnetized primarily by the Earth's magnetic field.

The ratio of the high to the low at each anomaly pair is listed next to each arrow in [Figure 15](#). These ratios range between 0.61 and 3.01. On average, each magnetic high and its paired low have about the same amplitude. If these objects were magnetized by the Earth's field, it would be expected that the high-low ratio would be about 6, and therefore higher than that of any of the individual ratios in the figure. This suggests that remanent magnetization could be strong in these objects, but that contradicts the finding of the orientation of the arrows, which suggested induced magnetization.

An initial analysis of the major magnetic anomaly at Salgir is given in [Figure 16](#). The

strength of the magnetic anomalies suggests that the source could be iron objects. The magnetic bodies were assumed to be magnetized by induction; this is reasonable since they are probably composed of old iron, whose induced magnetization is usually strong in comparison to its remanent magnetization. The induced magnetization of seven historical iron artifacts had been measured earlier (Bevan 2002a, p.4); the average of these values was $0.023 \text{ Am}^2/\text{kg}$. The total magnetization of the bodies in the magnetic model of Figure 16 is 40 Am^2 . Therefore these magnetic bodies at the Salgir fort could have a total mass of about $40 / 0.023$ or 1700 kg.

Note the blue magnetic lows in Figure 16; these are on the northern side of the red highs. These lows are much weaker in the calculated map (on the right) than in the measurements (on the left). Except for that, the patterns in the two maps are similar. These weak lows could be caused by magnetization that has a low angle of inclination.

Starting with the same bodies that are in Figure 16, a new magnetic model was created; the magnetic susceptibility of each body was changed to an intensity of magnetization (which is a magnetic moment per unit of volume, in A/m) and the inclination angle of this magnetization was then allowed to change for a more accurate model. Figure 17 shows the result. The lower inclination angle of magnetization for bodies 1 and 3 has strengthened the companion magnetic lows, and the calculations are now similar to the measurements.

A lower angle of magnetization could be caused by magnetic remanence, which may be found with steel. However, the magnetic map suggests that all of the magnetic bodies have about the same direction of magnetization. This would be unusual for steel, but more likely for old iron. If the iron bodies were rather flat and horizontal, the angle of magnetization could also be rather shallow. This could be the result of demagnetization; this effect is seen with a metal plate in Figure 44.

The total magnetic moment of the five bodies in Figure 17 is 57 Am^2 ; this is larger than the total moment of 40 Am^2 from the analysis in Figure 16. Since this model has remanent magnetization, the earlier value of induced magnetization ($23.3 \text{ mAm}^2/\text{kg}$) can be added to the value for remanent magnetization ($14.2 \text{ mAm}^2/\text{kg}$) for total of $0.037 \text{ Am}^2/\text{kg}$. The mass can then be estimated as $57 \text{ Am}^2 / 0.037 \text{ Am}^2/\text{kg} = 1540 \text{ kg}$.

In summary, these two analyses suggest that the total magnetic moment of the bodies that cause the anomalies is between 40 and 57 Am^2 . This is the best estimate of the source of the anomaly that was made before an excavation exposed the cannon balls. While a ceramic kiln could have a magnetic moment that is this large, the complexity of the anomaly and the fact that there appear to be several separate, but nearby, objects suggests that a kiln is unlikely. Several steel features are unlikely also; this is because the high-to-low directions of the anomalies are all about toward magnetic north. Iron appears to be more likely because induced magnetization is typical for iron.

An archaeological excavation revealed a large mass of iron. A photograph and a drawing of the excavation are in Figure 18. This excavation was a square whose sides were

5 m long. Two different types of projectiles were found in the excavation. One type is called a solid shot, or simply a shot; this is a sphere that is entirely iron. The other type is called a shell (or perhaps a grenade or a hollow shot); while this is also made of iron, it is hollow inside and filled with explosives that will break the iron into fragments that will be dangerous for the opponent. While many shells were found in the excavation, none of these had any explosive material inside; a cross-section through the middle of these shells has a shape like the letter C.

There is an old map of this fort on the Salgir River; this shows that the fort is located within a bend or meander of that river. [Figure 19](#) shows the angular bastions of the fort; the pattern applies the fortification geometry that was devised by Vauban (1737).

The terrain at and near Fort Salgir can be seen in the satellite image, [Figure 20](#). The magnetic map of [Figure 13](#) can be aligned with this map with three steps: First, the scale of the fort map ([Figure 19](#)) is adjusted to be the same as that of the magnetic map ([Figure 13](#)). Then, the orientation of true north in both maps is set to the same direction. Finally, the magnetic anomaly in [Figure 13](#) is shifted to where a powder magazine is found in [Figure 19](#); this match can only be made with powder magazine #1, as shown in [Figure 20](#).

So far, this study has analyzed a distinctive magnetic anomaly and also revealed its likely source, in the excavation pictured in [Figure 18](#). One could conclude the geophysical study at this stage. However, another step could be valuable and educational: One can also estimate the magnetic anomaly of the cannon balls that were discovered and compare that to the anomaly that was originally measured ([Figure 14](#)). There are two advantages to this further study. First, it will allow a better determination of the average magnetic properties of the cannon balls. Second, this additional study may also suggest if there are additional, but unexcavated, cannon balls (or other magnetic objects) below the depth of the excavation or outside the area of the excavation.

As a first step in this secondary, or post-excavation, analysis, the clusters of cannon balls are simplified to thin prisms with polygonal outlines where the excavation revealed the clusters; these are seen in [Figure 21](#). [Figure 21a](#) shows how the clusters of cannon balls are associated with high magnetic anomalies; these have yellow or red contour lines.

The second step in the post-excavation analysis of the magnetic survey: The magnetic moments of two iron balls that were excavated from the powder magazine of the Salfir fort were measured. [Figure 22](#) shows some readings that were the basis for calculating the magnetic parameters of one cannon ball. The magnetometer and its sensor remained stationary for these tests, and readings were automatically recorded at intervals of 0.2 s. During an initial few minutes, the ball was distant from the magnetometer; then the ball was moved close to the magnetic sensor and randomly rotated for a few more minutes, and then finally it was removed again. The black-line graph of [Figure 22](#) shows how the magnetic readings changed, from steady low values to high and variable readings, and then back to a steady low values when the ball was again distant from the magnetic sensor.

The variations in the middle of the graph are the result of remanent magnetization; as

the ball was rotated, that magnetization added or subtracted about 15 nT from the constant value of induced magnetization that resulted from the Earth's field (this induction caused a rise of 136 nT). The ratio of 136 to 15 indicates that induced magnetization is about ten times larger than remanent magnetization.

Before continuing the magnetic analysis, it is important to see if remanent magnetization must be considered. While the cannon balls appear to have mostly induced magnetization, it is necessary to check if randomly-oriented remanent magnetization has a significant effect on the magnetic anomalies. The result of this test is in [Figure 23](#). It shows that remanence will cause some irregularity in the magnetic maps, but it is minor, and it does not need to be considered further. Had the remanent magnetization been strong, the magnetic anomalies of the cannon balls would have been very complex, and therefore difficult to analyze.

Magnetic measurements on cannon balls from Salgir show that induced magnetization is much stronger than remanent magnetization. It would therefore be expected that the total magnetization of each cluster of cannon balls would be in the direction of the Earth's magnetic field. Calculated maps of the magnetic anomaly of the model prisms are plotted in [Figure 24](#) for a range of inclination angles. These maps show that an inclination angle of about 20 - 30° matches the measurements best; this angle is lower than the inclination of the Earth's field, which was 64°.

The findings of the excavation at the powder magazine are summarized and simplified in [Figure 21](#). The shape of each cluster of cannon balls was approximated with a polygonal disk; this shape and the location of each cluster remained constant during the following analysis. The depth of each cluster also remained fixed, and the declination of total magnetization of each cluster remained that of the Earth's magnetic field (52°). The thickness (vertical depth) of each polygonal body was set at a reasonable value that also remained constant. It was only the intensity of magnetization (in A/m) and its inclination that were iterated for a best fit to the measurements. The result is seen in [Figure 25](#).

The total mass of cannon balls that were excavated was about 2200 kg. The analysis in [Figure 25](#) estimates the total magnetic moment to be 37 Am². Therefore, the average magnetic moment per unit of mass for these iron balls is 17 mAm²/kg, which is almost the same as that the moment of a single cannon ball that was measured ([Figure 22](#), where it was about 19 mAm²/kg).

It can be educational to make a residual magnetic map after a magnetic model and its analysis have been completed; this residual map shows the difference between the magnetic measurements and the calculations of a computer program. [Figure 26](#) is an example. The usual goal would be to create a magnetic model and calculation that show no anomalies in this residual map, which is on the right side. While the major anomalies have been reduced, there are about four locations where anomalies remain outside the 5-m square of the excavation; these anomalies could be caused by iron cannon balls that remain buried in the soil. Additional anomalies in the residual map are caused by the fact that the magnetic

model of the excavation (shown in [Figure 21](#)) is not quite correct; the magnetic parameters could be improved.

The magnetic map of the Salgir site reveals many long and curved bands that are about 10 m wide ([Figure 13](#)). These bands are caused by now-buried meanders (curvatures or bends) of the Salgir River. They may also be called paleochannels of the river (Leopold and Langbein 1966; Mackey +8, 2000). The river flowed along different routes at different times in the past; the channels that were cut into the soil were later filled by nature (or by modern plowing) with sediments that were more magnetic than usual. While this subject has nothing to do with archaeological iron, this analysis still provides a valuable illustration.

The paths of prior river flows may also be revealed in conductivity maps, such as those that may be measured with the Geonics EM31 conductivity meter that explores to a depth of several meters (Conyers +3, 2008).

Part of the magnetic map that crosses a paleochannel is plotted in [Figure 27](#), revealing a black band of high magnetic readings. The black curve in the lower panel has the measurements after they have been smoothed by averaging; the bipolar anomaly is approximated by the two-dimensional calculations of either a deep (red) or a shallow (blue) feature that is outlined in the figure.

In [Figure 13](#), it appears that there are a somewhat greater number of anomalies within the band of the river meander on the right side of the map. This part of the map is enlarged as [Figure 28](#). There are a large number of anomalies in this area, and many of them have an amplitude of more than 20 nT; these are revealed with colored contour lines.

Cannon balls from an old fort in the USA

Several iron projectiles from the Civil War battlefield (1864) at Petersburg, Virginia, USA, were tested for their magnetic properties (Bevan, 2004b, p. C-14). The line between the magnetic sensor and a projectile was the direction of magnetic north and at the inclination of the Earth's magnetic field (70°). The background field of the Earth was measured, and then a sample was rotated in a search for the highest and lowest anomaly; the center-to-center spacing between the sample and the sensor was 82 cm. The three magnetic readings for each sample allowed a calculation of remanent and induced magnetization, in Am^2 . These were compared to their mass, and it was found that the induced magnetic moment of each sample was about the same, $20 \text{ mAm}^2/\text{kg}$.

Their remanent magnetic moments were always smaller than the induced moments; for example, a hollow shell cannonball (with a mass of 21.1 kg and diameter of 8 inches = 0.203 m) had an induced magnetization of $21 \text{ mAm}^2/\text{kg}$ and a remanent magnetization of $0.38 \text{ mAm}^2/\text{kg}$, for a Q ratio of 0.02 (Bevan 2002a, p. 4).

An iron-filled well

The magnetic survey at the Civil War battlefield discussed above detected a magnetic

anomaly that was high in amplitude (2763 nT) and broad in area (a diameter of 60 m). This anomaly is illustrated on the left side of [Figure 29](#). Nothing was visible at the surface in this area, but the source of the anomaly was interpreted as a likely well that contained a mass of iron that was greater than what would be possible from an iron pipe. A shallow archaeological excavation found a dug well at this location, and it exposed iron from a bed frame at the top of the well. This well was next to an earthen fortification from the Civil War, however the age of the well is not known and the well was not excavated further.

While the anomaly in [Figure 29](#) looks like a magnetic dipole, with a low to the north of the strong high, the anomaly has the slightly different pattern that is called a monopole. This pattern is caused by a magnetic feature that is both vertical and longer than it is wide. While it was possible to estimate the depth to the top of the well, it was not possible to estimate the depth to the bottom of the well. If the relative magnetic moment of the iron in the well was like iron (at $0.31 \text{ Am}^2/\text{kg}$), the mass of iron per unit of depth could be 620 kg/m.

The massive amount of iron in this well allowed it to be detected readily with a magnetic compass. Small changes in the direction of magnetic north were measured along the light blue line that is near the middle of the magnetic measurements in [Figure 29](#). These compass directions are plotted in [Figure 30](#); [Figure 31](#) clarifies the changing angles as the well is passed.

An industrial area in the 1800s

During the 1800s, the town of Harpers Ferry in the state of West Virginia (USA) had many industries; a nearby river provided water power for an iron foundry, a cotton mill, a wood pulp factory, and a manufacturer of military rifles. Floods from the nearby river have now covered the remains of those structures with about 1 m of sediments. A magnetic survey located large masses of magnetic artifacts that are underground. These must be mostly iron; see [Figure 32](#).

The magnetic highs in the map probably locate large features that may be spread over areas that are 10 - 20 m broad. Most of these anomalies do not appear as pairs of readings, high and low that are adjacent. However, paired anomalies were found at two locations, both are marked with black arrows in [Figure 32](#). In both locations, the direction from the anomaly high to the paired low is not toward magnetic north; furthermore, the magnetic lows at both locations are stronger in amplitude than the adjacent highs. These facts indicate that the artifacts that cause both anomalies are not magnetized by the Earth's field; instead, these objects must have strong remanent magnetization which is in differing directions.

Historical shipwrecks

Sunken ships from the last few centuries probably contained large quantities of iron in the engine, anchor, and hull. If this iron is now underwater at a shallow depth and hidden by sediments, a magnetic survey can be excellent for locating the ship.

Since the depth of a sunken ship may be the same as the depth of water, an estimate of depth from a magnetic survey is usually not necessary. Instead, it is typical to make an estimate of the mass of the ship from its magnetic anomaly. A 200-page report titled *Marine Geophysics* has detailed information about how magnetic surveys can be done to find shipwrecks and other objects that are underwater. That report includes a description of the Hall method for showing how the magnetic anomaly of a feature depends its spatial size, mass, and depth below the magnetometer (James 2025, p. 83). A similar description of the Hall calculation is found in another detailed report on magnetic surveys (Holt 2019, p. 19-21). Further information about the likely mass of iron objects that will be found at shipwrecks is in a report by Bright, Conlin, and Well (2014, p. 16-22); this report also compares the Hall method with the normal geophysical equation for the dipolar anomaly of a compact mass.

The iron in a modern ship may have a magnetic moment of 0.09 Am^2 per kilogram of mass (Watermann and Lam 1999, p. 8); this is a third of the relative magnetic moment that was mentioned by Breiner (1973, p. 42). Either value can aid the analysis of magnetic anomalies by converting magnetic moment to a mass of iron.

During the US Civil War in 1861 - 1865, hundreds of ships were sunk in rivers, by enemy action or by collision with trees that were hidden underwater (Gains 2008). Many of these ships had heavy iron armor, in addition to their steam engine. If possible, a sinking ship would be grounded on the nearby river bank, so that the passengers and crew could get to dry land, and the ship could be salvaged without difficulty. Many of the rivers in the central part of the USA shift their course from year to year, and many of those old ships are now found near a river, but on dry land, and perhaps at a depth of 5 - 10 m underground. It is very expensive to excavate a deeply-buried ship, and it is better to have a magnetic survey estimate the location, depth, and mass of a possible ship.

A steamboat sunk along the Red River in the southern US state of Louisiana in 1865. When the river later shifted its course, most of the boat was covered by sediments at the edge of the river, although one end of the ship was exposed at the river bank. A total-field magnetic survey (Simms and Albertson 2000, Fig 11) detected the ship next to the river as an elongated anomaly with an amplitude of about 2000 nT. The depth of the ship was known to be about 6 m and the sensor height was about 2 m. At the time and location of the survey, the Earth's field (B_e) was 51,000 nT at an inclination of 61° . If one assumes that the magnetic volume of the ship can be approximated with a rectangular box (10 by 30 m in size), having a thickness of 1 m and a susceptibility $k = 2.5$ (SI), then the magnetic moment of the ship can be approximated (with the Pdyke program from Geophysical Software Solutions) at about $30,000 \text{ Am}^2$. This moment is calculated from: $k * \text{volume} * B_e / 1257$.

At another location, a magnetic survey was done along a former river channel (now dry land) where the Missouri and Mississippi Rivers join in the central USA; historical records suggest the location of several ships that could now be buried there. The geophysical survey (Larson and Norris 2008, Fig. 4) did not find magnetic anomalies where wrecks were expected, but did locate a 90-nT anomaly at an unexpected location. As a supplement to the

authors' analysis of this anomaly, a square box-like feature (4 x 4 x 2 m) with an intensity of magnetization of 30 A/m and a depth of 8 m can create a calculated anomaly that is similar to the anomaly that they measured (see [Figure 33](#)); this body has a magnetic moment of 960 Am².

A magnetic survey detected anomalies of as much as 20 nT during a search for a wooden ship from the 1800s; this ship may be buried at a depth of about 8 m in the coastal sands of southern Australia (Stanley 1992). The legendary "Mahogany Ship" has been sought for many years (see Wikipedia).

It is not always necessary to use expensive equipment and software for locating shipwrecks. Edwin C. Bearss, a historian with the US National Park Service, wished to locate an ironclad gunboat that sunk during the US Civil War near the edge of the Yazoo River, and north of the city of Vicksburg, Mississippi. He detected this underwater shipwreck by exploring the river with a small boat and a magnetic compass (Jones and Peterson 1971, p. 35). There was a deflection of the needle of the compass when they passed over the location of the ship. A later survey for an iron-filled well with a compass is illustrated in [Figure 30](#).

As another illustration, during World War 2, many ships were sunk in the Yangtze River in China in order to block other ships from access to the river. A magnetic survey located seven ships; they each caused anomalies of more than 1000 nT (Wang, Qu, Qi and Shen 2006, Fig. 12).

An iron industry in Canada

In the 1800's there was a large iron industry near Trois-Rivieres in southeastern Canada. A geophysical survey with a cesium magnetometer mapped an area of 2.8 hectares. An analysis of the magnetic maps suggested that the total iron mass was as much as 15 Mg in the area; masses were estimated to be buried between a depth of 0 and 4 m (Bevan 1975a, 1975b). The estimate of mass was based on the magnetic parameters of three iron objects from the site; these measurements were made by rotating each object near the magnetic sensor and searching for its high and low magnetic anomalies.

parameter =>	mrm	mim	Q	ma	d
unit =>	mAm ² /kg	mAm ² /kg		kg	kg/m ³
Lump of cast iron	9.36	1.31	0.7	0.0113	5900
Lump of cast iron	43.6	47.4	0.9	0.0445	6600
Part of a spike	15.6	26.8	0.6	0.17	6100

The cast iron facade of a building

The iron face of an historic building in the USA ([Figure 34](#)) was removed and stored for later re-assembly. However, its location was lost after the storage area was covered with a thick layer of soil. A magnetic survey of the storage area located an anomaly whose spatial size, shape, and amplitude was reasonable for the facade ([Figure 35](#)). However, an excavation at that anomaly found only a huge mass of incinerated trash and rusted iron.

An abandoned town in the USA

A search for abandoned and lost towns in the state of Mississippi (southern USA) was made with a magnetic survey (Mason 1984). The area was dense with trees and bushes, and most types of geophysical survey would have been impossible. However, the area could be mapped with the help of several people, each carrying a proton magnetometer. Most of the anomalies were caused by iron wire from broken-down fences and other iron trash; however, three filled wells (2 m in diameter and 5 m deep) were detected because their fill contained thousands of nails or a cast iron kettle. These caused anomalies of about 30 nT at a sensor height of 1.2 m. Others have also found magnetic surveys to be suitable for locating iron artifacts within wooded sites (Hodgetts, Millaire, Eastaugh, and Chapdelaine 2016; and Sampson and Horsley 2020).

Buried aircraft parts

Historical records suggested that aircraft parts were buried at an airport in the central USA state of Indiana during World War 2. An exploration with a proton magnetometer (a Geometrics model G-856) discovered a large magnetic mass, as shown on the left side of [Figure 36](#).

An excavation at that location found a large pit that had been filled with incinerated trash, and none of the aircraft parts that were sought. Would it have been possible to predict that this mass was burned trash? Perhaps there is no reliable method for distinguishing somewhat small particles of trash from the larger iron objects that were wanted. It is possible that seismic velocity might allow this distinction, but it may be easier to make a small excavation to identify the source.

Since aircraft contain much less iron than most ships, magnetic exploration for aircraft is less suitable. The magnetic moments of several engines for driving aircraft propellers were measured by Weiss +6 (2007); an average of their values was: induced = 9.5 Am^2 and remanent = 4 Am^2 .

Magnetic directions in a farmed field

The magnetic map of a plowed field is plotted as [Figure 37](#). All of the anomalies in this map are probably caused by metallic iron. The soil here is mostly non-magnetic sand, and the few small stones are also not magnetic. However, the area has been farmed for

more than 100 years, and it was also the site of a battle of the US Civil War on 1 July, 1862. Most of the magnetic anomalies are probably caused by now-buried parts of farming equipment, although some anomalies may reveal artifacts from the battle.

While [Figure 37](#) allows many buried iron objects to be located, the magnetic patterns provide additional information that may not be immediately apparent: Estimates of the direction of total magnetization of the objects that cause the anomalies. Many of the anomalies shown in [Figure 37](#) are bipolar, with a magnetic low (blue) immediately adjacent to a high (red); these anomalies can be analyzed, perhaps with the MagPick computer program that has been written by Mikhail Tchernychev. [Figure 38](#) has a plot of these magnetic directions for 125 anomalies.

If all of these objects were compact and magnetized only by induction (that is, they were without remanent magnetization), all of these symbols would be near the black square; that square marks the direction of the Earth's field. Instead, most symbols are distant from that square, and an unusually large fraction of directions are rather horizontal (near the large black circle that encloses the data points). If the symbols had been distributed rather uniformly within the area of the large circle, this could mean that the magnetization of the objects was primarily remanent. This map shows neither possibility.

Many iron objects are elongated; they may be rather flat or they may be like thin and long rods or bars. These objects will lie rather flat on the ground surface after falling, and they may remain rather horizontal after they are buried. Iron objects are usually so magnetic that they are magnetized primarily in the direction of their length, and this is therefore often horizontal. While no excavation tests have been made to check this idea, it is the most reasonable explanation for this pattern.

The axle of a Ferris wheel

Perhaps the heaviest steel object that was buried and later located with a magnetic survey weighed about 40,000 kg. This was the steel axle of a tall Ferris wheel. This axle was the central part of a rotating platform that gave an elevated view at a world's fair that was held in the city of St. Louis (Missouri, USA), in 1904. The wheel was destroyed after the fair, but the axle was so big (15 m long) that it was just buried nearby, and then forgotten.

Sheldon Breiner found the buried axle with the help of a cesium magnetometer from Geometrics (Breiner 2007). He made a reconnaissance survey in downtown St. Louis in a little more than a day, measuring the total magnetic field with his sensor at a height of 2 m. The axle gave an anomaly of about 24,000 nT, and he found no anomaly that was stronger; the anomalies of passing or parked cars were small relative to this. He could delineate the axle by the characteristic shape of the anomaly, and he determined that the axle was buried about 60 m from where the Ferris wheel was operated. While he did not analyze his magnetic measurements for a determination of the depth of the axle, it is probably about 3 m underground.

The remaining illustrations review the magnetic maps of features that usually have little or no archaeological importance. However, their anomalies must be understood, for these patterns will be found at many locations where magnetic surveys are done. The order of these examples will be roughly in the sequence of decreasing iron mass.

A passing train or another distant feature

While magnetic objects such as iron artifacts create magnetic highs in their vicinity, these magnetic objects also create magnetic lows at a greater distance. These low readings may sometimes be too faint to be visible in the magnetic map. These magnetic lows have a simple explanation: The magnetic flux from the Earth concentrates in the magnetic feature, and therefore the flux must be depleted outside the feature, causing the magnetic low.

In any map of magnetic anomalies (that has the Earth's field subtracted), a summation of all of the measurements (positive and negative) will be about zero. Stated in a different way: Add all of the measurements that are magnetic highs and separately, add all of the lows; the magnitude of the two sums should be about the same. The summation to zero is related to the general fact that the net magnetic flux outward from an enclosed volume or across an infinite plane is zero.

During a magnetic survey, these lows from a nearby iron object are usually most apparent when a car or truck passes near the area of survey; the magnetic readings will be low for one or more readings along a line of traverse, when the car was nearest. This unwanted effect will be seen much more with a total-field magnetometer than with a gradiometer. [Figure 39](#) illustrates measurements of the magnetic lows of passing cars.

In addition to cars and trucks, even larger masses of iron may be nearby; these may be trains or modern ships (see [Figure 0](#)). If these large masses are moving, their magnetic effect will be most apparent in a plot of temporal changes in the magnetic field. [Figure 40](#) has an example; note the two small dips in the readings when trains passed.

A distant magnetic low can be explained by the calculation of [Figure 41](#), where a spatial map approximates the temporal measurements of [Figure 40](#). The calculations show that almost all space around a magnetic object has a reduced magnetic field; it is only when measurements are made directly over the object that magnetic high readings are found.

[Figure 42](#) shows another view of the reduction of the magnetic anomaly as a large mass of iron becomes more distant. At a distance of 10 m, this graph shows that a total-field magnetometer will find an anomaly of 100 nT, while a gradiometer will detect a weaker anomaly of only 5 nT.

An understanding of these magnetic lows will allow a correct interpretation of a magnetic map that has a strong low at the edge of the map (without a companion high); the magnetic object is simply outside the area of survey (see [Figure 37](#)).

Further information about the magnetic lows that are caused by objects is plotted in [Figure 43](#). These unwanted anomalies that are measured with a total-field magnetometer can be much reduced with a magnetic gradiometer.

Aeromagnetic anomalies

Aeromagnetic surveys are often flown at an altitude of 1000 m or higher. However, for a better spatial resolution of underground features, the height may be reduced below 150 m. At this lesser height, heavy iron features such as oil wells, water towers, television antennas, trains, and steel-framed buildings can add confusing anomalies (Hassan +3, 1998). These unwanted anomalies are called “cultural noise” in the discipline of geophysical exploration for minerals. This interference may usually be identified in the magnetic map by searching for anomalies that have a high amplitude and a small area (spikes). Further information about the effect of vertical pipes and similar unwanted features in magnetic maps is available (Muszala, Stoffa, and Lawver, 2001; Hassan and Pierce 2005); the procedures that are applied to cultural editing may benefit magnetic surveys at archaeological sites also.

A nearby car can cause an anomaly that is normally an unwanted interference to a magnetic survey. However, if a buried car is sought, a magnetic survey can readily locate it, for the mass of iron and steel in a car is about 1000 kg. A magnetic search for a buried car (Witten 2003, Fig. 3) could definitely show that no car was buried in the area of search.

Large and heavy plates

The magnetic anomaly that is mapped in [Figure 44](#) has an interesting pattern: A linear magnetic low that is north of, and parallel to, a rather linear high. The anomaly is caused by a steel plate that is at the surface of the ground. This plate is called a Marston Mat (see Wikipedia) or perforated steel planking. They are found near many airfields that operated during World War 2; after the war, many of these plates were converted to domestic use, and they may now be found as pavements, walls, or fencing.

The magnetic measurements in [Figure 44](#) were approximated by the calculated anomalies in [Figure 45](#). Note that the inclination angle of magnetization of the plate on the right is nearly horizontal (inclination = -0.8°) and much shallower than the Earth's field (inclination = 63°).

Buried fuel tanks

Petroleum fuel for heating houses or powering cars is usually stored in large steel tanks that are buried underground. A magnetic survey can locate these tanks by their high amplitude anomaly (perhaps several thousand nanoteslas); this anomaly may have a breadth of several meters.

One example is seen in [Figure 46](#); three buried tanks were expected at this location. The strong magnetic anomaly (over 9000 nT) made it certain that the tanks were there.

A magnetic analysis of [Figure 46](#) shows that a rectangular box with a magnetic susceptibility of 15 (SI), which is a magnetic moment of about $40,000 \text{ Am}^2$, has a calculated anomaly that is similar to the measurements. The effective susceptibility was less than 6 (SI) after an approximate correction was made for demagnetization. However, the magnetic anomaly of a magnetic shell will be different from that of a filled shell (because of demagnetization); therefore, this analysis is poor for estimating the mass of the steel that makes these tanks. However, as mentioned with the demagnetization section, comparisons to similar tanks may be accurate.

As another example, a magnetic survey with its total-field sensor at a height of about 2.5 m detected an anomaly of 6000 nT at one location. An excavation at the anomaly found a steel storage tank with a capacity of 42,000 liters at a depth of 1 m (Schlinger 1990, Fig. 7A)

Drums for storing chemicals

In many countries, chemicals for manufacturing processes have been stored and shipped in large steel cans called 55-gallon drums (with a volume of about 0.2 m^3 or 200 liters). Unwanted chemicals may also be put in these drums and then buried. These locations may be lost or forgotten and many geophysical surveys have been done to find their burial locations. Perhaps the first article that illustrated the magnetic anomaly of a typical 55-gallon steel drum was written by Tyagi and Lord (1983).

Barrows and Rocchio (1990, Fig. 3) show how the magnetic anomaly of a drum may be measured by elevating it above the magnetic sensor; this is easier than burying the drum.

The magnetic properties of a variety of steel drums and their magnetic maps are illustrated by Emerson +3 (1992); these authors also discuss the difficulty of including the effect of demagnetization and how it varies with the thickness of the steel.

Detailed magnetic measurements were made on steel that had been cut from drums (Ravat 1996). These tests were followed by the creation of models from the magnetic maps of steel drums; his analysis found that the remanent magnetic moment of the steel was roughly $130 \text{ mAm}^2/\text{kg}$ and that the induced moment was about $420 \text{ mAm}^2/\text{kg}$. Therefore, the Q ratio was low, at about 0.31 and that is also reasonable.

Detailed magnetic model of steel drums may be calculated (Furness 2002 and 2007); the publication includes the effect of the shape of the steel shell of the drum.

A recent review of the problem of detecting steel drums (Marchetti, Sapia, and Settimi 2013) also includes maps of buried drums that have been measured with a gradiometer and a total-field magnetometer.

An analysis of the magnetic map of a drum in its upright orientation is in [Figure 47](#). This analysis assumed that the anomaly was caused by both remanent and induced magnetization. The drum was modeled as a circular cylinder that is vertical, and filled with a magnetic material. The susceptibility of the model ($k = 6.7 \text{ SI}$) can be multiplied by the

intensity of the Earth's magnetic field ($H_e = B_e / 1257$) to give an induced intensity of 295 A/m. The Q ratio is then $44.5 / 295 = 0.15$. This agrees with the simpler analysis of [Figure 48](#) that found that induced magnetization predominates in this iron object.

An overhead object

The iron objects that cause distinct magnetic anomalies are not always buried or at the ground's surface. They may also be overhead, and then their magnetic anomalies will be quite different; see [Figure 49](#). [Figure 43](#) also illustrates the anomaly of an elevated object.

Underground pipes

Underground steel or iron pipes can be detected by magnetic surveys at many archaeological sites, particularly those that were occupied in the historic period. [Figure 50](#) reveals segments of four buried pipes; their magnetic anomalies probably hide archaeological structures in their vicinity. An excellent discussion of the magnetic anomalies caused by iron pipes has been prepared by Sowerbutts (1988).

The magnetic map of the underground pipe in [Figure 51](#) is rather uniform along its east-west length; unlike many other magnetic maps of pipes, this does not show the string-of-beads pattern. An analysis of this magnetic map indicates that the direction of total magnetization of the pipe is close to that of the Earth's magnetic field. This pipe was probably constructed by rolling sheet iron into a cylinder and adding corrugations that encircle the pipe for greater strength.

There is no evidence of different directions of magnetization along the length of this pipe, and it is possible that the pipe is constructed of iron that has little remanent magnetization. It is also possible that the metal has remanent magnetization, but its effect has been lost because that magnetization is now cylindrical, therefore canceling out the remanence, just like the underground cylindrical magnetization of a lightning strike.

A grounding rod

A magnetic survey revealed the anomaly shown in [Figure 52](#). A later excavation found that the anomaly was caused by an iron grounding rod. Since the rod was vertical, and also long and thin, it has created an anomaly that is similar to that of a single monopole, as shown in [Figure 29](#).

Unexploded ordnance

During about 1960 in Canada, and 2010 in the USA, and at other periods in Europe, there were many studies done on the application of magnetic surveys to locate underground explosives in steel containers. These were important to find because of the danger of unexpected explosions. These modern explosives are found at training bases for the military, and also where bombs failed to explode during wars. These buried iron objects are

called UneXploded Ordnance, and abbreviated UXO. The many articles and reports that were published on this topic are also valuable for the search for archaeological artifacts of iron; do a web search for "magnetic UXO" to find many of these informative reports and articles. Explosive land mines are constructed so that they contain very little iron; magnetic surveys are seldom applied to their search.

Here are a sample of publications that describe the application of magnetic surveys to locating UXO:

McFee +3 (1993) made a detailed study in Canada about the detection of buried iron; these authors also wrote many other important publications on this topic at about this time, including the earlier article McFee, Das, and Ellingson (1990).

Butler +4 (2012) found that a spheroidal model (elongated sphere) was more suitable than a sphere for approximating the magnetic anomaly of UXO by an estimation of shape.

Billings (2003) found that an estimation of the direction of remanent magnetization aided the discrimination between UXO and non-hazardous metal that is also underground; this work was extended in a later report (Billings 2009).

Krahenbuhl +3 (2011) studied a method for distinguishing UXO from other metal, soil contrasts, and magnetic stone by applying Euler deconvolution and estimating the shape of the buried objects. These ideas are also described in an article (Davis +3, 2010).

While unexploded weapons are a hazard for magnetic surveyors of archaeological sites, already-exploded weapons can also cause serious interference to magnetic exploration. During many wars in the 1900s, explosives were designed to spread fragmented steel over a wide area. These fragments are usually more magnetic than most archaeological artifacts. It may therefore be necessary to search an area with a fast metal detector and remove all shallow metal in order that larger, deeper, but less magnetic, archaeological features can be detected with a magnetometer. Perhaps in some areas, it may be best to raise the magnetic sensor to a greater height than usual; this can reduce the anomalies of shallow objects more than deep objects. An alternative would be an exploration with resistivity or ground-penetrating radar, for both techniques are less sensitive to metal than are magnetic surveys.

Temporal noise in magnetic data

Magnetic surveys are affected by unwanted temporal changes caused by lightning, electrical power lines, and electrified railroads. [Figure 53](#) shows how lightning flashes may be detected by a magnetometer. These are temporal anomalies in the magnetic field; if an area was being mapped during this thunderstorm, many small-area anomalies would appear as spatial noise in the magnetic map, and these anomalies could be confused with small features that are buried.

Meteorites

Most geological iron has no importance for archaeology. Meteorites are an exception, for these have been a source for iron in ancient times (Appelt +5, 2015). Magnetic maps that were measured over meteorites in Greenland found anomalies of more than 1000 nT (Appelt +5, 2015, Fig. 58 and 60); the height of the magnetic sensor was not noted in the report.

The magnetic susceptibility meter manufactured by ZH Instruments (a model SM-30) was applied to the measurement of meteorites (Folco +3, 2006). The SM-30 instrument was also used in another study (Macke 2010, Fig. 14 and p. 45-50). The simple design of a portable electronic meter for measuring the magnetic susceptibility and electrical conductivity of objects such as meteorites has been described by Uehara and Gattacceca (2023). A procedure for the measurement of the magnetic moment of very heavy meteorites has also been developed (Clave +6, 2020).

Magnets must not be used for testing if a rock may be an iron meteorite, for this may alter the remanent magnetization that is important to the study of interplanetary magnetic fields (Vervelidou +2, 2023). A proton magnetometer should probably not be applied to this test (unless the sensor remains at a distance of a few meters); most sensors create a strong magnetic field during their measurement.

Some large impact craters on Earth have been created by the fall of heavy iron meteorites. The magnetic maps of these craters usually appear to be complex rather than showing simple or dipolar patterns. The magnetic map of the impact site of an iron meteorite did not reveal a concentration of iron (Wynn 2002); this was because molten iron was mixed with sand and scattered around the area of impact. The magnetic maps of most meteorite impacts can show primarily a magnetic low, with weaker and more complex magnetic highs (Therriault, Grieve, and Pilkington 2002).

Iron mines

Magnetic surveys have been applied for several centuries for locating where iron deposits may be mined. Early sensors were mechanical and not electronic. They were much like today's magnetic compasses; they revealed an unusual magnetic declination where iron was near. A dip needle is much like a magnetic compass, but the inclination of a magnetic needle that swings in a vertical plane was noted. Early developments and applications of these mechanical magnetometers were made in Europe. At a later time, explorations for iron began in the USA, with puzzling results: There could be strong indications of buried iron where little iron was found. This was later revealed to be caused by the fact that small amounts of magnetite created huge anomalies (Hinze 2022, p. 5). Unfortunately, large amounts of hematite caused insignificant anomalies. Hematite is weakly magnetic but it is an excellent source for iron ore.

Magnetite in sediments

Another source of natural iron that can create unwanted magnetic anomalies is magnetite. This is often found on beaches and at the edge of rivers that have sandy sediments; this magnetite is also called black sand. It is readily detected by measurements with a magnetometer or magnetic susceptibility meter (El-Sadek, Ammar, and Elkhateeb 2012, Fig. 3 and 9). Magnetite can be identified by pouring dry sand or soil over a strong permanent magnet. Magnetic minerals are also found in other sedimentary deposits, such as laterites (Grant 1984, p.319). The Salgir River that has been discussed here is an example of the detection of magnetic sediments. Magnetic surveys may be more difficult in areas that were formerly glaciated (Gay 2004), for igneous stones that are quite magnetic may have been imported (plowed by the glacier) to the area.

Conclusions

This is the fourth report of a series about Magnetic Mapping. These reports have suggested that there may be significant differences in the Q ratio between archaeological features. (The Q ratio is remanent magnetization divided by induced magnetization)

The Q ratio for **iron** is usually less than 1 and can be near 0.1; see this report, p. 4.

The Q ratio for **soil** is about 1 (Bevan and Smekalova 2023, p. 9-11).

The Q ratio for **fired earth** is often about 10 (Bevan and Smekalova 2025b, p. 57).

The Q ratio for **stone** is variable over a wide range (Bevan and Smekalova 2021). However, many more measurements are needed to check if these values are typical and reasonable. Still, when local data are not available, these values can be applied to an analysis.

In addition to a low Q ratio, iron artifacts usually have important differences from other artifacts. Iron often has an elongated shape; it can be either long like a rod or a bar, or it can be thin like a plate or disk. When discarded, these artifacts will often lie flat on the earth, and they will remain flat when they are buried. Being horizontal and very magnetic, these artifacts will then have an inclination of magnetization that is very much less than the angle of the Earth's magnetic field, and perhaps very close to zero. This low inclination may be apparent in a bipolar magnetic anomaly if the amplitude of the magnetic high is similar to the magnitude of the associated magnetic low. A magnetic model will allow a better estimation of the inclination of magnetization, and it will also furnish an approximation of the declination angle (Bevan 2020) of that magnetization. [Figure 38](#) illustrates how directions of magnetization may be rather horizontal, although at many different declinations (horizontal angles); this suggests that many of the iron objects that were detected are both elongated and horizontal.

A simple visual examination of a magnetic map will also provide helpful information. [Figure 15](#) has an example of five objects that each have a declination angle that is about the same as that of the Earth's field; this suggests that induced magnetization might

predominate. This differs from the pattern in [Figure 32](#); the two dipolar directions (marked with black arrows) are quite different from each other and they are also different from the direction of the Earth's field; this means that these objects have remanent magnetization.

Iron objects are more magnetic than anything else; [Figure 2](#) indicates that the relative magnetic moment of iron can often be assumed to be about $0.1 \text{ Am}^2/\text{kg}$. This means that demagnetization may have an effect on the orientation of magnetic anomalies. The clusters of cannon balls in [Figure 18](#) have primarily induced magnetization. However, the layers are relatively thin and rather flat, so the direction of their magnetization is much more horizontal than the inclination of the Earth's magnetic field.

If a magnetic survey is to be done in an area where both iron and earthen contrasts are to be discovered, it will probably be important that the magnetic map displays a very wide range in the amplitude of magnetic anomalies. For this situation, it may be best that the magnetic map has combined both gray scale images (for weak contrasts) and also contour line images (for high amplitude anomalies). [Figure 37](#) has an example of this type of map.

Only a fraction of geophysical surveys are followed by an archaeological excavation. Even fewer projects include a post-excavation geophysical survey and evaluation. A magnetic map that is measured after an excavation can indicate if further magnetic features remain below or just outside the area of the excavation. Many geophysical anomalies are caused by rubble and other complex strata that have no importance for archaeology. Magnetic mapping in an excavation can clarify the anomalies caused by intact and simpler archaeology; tests in the excavation can also quantify the geophysical contrasts of the features. Magnetic models of the excavated features can then improve the reliability of the interpretation of future geophysical surveys.

References

Alberts, Robert C., 1975, A charming field for an encounter, the story of George Washington's Fort Necessity, US National Park Service, US Government Printing Office.

Appelt, Martin, Jens Fog Jensen, Mikkel Myrup, Henning Haack, Mikkel Sorensen, and Michelle Taube, 2014, The cultural history of the Innaanganeq / Cape York meteorite, Technical report 2015, The Greenland National Museum & Archives. Free at https://anthropology.ku.dk/research/research-projects/completed_projects_/now/Meteorit2014FinalReportLight.pdf

Barrows, Larry, and Judith E. Rocchio, 1990, Magnetic surveying for buried metallic objects, Ground Water Monitoring Review, Free at <https://www.geometrics.com/wp-content/uploads/2018/10/M-TR34.pdf>

Bevan, Bruce, 1975a, A magnetic survey at les Forges du Saint-Maurice, 92-page report from the Museum Applied Science Center for Archaeology, The University Museum, University of Pennsylvania, and prepared for Pierre Nadon and John P. Wilson (Parks Canada). Free at <http://core.tdar.org/document/381133>

Bevan, Bruce, 1975b, A magnetic survey at les Forges du Saint-Maurice, MASCA Newsletter, vol. 11, no. 1, 1p.

Bevan, Bruce, 1980, Iron in the park: A magnetic survey, a 13-page report prepared for Craig Blakely, Philadelphia Historic Preservation Corporation. Free at <http://core.tdar.org/document/381158>

Bevan, Bruce, 1981, A geophysical survey at New Windsor Cantonment, 21-page Geosight report prepared for Charles Fisher (New York State Parks and Recreation).

Bevan, Bruce W., 1983, Quantitative magnetic analysis of landfills, 26-page Geosight report. Free at <https://www.geometrics.com/wp-content/uploads/2018/10/M-TR26.pdf>

Bevan, Bruce, 1987, A geophysical survey on Virginius Island, a 16-page report from Geosight prepared for Stephen Potter and Susan Frye (US National Park Service). Free at <http://core.tdar.org/document/381210>

Bevan, Bruce, 1988, A geophysical survey at Fort Necessity, 31-page report prepared for David Orr (US National Park Service). Free at <http://core.tdar.org/document/381182>

Bevan, Bruce, 1993, How distant can a base station be, 28-page Geosight report prepared for William Brennan, Rolf Ehrat, Don Heimmer, Douglas Londry, Alan Scott, and John

Weymouth. Free at <https://www.researchgate.net/publication/318826550>

Bevan, Bruce, 1996, Geophysical exploration in the U.S. national parks, *Northeast Historical Archaeology*, vol. 25, p. 69-84. Free at <https://www.academia.edu/26462162> and at <https://www.researchgate.net/publication/304248165>

Bevan, Bruce 2000, A geophysical survey at Appomattox Court House, 120-page Geosight report prepared for Allen Cooper and Joe Williams (US National Park Service). Free at DOI:10.13140/RG.2.2.11734.65603 and at <https://www.researchgate.net/profile/Bruce-Bevan/publication/311677774>

Bevan, Bruce W., 2002a, The magnetic properties of archaeological materials, 13-page Geosight report (Technical Report no. 5, 2nd edition). Free at <https://www.geometrics.com/wp-content/uploads/2018/10/M-TR124.pdf> and at DOI:10.13140/RG.2.1.3505.5603 and at <http://core.tdar.org/document/381526>

Bevan, Bruce, 2002b, A geophysical survey at the West House, Richmond National Battlefield, a 125-page report prepared by Geosight for Benjamin Ford (Rivanna Archaeological Consulting). Free at <http://core.tdar.org/document/381212> and at <https://www.researchgate.net/publication/311678335>

Bevan, Bruce W., 2004a, Geophysical Exploration for Archaeology, Volume C: Detailed survey procedures, 227-page Geosight report. Free at <http://core.tdar.org/document/381097>, or at DOI: 10.13140/RG.2.2.15085.59364 or at <https://www.academia.edu/26462148>

Bevan, Bruce W., 2004b, Geophysical Exploration for Archaeology, Volume B: Introduction to geophysical exploration, a 242-page Geosight report. Free at <http://core.tdar.org/document/381094> and at DOI: 10.13140/RG.2.2.33540.53120, and at <https://www.academia.edu/31116829> and at https://digitalcommons.unl.edu/cgi/viewcontent.cgi?params=/context/natlpark/article/1090/&path_info=spec1.pdf

Bevan, Bruce, Tatyana Smekalova, and Sergei Smekalov, 2005, Magnetic maps of three Danish slag blocks, which includes: 2006 Supplement: Analysis of the magnetic maps, 72-page report prepared for Olfert Voss (Nationalmuseum) from St. Petersburg State University and Geosight. Free at <http://core.tdar.org/document/381130> and at <https://www.researchgate.net/publication/305587882>

Bevan, Bruce W., 2006, Understand magnetic maps, 74-page Geosight report. Free at

<https://www.researchgate.net/publication/272487686> and at
<https://www.academia.edu/26462122>

Bevan, Bruce W., 2009, Directions of magnetization, the 9-page summary of a poster at the Computer Applications to Archaeology conference in Virginia. Free at
http://proceedings.caaconference.org/files/2009/03_Bevan_CAA2009.pdf and at
<http://core.tdar.org/document/381083> and at <https://www.academia.edu/26462287>

Bevan, Bruce, 2020, Orientations of dipolar magnetic anomalies, 29-page Geosight report. Free at <https://www.researchgate.net/publication/345422018> and at
<https://www.academia.edu/44450180>

Bevan, Bruce W. and Tatiana N, Smekalova, 2021, Magnetic mapping of archaeological stone, 214-page report from Geosight and the V. I. Vernadsky Crimean Federal University. Free at DOI: 10.13140/RG.2.2.25475.84001 and at <https://www.academia.edu/51629240/>

Bevan, Bruce W., and Tatiana N. Smekalova, 2023a, Magnetic mapping of earthen archaeology, 128-page report prepared by Geosight and V. I. Vernadsky Crimean Federal University. Free at <https://www.researchgate.net/profile/Bruce-Bevan/publication/374807603> and at DOI: 10.13140/RG.2.2.16658.84161 and <https://www.academia.edu/108047776>

Bevan, Bruce W., 2025a, The polarity of magnetic anomalies, or: Magnetic dipoles around the world, 12-page Geosight report. Free at DOI: 10.13140/RG.2.2.18817.06249 and at Academia.edu

Bevan, Bruce W. and Tatiana N, Smekalova, 2025b, Magnetic mapping of fired archaeology, 224-page report from Geosight and the V. I. Vernadsky Crimean Federal University. Free at DOI: 10.13140/RG.2.2.34535.36007 and at <https://www.academia.edu/129379160>

Billings, Stephen D., 2003, Discrimination and classification of buried unexploded ordnance using magnetometry, 25-page report from the University of British Columbia - Geophysical Inversion Facility. Available at <https://ieeexplore.ieee.org/document/1304891> and free at <https://www.researchgate.net/publication/3203499>

Billings, Stephen, 2009, Advanced UXO discrimination using magnetometry: Understanding remanent magnetization, SERDP Project MM-1380, 83-page final report from Sky Research. Free at <https://apps.dtic.mil/sti/tr/pdf/ADA520702.pdf>

Birkmire, Wm. H., 1892, Architectural iron and steel, and its application in the construction of buildings, second edition, Wiley. Free at archive.org.

References

- Breiner, Sheldon, 1973, Applications manual for portable magnetometers, 58-page Geometrics report. Free at <https://www.geometrics.com/wp-content/uploads/2018/10/m-ampm-05Apr06.pdf>
- Breiner, Sheldon, 2007, Magnetic survey to find axle from observation (Ferris) wheel used in the 1904 St Louis World's Fair, 8-page report. Free at <http://www.breiner.com/sheldon/papers/Magnetometer%20survey%20for%20buried%20Axle%20in%20St%20Louis%20May,%202007.pdf>
- Bright, John C., David Conlin, and Sage Well, 2014, Marine magnetic survey modeling: Custom geospatial processing tools for visualizing and assessing marine magnetic survey for archaeological resources, 240-page report from the Submerged Resources Center of the National Park Service in the USA. Free at <https://www.boem.gov/Marine-Magnetic-Survey-Modeling/>
- Butler, Dwain K., Janet E. Simms, John S. Furey, and Hollis H. Bennett, 2012, Review of magnetic modeling for UXO and applications to small items and close distances, *Journal of Engineering and Environmental Geophysics*, vol. 17, no. 2, p. 53-73. Available at DOI:10.2113/JEEG17.2.53
- Chadebec, Olivier, Jean-Louis Coulomb, Vincent Leconte, Jean-Paul Bongiraud, and Gilles Cauffet, 2000, Modeling of static magnetic anomaly created by iron plates, *IEEE Transactions on Magnetics*, vol. 36, no. 4, p. 667-671. Available at DOI: 10.1109/20.877537 and free at <https://www.researchgate.net/publication/3101860>
- Clark, D. A., 1980, Reliability of susceptibility measurements on conductive samples - A comparison of commercially available instruments, 11-page report (1173R) from CSIRO, Australia. Free at <https://research.csiro.au/potential-fields/wp-content/uploads/sites/398/2023/12/26575948.pdf>
- Clark, D.A., and D.W. Emerson, 1999, Self-demagnetization, Preview (ASEG publication), April, p. 22-25. Free at <https://www.aseg.org.au/sites/default/files/PVv1999n079.pdf>
- Clave, Elise, Clara Maurel, Eduardo A. Lima, Jay Shah, Elias N. Mansbach, Minoru Uehara, and Benjamin P. Weiss, 2020, A portable magnetometer for magnetic measurements of meter-sized meteorites, *Geochemistry, Geophysics, Geosystems*, vol. 21, e2020GC009266. Free at <https://doi.org/10.1029/2020GC009266>
- Conyers, Lawrence B., Eileen G. Ernenwein, Michael Grealy, and Kelsey M. Lowe, 2008, Electromagnetic conductivity mapping for site prediction in meandering river floodplains,

- Archaeological Prospection, vol. 15, p. 81-91. Available at DOI: 10.1002/arp.326
- Davis, Kristofer, Yaoguo Li, and Misac Nabighian, 2010, Automatic detection of UXO magnetic anomalies using extended Euler deconvolution, *Geophysics*, vol. 75, no. 3, p. G13-G20. Available at 10.1190/1.3375235
- El-Sadek, Mohamed A., Ahmed A. Ammar, and Sayed A. Elkhateeb, 2012, Analysis and interpretation of the field and laboratory geophysical measurements of black-sand beach deposits, East Rosetta, Egypt, *International Journal of Geophysics*, Article ID 435216, 10 pages. Available at doi:10.1155/2012/435216
- Emerson, D.W., J. E. Reid, D. A. Clark, M. S. C. Hallett, P. B. Manning, 1992, The geophysical responses of buried drums - Field tests in weathered Hawkesbury sandstone, Sydney basin, NSW, *Exploration Geophysics*, vol. 23, p. 589-617. Available at <https://doi.org/10.1071/EG992589>
- Eskola, L., T. Jokinen, H. Soininen, T. Tervo, 1993, Some remarks on static field thin sheet models, *Journal of Applied Geophysics*, Vol. 30, p. 229-234. Available at [https://doi.org/10.1016/0926-9851\(93\)90029-X](https://doi.org/10.1016/0926-9851(93)90029-X)
- Eskola, L., R. Puranen, and H. Soininen, 2001, Measurement of magnetic properties of steel sheets, *Geophysical Prospecting*, Vol. 47, p. 593-602. Available at <https://doi.org/10.1046/j.1365-2478.1999.00141.x>
- Everett, M.E., C.J. Pierce, N. Save, R.R. Warden, D.B. Dickson, R.A. Burt, and J.C. Bradford, 2006, Geophysical investigation of the June 6, 1944 D-Day invasion site at Pointe du Hoc, Normandy, France, *Near Surface Geophysics*, p. 289-304. Available at <https://doi.org/10.3997/1873-0604.2005052> and free at <https://www.researchgate.net/publication/236901679>
- Folco, Luigi, Pierre Rochette, Jerome Gattacceca, and Natale Perchia, 2006, In situ identification, pairing, and classification of meteorites from Antarctica through magnetic susceptibility measurements, *Meteoritics & Planetary Science*, vol. 41, p. 343-353. Free at <https://doi.org/10.1111/j.1945-5100.2006.tb00467.x>
- Freed, Chad H., Edward L. Doheny, and Timothy D. Bechtel, 2009, Determination of the magnetic viscosity for cold rolled carbon-steel 55-gallon drums in the Earth's magnetic field, *Symposium on the Application of Geophysics to Engineering and Environmental Problems* Available at <https://doi.org/10.4133/1.3176739> and free at <https://www.researchgate.net/publication/269122724>

References

- Furness, Peter, 2002, The magnetic fields of steel drums, *Journal of Applied Geophysics*, vol. 51, no. 2-4, p. 63-74. Available at [https://doi.org/10.1016/S0926-9851\(02\)00211-2](https://doi.org/10.1016/S0926-9851(02)00211-2) and free at <https://repository.geologyscience.ru/server/api/core/bitstreams/84e4aee4-e925-4469-852f-0603f4106b0d/content>
- Furness, Peter, 2007, Modelling magnetic fields due to steel drum accumulations, *Geophysical Prospecting*, vol. 55, p. 737-748. Available at <https://doi.org/10.1111/j.1365-2478.2007.00635.x>
- Gains, W. Craig, 2008, *Encyclopedia of civil war shipwrecks*, 265-page book from the Louisiana State University Press. Available at <https://lsupress.org/9780807134245/encyclopedia-of-civil-war-shipwrecks/> and free at <https://archive.org/details/encyclopediaofcivilwarshipwrecks>
- Gay, S. Parker, Jr., 2004, Glacial till: A troublesome source of near-surface magnetic anomalies, *The Leading Edge*, p. 542-547. Available at DOI:10.1190/1.1766241k and free at <https://watermark02.silverchair.com/1.1766241.pdf> and at <https://www.researchgate.net/publication/249866984>
- Ghirotto, A., A. Zunino, E. Armadillo, and K. Mosegaard, 2021. Magnetic anomalies caused by 2D polygonal structures with uniform arbitrary polarization: New insights from analytical / numerical comparison among available algorithm formulations, *Geophysical Research Letters*, vol. 48, e2020GL091732. Available at <https://doi.org/10.1029/2020GL091732> and free at https://essopenarchive.org/users/550578/articles/604039/master/file/data/ghirotto_et_al-2020-grl-supporting_information/ghirotto_et_al-2020-grl-supporting_information.docx
- Grant, F.S., 1984, *Aeromagnetics, geology and ore environments*, I. Magnetite in igneous, sedimentary and metamorphic rocks: An overview. *Geoexploration*, vol. 23, p. 303-333. Available at [https://doi.org/10.1016/0016-7142\(85\)90001-8](https://doi.org/10.1016/0016-7142(85)90001-8)
- Hassan, H.H., J.W. Peirce, W.C. Pearson, and M.J. Pearson, 1998, Cultural editing of HRAM data: Comparison of techniques, *Canadian Journal of Exploration Geophysics*, vol. 34, no. 1 and 2, p. 16-22. Free at <https://www.terraquest.ca/FileServer/sites/260/resources/Cultural-Editing-of-Aeromag-Data.pdf>
- Hassan, Hassan H., and John W. Pierce, 2005, SAUCE: A new technique to remove cultural noise from HRAM data, *The Leading Edge*, p. 246-250. Available at

<https://doi.org/10.1190/1.1895307>

Hillan, Dean, and Clive Foss, 2012a, Correction schemes for self-demagnetisation, ASEG Extended Abstracts, 22nd International Geophysical Conference, Brisbane, 4 pages. Available at <https://doi.org/10.1071/ASEG2012ab402>

Hillan, Dean, Clive Foss, James Austin, Phil Schmidt, and Dave Clark, 2012b, Direction to magnetic source analysis of single string of down-hole magnetic tensor data, SEG SEG Technical Program Expanded Abstracts, 5 pages. Available at DOI <http://dx.doi.org/10.1190/segam2012-1130.1> and free at <https://www.academia.edu/87601732>

Hinze, William J., 2022, From compass to drone: The evolving role of magnetics in mapping the geology and ore deposits of the Lake Superior region, Minnesota Geological Survey Open File Reprint OFR-22-8. Free at <https://conservancy.umn.edu/items/c79bf14d-8271-441a-b2f4-4bf15b50c895>

Hodgetts, Lisa, Jean-Francois Millaire, Edward Eastaugh, and Claude Chapdelaine, 2016, The untapped potential of magnetic survey in the identification of precontact archaeological sites in wooded areas, *Advances in Archaeological Practice*, p. 41 - 54. Available at DOI: 10.7183/2326-3768.4.1.41 and free at <https://www.researchgate.net/publication/293011522>

Holt, Peter, 2019, Marine magnetometer processing, 2nd edition, 44-page report from 3H Consulting Ltd. Free at <https://www.3hconsulting.com/Downloads/MagnetometerProcessing.pdf>

James, Mark, and 5 others, 2025, Marine Geophysics, 2nd edition, Historic England. Free at <https://historicengland.org.uk/images-books/publications/marine-geophysics-data-acquisition-processing-interpretation/>

Jones, Virgil Carrington, and Harold L. Peterson, 1971, U.S.S. Cairo, the story of a Civil War gunboat, National Park Service. Free at https://www.nps.gov/parkhistory/online_books/vick/cairo.pdf

Krahenbuhl, Richard, Yaoguo Li, Misac Nabighian, and Kris Davis, 2011, Advanced UXO detection and discrimination using magnetic data based on extended Euler deconvolution and shape Identification through multipole moments, 118-page final report from the Colorado School of Mines. Free at <https://apps.dtic.mil/sti/tr/pdf/ADA548972.pdf>

Krahenbuhl, Richard A., and Yaoguo Li, 2017, Investigation of magnetic inversion methods in

References

highly magnetic environments under strong self-demagnetization effect, *Geophysics*, vol. 82, no. 6, p. J83-J97. Available at 10.1190/GEO2016-0676.1

Kristjansson, L., 1983, Magnetic field measurements near a steel plate, *European Journal of Physics*, p. 48-52. Available at DOI: 10.1088/0143-0807/4/1/011 and free at researchgate.net/publication/230965279

Ladynin, A.V., A.N. Vasilevskii, A.F. Pavlov, and A.A. Popova, 2002, Vector magnetic surveys in iron prospecting, *Russian Geology and Geophysics*, Vol. 43, No. 1, p. 75-85. Free at <https://pubs.geoscienceworld.org/nsu/rgg/article/43/1/75/591132/VECTOR-MAGNETIC-SURVEYS-IN-IRON-PROSPECTING?searchresult=1>

Larson, Timothy H., and F. Terry Norris, 2008, Magnetometer survey for buried steamboats near the mouth of the Missouri River, 21st Symposium on the Application of Geophysics to Engineering and Environmental Problems, p. 515-524. Available at <https://doi.org/10.4133/1.2963307>

Leopold, Luna B., and W. B Langbein, 1966, River meanders, *Scientific American*, p. 60 - 70. Free at: <https://facultyweb.kennesaw.edu/jdirnber/docs/Leopold%20Riv%20Meand%201966.pdf>

Levanto, Arto E., 1963, On magnetic measurements in drill holes, *Geoexploration* Vol. 1, No. 2, p. 8 - 20. Available at [https://doi.org/10.1016/0016-7142\(63\)90009-7](https://doi.org/10.1016/0016-7142(63)90009-7)

Li, Feng, Guo Wenjian, 2016, Analysis on data processing of a three-component magnetic survey in a well, *International Journal of Geology*, vol. 1 no. 1, p. 1-5. Available at doi: 10.18282/IJG.2016.004 and free at <https://www.researchgate.net/publication/319861598>

Liu, Shuang, and Xiangyun Hu, 2017, Inversion and interpretation of magnetic anomaly in the presence of significant remanence and self-demagnetization based on magnetic amplitude, chapter 3, *Intechopen*, Free at <http://dx.doi.org/10.5772/intechopen.71027>

Liu, Shuang, Xiangyun Hu, Tianyou Liu, Jie Feng, Wenli Gao, and Liquan Qiu, 2014, Magnetization vector imaging for borehole magnetic data based on magnitude magnetic anomaly, *Geophysics*, vol. 78, no. 6, p. D429-D444. Available at doi.org/10.1190/GEO2012-0454.1

Macke, Robert J., 2010, Survey of meteorite physical properties density porosity and magnetic susceptibility, Doctoral dissertation, University of Central Florida. Free at

<https://stars.library.ucf.edu/etd/1638>

Mackey, T., K. Lawrie, P. Wilkes, T. Munday, N. Kovacs, R. Chan, D. Gibson, C. Chartres, and R. Evans, 2000. Palaeochannels near West Wyalong, New South Wales: A case study in delineation and modelling using aeromagnetics. *Exploration Geophysics*, Vol. 31, p. 1-7. Available at DOI:10.1071/EG00001

Marchetti, Marco, Vincenzo Sapia, and Alessandro Settimi, 2013, *Annals of Geophysics*, vol. 56, no. 1, p. 1-12. Available at doi:10.4401/ag-6201 and free at <https://www.researchgate.net/publication/236268721>

Mason, Randall J., 1984, An unorthodox magnetic survey of a large forested historic site, *Historical Archaeology*, vol. 18, p.54 - 63. Free at <https://www.jstor.org/stable/25615497>

McFee, John E., Yodadhish Das, and Robert O. Ellingson, 1960, Locating and identifying compact ferrous objects, *IEEE Transactions on Geoscience and Remote Sensing*, vol. 28, no. 2, p.182-193. Available at <https://ieeexplore.ieee.org/document/46697> and free at <https://www.researchgate.net/profile/John-Mcfee/publication/3200668>

McFee, John E., Robert Ellingson, and Yogadhish Das, 1993, Experimental study of location and identification of ferrous spheroids using a "smart" total field magnetometer, 110-page report from the Defence Research Establishment Suffield. Free at <https://apps.dtic.mil/sti/html/tr/ADA263661/index.html>

Muszala, Stefan, Paul L. Stoffa, and L. A. Lawver, 2001, An application for removing cultural noise from aeromagnetic data, *Geophysics*, vol. 66 no. 1, p. 213-219. Available at <https://doi.org/10.1190/1.1444897>

Parasnis, D.S., 1966, *Mining geophysics*, Elsevier.

Pearce, J. G., 1945, *Cast iron in building*, George Allen and Unwin Ltd. Free at archive.org.

Phillips, Jeffrey D., 2007, Geosoft eXecutables (GXs) Developed by the U.S. Geological Survey, Version 2.0, with notes on GX development from Fortran code, 118-page Open-File Report 2007-1355. Free at <https://pubs.usgs.gov/of/2007/1355/>

Purss, Matthew B. J. and James P. Cull, 2005, A new iterative method for computing the magnetic field at high magnetic susceptibilities, *Geophysics*, vol. 70, no. 5, p. L53-L62. Available at: 10.1190/1.2052469

References

- Rambabu, H. V, and G. D. J. Sivakumar Sinha, 1986, Magnetic anomalies over thin plates and their analysis, *Proceedings of the Indian Academy of Science*, Vol. 95, No. 3, p. 331-341. Free at <https://www.ias.ac.in/article/fulltext/jess/095/03/0331-0341>
- Ravat, Dhananjay, 1996, Magnetic properties of unruled steel drums from laboratory and field-magnetic measurements, *Geophysics*, vol. 61, no. 5, p. 1325-1335. Available at DOI:<https://doi.org/10.1190/1.1444056>
- Saltus, Richard W., and Richard J. Blakely, 2011, Unique geologic insights from non-unique gravity and magnetic interpretation, *GSA Today*, vol. 21, p.4-11. Available at doi:10.1130/G136A.1
- Sampson, Christina Perry, and Timothy J. Horsley, 2020, Using multistaged magnetic survey and excavation to assess community settlement organization: A case study from the central peninsular Gulf Coast of Florida, *Advances in Archaeological Practice*, vol. 8, no. 1, p. 53 - 64. Available at DOI:10.1017/aap.2019.45
- Scheiblecker, Marion, 2021, Can magnetic directions of kilns help us to distinguish settlement phases?, *Archaeosciences*, 45-1, 5 pages. Free at <https://www.cairn.info/revue-archeosciences-2021-1-page-201.htm>
- Schenck, Helen, 1978, Archaeological prospecting at Valley Forge, *MASCA Newsletter*, Museum Applied Science Center for Archaeology, University Museum, University of Pennsylvania December, p. 16-17.
- Schlinger, Charles M., 1990, Magnetometer and gradiometer surveys for detection of underground storage tanks., *Bulletin of the Association of Engineering Geologists*, vol. 27, no. 1, p. 37-50. Free at <https://www.geometrics.com/wp-content/uploads/2018/10/M-TR3.pdf>
- Schnetzler, C.C., and P.T. Taylor, 1984, Evaluation of an observational method for estimation of remanent magnetization, *Geophysics*, vol. 49, nno. 3, p. 282-290. Available at DOI:10.1190/1.1441660 and free at <https://watermark02.silverchair.com/282.pdf>
- Silva, Joao B. C., and Gerald W. Hohmann, 1981, Interpretation of three-component borehole magnetometer data, *Geophysics*, vol. 46, no. 12, p. 1638 - 1748. Available at <https://library.seg.org/doi/pdf/10.1190/1.1441179>
- Simms, Janet E. and Paul E. Albertson, 2000, Multidisciplined investigation to locate the Kentucky shipwreck, *Geoarchaeology*, vol. 15, no. 5, p. 441-468. Available at [https://doi.org/10.1002/\(SICI\)1520-6548\(200006\)15:5<441::AID-GEA3>3.0.CO;2-8](https://doi.org/10.1002/(SICI)1520-6548(200006)15:5<441::AID-GEA3>3.0.CO;2-8)

Smekalova, Tatyana N., and Bruce W. Bevan, 1993, A geophysical test at Scythian Neapolis, a 120-page report prepared for Prince Hans-Werner von Sachsen-Altenburg from St. Petersburg State University and Geosight Free at <http://core.tdar.org/document/381117> and at <https://www.researchgate.net/publication/305723529>

Smekalova, Tatiana N., 2006, Geomorphological and geophysical survey on the archaeological site at Dime, Fayyum, Egypt, a 12-page report prepared for Mario Capasso and Paola Davoli, Soknopaiou Project, Università degli Studi di Lecce, Italy, by the St. Petersburg State University, Russia. The survey is also described in a 24-page report: Geophysical survey at Dime, Fayyum, Egypt, November, 8-18, 2006, also prepared for the project leaders. Summary available at https://doi.org/10.1007/978-3-319-01784-6_7

Smekalova, Tatiana, and Bruce Bevan, 2009, A geophysical evaluation of Avaldsnes, a 69-page report prepared for Dagfinn Skre (University of Oslo) from the Moesgaard Museum and Geosight . Free at <https://www.khm.uio.no/forskning/prosjekter/avaldsnes/dokumenter/forprosjekt-rapporter/2009-smekalove-bevan.pdf> and at <https://www.academia.edu/31116811> and at <http://core.tdar.org/document/381142>

Smekalova, Tatiana, and Bruce Bevan, 2015, A magnetic survey at Eltigen 4, 12-page report prepared for Mark Kotin. Free at <https://www.researchgate.net/publication/374228034>

Smekalova T.N., Belik Yu.L. 2016, A.V. Suvorov and the annexation of Crimea to Russia, History of forgotten fortresses, St. Petersburg, Aleteya Publ. 2016. (Materials for the archaeological map of Crimea, vol. XVI).

Смекалова Т. Н., Белик Ю. Л., 2016, А. В. Суворов и присоединение Крыма к России. История забытых крепостей. – СПб.: Алетея, 2016. – 228 с. (Материалы к археологической карте Крыма. Вып. XVI).

Smekalova, T.N., A.G. Gertsen, A.S. Devayev, Yu.L. Belik, A.N. Gavriluk, L.L. Leonov, A.V. Antipenko, 2022, Archaeological and geophysical studies of the Salgir retrenchment, the first Russian fortress in the Crimea, Journal of Historical, Philological and Cultural Studies
Смекалова Т.Н., Герцен А.Г., Деваев А.С., Белик Ю.Л., Гаврилюк А.Н., Леонов Л.Л., Антипенко А.В. Салгирский ретраншемент: локализация и междисциплинарные исследования первой русской крепости в Крыму // ПИФК. 2022. № 3. С. 78–94.

Smekalova, T.N., A.S. Devayev, A.G. Gertsen, and A.N. Gavriluk, 2023, Current investigation of Salgir earthworks: Excavations of the artillery cellar with cannonballs, Journal of Historical, Philological and Cultural Studies, no. 4, pp. 178 - 188. (in Russian with an abstract and figure captions in English)

Смекалова Т.Н., Деваев А.С., Герцен А.Г., Гаврилюк А.Н. Новые исследования Салгирского фельдшанца: раскопки артиллерийского погреба с пушечными ядрами // Проблемы истории, филологии, культуры (ПИФК). 2023. № 4. С. 178–188.

References

- Sowerbutts, W.C., 1988, The use of geophysical methods to locate joints in underground metal pipelines, *Quarterly Journal of Engineering Geology*, vol. 21, p. 273-281. Available at <https://www.lyellcollection.org/doi/abs/10.1144/GSL.QJEG.1988.021.03.02?download=true>
- Stanley, John M., 1992, Search for the 'Mahogany ship', *Preview* (ASEG magazine), issue 37, p. 8-9.
- Swain, Er. Mayadhar, 2021, Iron pillars of India, *Odisha Review*, August, p. 26-29. Free at https://www.academia.edu/50944588/Iron_Pilars_of_India
- Therriault, Ann, M., Richard A.F. Grieve, and Mark Pilkington, 2002, The recognition of terrestrial impact structures, *Bulletin of the Czech Geological Survey*, Vol. 77, No. 4, p. 253-263. Free at <http://www.geology.cz/bulletin/fulltext/02therriaultfinal.pdf>
- Tyagi, S., and W.E. Lord, Jr., 1983, Use of a proton precession magnetometer to detect buried drums in sandy soil, *Journal of Hazardous Materials*, vol. 8, p. 22-23. Free at <https://www.geometrics.com/wp-content/uploads/2018/10/M-TR1.pdf>
- Uehara, Minoru, and Jerome Gattacceca, 2023, The Meteorite meter: A handheld instrument for the combined measurement of magnetic susceptibility and electrical conductivity, with application to meteorite identification and classification, *Meteoritics and Planetary Science*, vol. 58, p.1629-1641. Available at <https://onlinelibrary.wiley.com/doi/pdf/10.1111/maps.14087> and free at <https://hal.science/hal-04248767v1>
- Vauban, Sebastien Le Prestre de, 1737, *De l'attaque et de la defense des places*, A La Haye : Chez Pierre de Hondt. Free at archive.org
- Vervelidou, Foteini, Benjamin P. Weiss, and France Lagroix, 2023, Hand magnets and the destruction of ancient meteorite magnetism, *Journal of Geophysical Research: Planets*, vol. 128, e2022JE007464. Free at <https://doi.org/10.1029/2022JE007464>.
- Wang, Chuanlei, Zan Qu, Mingsong Qi and Bo Shen, 2006, The magnetic detection of sunken ships in the Madang section of the Yangtze River, *Journal of Environmental and Engineering Geophysics*, vol. 11, no. 2, p. 123-131. Available at <https://doi.org/10.2113/JEEG11.2.123>
- Watermann, J. and J. Lam, 1999, Distributions of magnetic field variations, differences and residuals, 84-page report SACLANTCEN SR-304 from the SACLANT Undersea Research Centre. Free at <https://apps.dtic.mil/sti/pdfs/AD1113041.pdf>

Weiss, Eyal, Boris Ginzburg, Tsurriel Ram Cohen, Hovav Zafrir, Roger Alimi, Nizan Salomonski, and Jacob Sharvit, 2007, High resolution marine magnetic survey of shallow water littoral area, *Sensors* 2007, vol. 7, p. 1697-1712. Free at <https://doi.org/10.3390/s7091697>

Witten, Alan, 2003, An eventful semester teaching field geophysics, *The Leading Edge*, July, p. 616-620. Available at DOI: 10.1190/1.1885523

Wynn, J.C., 2002, Mapping an iron-meteorite impact site with a magnetometer, and implications for the probability of a catastrophic impact on Earth, *Journal of Environmental and Engineering Geophysics*, vol. 7, no.4, p. 143 - 150. Available at <https://pubs.geoscienceworld.org/eegs/jeeeg/article/7/4/143/655054> and free at <https://www.researchgate.net/publication/250377110>

Ziegler, Robert J. (editor), 2001, Historical archaeology at locality 6 of the Fort Ellsworth site (14EW26), 394-page report, U.S. Army Corps of Engineers, Kansas City District. Free at <https://apps.dtic.mil/sti/tr/pdf/ADA409515.pdf>

details Figure 0: This photo was taken on 26 September 2009 by Marit Synnove Veia (Nordvegen Historic Center). Further information about this survey can be found in a 69-page geophysical report: A geophysical evaluation of Avaldsnes, prepared for Dagfinn Skre (University of Oslo) by Tatiana Smekalova (Moesgaard Museum) and Bruce Bevan (Geosight). If one wished to eliminate the broad-area caused by the ships, a magnetic gradiometer could be applied.

details Figure 1: Earthen contrasts are likely to be less magnetic than random brick.

details Figure 2: The estimate from Breiner (1973, p. 42) is from his monograph; the estimate Navy, noted with green text, is for a modern navy ship (Watermann and Lam 1999, p. 8). Note that all of these moments are the sum of both induced and remanent magnetization, and those values have been divided by the mass of the object. Most of these measurements are from Bevan (2002a). A valuable collection of many magnetic measurements on modern steel is found in Ravat (1996). Rough averages from the analyses of the dozens of magnetic maps that were modeled with magnetic dipoles yielded a relative remanent moment of $130 \text{ mAm}^2/\text{kg}$ and induced moment of $420 \text{ mAm}^2/\text{kg}$, for a Q ratio of 0.31. The density of these artifacts was measured for only four items: 18th century iron (5900, 6600, and 6100 kg/m^3) and medieval nail (5240 kg/m^3). The 18th century cannonballs were found at the Salgir fort in Crimea; one typical ball (5.5 kg) had $m_r = 9.12 \text{ mAm}^2$ and $m_i = 94.2 \text{ mAm}^2$; this was determined by rotating it near a magnetic sensor. The hat wire had a mass of 6.2 g; this circled the perimeter of the hat and allowed it to remain rigid; this wire had the following magnetic moments: induced = 1.72 mAm^2 and remanent = 2.34 mAm^2 . The possible medieval iron bar is analyzed in [Figure 10](#).

details Figure 3: The Magnaprobe is a simple tool for approximating the direction of the magnetic field near any strongly-magnetic object. This instrument is available for sale at several sites that are listed on the internet. Note that the red-blue magnet can change its angle of inclination about one white-framed axis, and its angle of declination about the second axis. A plastic bar at the left allows the probe to be held and moved easily. As shown here, the red side of the magnet dips down toward the north, like a three-dimensional compass. In this illustration, the magnetic probe and the compass are so near that they affect each other. The steel rod at the upper right is 8 cm long; this rod has primarily remanent magnetization. At the lower left, the broken head of a hammer has primarily induced magnetization; the fractured end of the broken hammer is apparent by its granular appearance. The diameter of the hammer head is 3 cm. If an object has both induced and remanent magnetization, it may be more difficult to test. The magnetic properties of this hammer fragment, and also the steel rod, were measured and are described in a later section titled [Measuring and calculating magnetic parameters](#).

details Figure 4: A photograph of the hammer head that was tested is seen in [Figure 3](#); this shows that the front part of the hammer head broke from the rear end, leaving a very rough surface and a rather compact mass of iron. No special care was made to keep the head stationary for a period of a few hours before moving it close to the magnetic sensor in a

different orientation. The fluxgate sensor was so close to the hammer head that only a slight movement would create a large change in the magnetic reading. The possibility of magnetic viscosity from the nearby house was not tested. The Earth's magnetic field at the test site was about 50,600 nT. Earlier evidence of magnetic viscosity was detected during some magnetic measurements at the prehistoric site of Hopeton in the central US state of Ohio (Bevan 2006, Fig. 18). Archaeological work in a section of a trench at the site was protected from the sun and rain by a moveable roof framed with steel pipes and covered with sheet plastic; the mass of steel was probably about 70 kg. This steel frame was moved to a distance of perhaps 5 m about an hour before magnetic measurements were made in the trench. During a period of 4 minutes, while the frame remained stationary, the magnetic measurements increased by about 100 nT. This rise is likely caused by magnetic viscosity.

details Figure 5: This survey was done on 12 November 2006 with a Gem Systems model GSM-19WG Overhauser magnetometer. A second Gem magnetometer was a base station that corrected temporal changes in the spatial readings. Measurements were made along north-south lines that were spaced by 0.5 m. The interval between readings on each line was 0.2 s and about 0.25 m. The ancient settlement was called Soknopaiou Nesos; it is north of Lake Birket Qarun and at coordinate E30.7° N29.5°. This magnetic feature was detected on the western side of the temple; the survey is described by Smekalova (2006). It is not impossible that the doubling of the magnetic low has been created by an error in one magnetic measurement near E115.25 N156.5, but that error is unlikely.

details Figure 6: This sword is very similar to three swords that are seen in a relief from Palmyra that is now in the Louvre. This sword is probably from the first or second century AD. Some or all of these photos may have been taken by Giuseppe Alvar Minaya. The sword was oriented in about a north-south direction, and its point was toward the south. The metal of the knob (pommel) at the northern end of the sword appears to be quite different from the rusty iron of the blade. The soil in these photos is quite sandy. The mass of the cleaned sword is not known. An excellent source of information about steel and ancient swords is found at <https://www.tf.uni-kiel.de/matwis/amat/>

details Figure 7: These models and calculations were made with the Potent program from Geophysical Software Solutions. The horizontal prism has a rectangular cross-section of 0.1 by 0.1 m. The parameters of the Earth's magnetic field and the survey are listed with the map of measurements. The susceptibility values that are listed for models #1 and #3 are the values before demagnetization was applied to the calculation. An approximate correction for demagnetization reduced the susceptibility values as follows: #1 from 4.6 to 1.4 SI; #3 from 8.2 to 1.7 SI. This correction for demagnetization was also applied to those bodies with remanent magnetization. The magnetic moments of the bodies in the three models were:

#1: bar = 1.57 Am², sphere = 0.39 Am²;

#2: bar = 1.95 Am², sphere = 1.09 Am²;

#3: left bar = 2.79 Am², right bar = 0.86 Am²

Based on the finding of the excavation, models #2 and #3 are incorrect (for #2, there were

not two swords), and in #3, the sword did not have a separate object at its middle (the sphere is difficult to see). While the excavation exposed the sword at a depth of 0.8 m, all of these magnetic models suggest that the elongated feature in the magnetic maps (the model of the sword) is at a depth of about 0.4 m, much shallower than the correct value; the cause of this error is not known.

details Figure 8: The conversion to total gradient was made with a GX routine from the US Geological Survey (Phillips 2007). This routine was added to the Oasis montaj viewer from Geosoft. The magnetic model for the sword, on the right, is a magnetic bar that is at a depth of 0.5 m and which is 1 m long and with a cross section of 0.1 by 0.1 m. The total gradient of that model is plotted on the right side of this figure.

details Figure 9: This iron bar was discovered in 1926 during the plowing of a field near the town of Vandel, on Jutland; it is now in the museum at Vandal as specimen number 1998/119-EM3. This bar was probably imported from southern Germany or from Switzerland. Its age is not known. Neither the mass nor the volume of this bar was measured, but its volume can be approximated from a pair of cones whose circles meet at the middle; this volume is 385 cm^3 . This test was coordinated by Olfert Voss (Nationalmuseet in Denmark); this test and other magnetic tests on blocks of Danish iron slag are described in a report (Bevan, Smekalova, and Smekalov 2005). The tri-axial fluxgate magnetometer was a model FGM-5DTAA from Walker Scientific; the magnetic field of three perpendicular components of the Earth's field was measured along the 1-m length of the traversing board at intervals of 2 mm and 57 ms. A small computer controlled the magnetometer, but it is not shown in the figure. The total field, inclination, and declination were calculated from the three magnetic components (in the X, Y, and Z directions, or East, North, and Up) of the total field. The adjacent concrete blocks were not magnetic.

details Figure 10: Since the amplitude of the anomaly was huge, no base station was needed. Vectorial magnetic measurements are seldom done; this is because of the high sensitivity of the readings to the rotation of the magnetic sensor; note that the inclination and declination are noisier than the total field. However, the L-shaped cross-section of the traversing board defined the line of measurement and minimized angular rotation of the sensor. The computer that controlled the measurements gave audible beeps at intervals when 10-cm points were to be passed; this allowed good accuracy in locations. While it was easy to make an accurate profile along one line of measurement, it would be more difficult to orient the sensor on multiple parallel lines if a magnetic map was wished. These vector magnetic measurements are similar to magnetic measurements in a borehole, and several articles provide a good summary of procedures: Hillan, Foss, Austin, Schmidt, and Clark (2012b) illustrate how the technical measurement of the magnetic gradient tensor may assist with locating a magnetic body near a bored hole. Li and Wenjian (2016) show how three-component magnetic data may be plotted to show the amplitude and direction of the magnetic field along the line of measurement. A method for estimating the direction of magnetization of a feature near a bored hole was explained by Liu +5, (2014). Ladynin (+3,

2002) show how a vectorial analysis may aid a search for iron ore. A graphical display of magnetization in a bored hole has been shown by Levanto (1963). Silva and Hohmann (1981) show how a prismatic body near a bored hole may be investigated and interpreted with 3-component magnetic data.

details Figure 11: This calculation was done with the MdMagC program (Multi-dipole Magnetic, Constrained); most of the parameters were iterated for a minimum RMS error between the measured and calculated fields. The model has a line of 8 dipoles that extend along the middle of the iron block. The magnetic moment of each dipole could vary independently of the other dipoles. While the inclination and declination of each dipole could change, all dipoles were forced to have the same direction as every other dipole. The X and Z locations for each dipole were fixed and did not change during the iterations of the analysis.

details Figure 12: This magnetic model was calculated with the Potent program. While the shape of the model is similar to the bar, it was necessary to reduce the length of the model to a value less than its known length. An approximate correction for demagnetization has been made.

details Figure 13: This magnetic survey and its findings are described in a pair of publications (Smekalova +6, 2022; and Smekalova, Devayev, Gertsen, and Gavriluk 2023). The total-field magnetic survey was done with a Gem Systems model GSM-19 Overhauser magnetometer during the month of October, in 2021. Traverses were made in grid east-west directions with a line spacing of 1 m; along each traverse the measurement spacing was less than 0.5 m. The long and curving bands of anomalies are caused by former meanders of the Salgir River; these will be discussed later in this report. Several years before this Salgir survey, another 18th century fort was also located in Crimea with a geophysical survey and aerial photography (Smekalova, and Belik 2016). This magnetic map, along with the magnetic measurements that are plotted in [Figure 22](#), were made with the expert assistance of Sergei Fridrikhson (on the staff of the Vernadsky Crimean Federal University).

details Figure 14: This is a localized anomaly, for there are only a few weak anomalies near the major anomalies. This is fortunate, for it simplifies the analysis.

details Figure 15: This map has also been extracted from [Figure 13](#). Hachures mark contour lines that enclose low readings in this map. One likely dipolar pair does not have a high / low ratio listed in this figure; this is because the amplitude of the high cannot reliably be determined. The Pdyke program from Geophysical Software Solutions was applied to the calculation of the ratio of the magnetic high to the low of a 1-m cube with it top at a depth of 1 m; its susceptibility was set to 0.01 (SI). The magnetic field of the Earth was assumed to be 49,871 nT at an inclination of 63.5°. The calculation finds a peak high of 19.2 nT and a low of -2.9 nT; this ratio (6.6) is expected if there is only induced magnetization. In order to make the high / low ratio about 1 (an average of the measurements), it would be necessary to reduce the inclination of the Earth's magnetic field from its actual value of 63° to about 28°.

details Figure 16: This analysis was made with the Potent program from Geophysical

Software Solutions. The parameters of the bodies that resulted from this analysis were as follows:

body #	type	susceptibility SI	depth m	volume m ³	moment Am ²
1	disk	0.297	1.32	1.66	19.47
2	sphere	0.24	0.62	0.52	4.97
3	ellipsoid	0.29	0.98	0.53	6.08
4	sphere	0.040	0.09	0.52	0.82
5	sphere	0.44	0.89	0.52	9.06

The polygonal disk #1 has a thickness of 0.15 m; depths are to the top of each body.

details Figure 17: The parameters of these bodies are as follows:

body	type	intensity A/m	depth m	volume m ³	moment Am ²	inclination degrees
1	disk	10	0.97	1.66	16.6	32
2	sphere	9	0.56	0.52	4.71	37
3	ellipsoid	38	1.43	0.53	20.18	10
4	sphere	10	0.65	0.52	5.24	67
5	sphere	19	0.77	0.52	9.96	13

This table lists the intensity of magnetization of each body, its depth and volume, magnetic moment, and its magnetic inclination angle. The disk (body #1) is a polygonal slab that is horizontal and has a thickness of 0.15 m. The ellipsoid has a length of 2 m, a width of 1 m, and a height of 0.5 m. Depths are to the tops of bodies.

details Figure 18: This archaeological excavation was made in 2022. Squared stones locate some of the walls of the powder magazine (also called an artillery cellar). Colors mark different clusters of cannon balls; these clusters are numbered 1 - 4 (and cluster 4 has three adjacent groups). The major masses and quantities of cannon balls were as follows: A total of 216 six-pound shells were distributed among the clusters; the average mass of each was 2.28 kg. A total of 286 cannon balls were twelve-pound solid shot; almost all of these were found in cluster #3 and each had a mass of about 5.4 kg. The total mass of the cannon balls in cluster 3 was 1620 kg. The density of a solid shot cannon ball was found to be 6.8 g/cm³; pure iron has a density of 7.9 g/cm³. At the time of this fort, the mass of each cannon ball was usually described world-wide with a British convention and weight was specified in pounds (see <https://www.arc.id.au/Cannonballs.html>),

details Figure 19: Powder magazines were constructed for the storage of military

projectiles. It was most important to protect explosives that could be ignited by an opponent. For this reason, powder magazines were usually underground, and each had a thick layer of soil on its roof to prevent explosions inside the powder magazine. Rotate this map by about 180° to match its orientation in the other maps here. The north direction marked on this map appears to be true north. At the time that this map was drawn, magnetic north was 10° West of true north. At the time of the magnetic survey, magnetic north was 8° East of true north. The historical values for magnetic declination were found at the web site:

<https://www.ncei.noaa.gov/maps/historical-declination/> The text with this map is in Russian, although it has Latin letters for the labels in the legend. A cross-section at the lower right side of the map indicates the shapes of parapets and trenches at the sides of the fort. This fort at the Salgir River has similarities to Fort Morton at the USA Civil War (1864) battlefield at Petersburg, in the eastern state of Virginia. The earthwork of Fort Morton was leveled after the war and that fort is also invisible at the surface. Like Salgir, there is an excellent map of Fort Morton. In Virginia, the two powder magazines were detected with a deep-exploring (2 m) conductivity meter, a model EM31 from Geonics, rather than with a magnetic survey (at Fort Salgir). While it was the cannon balls at Salgir that allowed its location and identification, it was the base of filled trenches and pits (profiled with a ground-penetrating radar) at Petersburg that defined the location of that fort (Bevan 2004a, Fig. B133). It is possible that some of the buildings that are shown inside the Salgir fort were detected by the magnetic survey in [Figure 13](#); these may be investigated at a future time. It appears that this Salgir fort was never attacked or involved in a battle.

details Figure 20: North is parallel to the sides of this photograph from Google Earth. The green line shows the perimeter of the magnetic survey. The ridge of the earthwork was not revealed by the magnetic survey. If the #2 powder magazine was placed at the magnetic anomaly, the western side of the fort would have the Salgir River flowing through it. The northwestern bastion of the fort extends into a slight bend in the river; this may be a coincidence or perhaps it was deliberate. By comparison with the magnetic map ([Figure 13](#)), it is seen that some of the old river channels or meanders are faintly visible here as light-toned bands. However, no trace of the early fort can be seen in this photograph. The Salgir is the longest river in Crimea; it begins in the mountains south of Simferopol and ends near the Sea of Azov. Trees are seen growing next to the Salgir River. Traces of farming are apparent in two fields as lines that extend toward the upper right; plowing has probably been the major reason that the shape of the fort's earthwork has been lost.

details Figure 21: The stones that were also exposed are not located here. Since some of the clusters extend to the edge of the excavation, it is reasonable that some additional cannon balls remain in unexcavated soil. Some of the clusters contain more than one type of cannon ball, as a shot or a shell; therefore, a comparison between total mass and the number of balls may differ from one cluster to another. The counts and masses here are approximate.

details Figure 21a: This figure is a combination of [Figure 14](#) and [Figure 21](#). Cluster #3

is located between the peak of the strongest magnetic high and a magnetic low that is toward the north.

details Figure 22: The magnetic parameters are calculated as follows (Bevan 2002a, Fig. C40):

Remanent magnetic moment, $Am^2 = mr = r^3 (Bh - BI) / 400$

Induced magnetic moment, $Am^2 = mi = r^3 (Bh + BI) / 400$

The line between the two centers (ball and sensor) was in the same direction of the Earth's magnetic field. The induced magnetization of the ball causes the magnetic readings to rise from 49,751 nT to midway between the red and blue line. There is a puzzling change in the temporal noisiness of the readings when the cannon ball was near the magnetic sensor. It has a period of about 0.8 s ; the cause of this is not known, but it has no serious effect on the magnetic parameters. The parameters of another projectile were as follows: A 6-pound grenade or hollow shell had $mr = 3.3 \text{ mAm}^2$, $mi = 48.5 \text{ mAm}^2$, and mass = 2.5 kg.

details Figure 23: The magnetic moments that were assumed (90 and 9 mAm^2) were about those of a solid cannon ball from the Salgir fort. The central depth for each ball was 0.3 m below the calculation surface; the center-to-center spacing between balls was 0.2 m. The directions of remanent magnetization were randomly distributed over a sphere; there are infinitely many different random magnetic maps that are as likely as this example. The map of total magnetization (the vectorial sum of the induced and remanent magnetization here) would be very similar to the map of induced magnetization; there would only be small shifts of the contour lines, by about 20% of the spacing between the lines. The Earth's magnetic field was 49,700 nT at an inclination of 64° and a declination of 52° . Calculations that are similar to this are found in another report (Bevan 2006, Fig. 30).

details Figure 24: The clusters of cannon balls are indicated with black polygonal lines; these differ from the oval contour lines of the magnetic anomaly. As the inclination angle increases, magnetic highs become closer to the centers of the magnetic features.

details Figure 25: These calculations were done with the Potent program. Note that the polygonal disks are not centered over the magnetic highs. The separated parts of cluster #3 are each outlined with a brown color. The magnetic moment of 37Am^2 also includes the magnetic effect of cannon balls that remain unexcavated and outside the area of the excavation. Therefore, the average magnetic moment per unit of mass for the balls should be less than $17 \text{ mAm}^2/\text{kg}$.

details Figure 26: One could make a further analysis of the residuals and estimate the location and mass of iron that remains.

details Figure 27: The magnetic measurements in the upper panel have been extracted from [Figure 13](#). At a contour interval of 1 nT, the map shows high spatial noisiness. This was reduced by averaging the 61 lines of measurement that cross this part of the meander in a left-right orientation. The black line in the lower graph is a plot of those averages. The measurements have been approximated by the calculated magnetic anomaly of two simple prismatic features. While the shallow and triangular cross-section is more

reasonable, both calculated curves are similar, and the measurements themselves cannot indicate the best magnetic model. The magnetic moment per unit of length (perpendicular to the page) for the triangular feature is $0.12 \text{ Am}^2/\text{m}$; it is $0.21 \text{ Am}^2/\text{m}$ for the 4-sided feature (this is greater because it is deeper). These 2-D models and calculations were made with aid of the Mag2dc program from Gordon Cooper (University of Witwatersrand). This graph shows that two quite-different magnetic models can give almost the same calculated magnetic field; in geophysics, this is called non-uniqueness (Saltus and Blakely 2011) and it must always be remembered. Perhaps a supplemental survey, such as a resistivity sounding or pseudosection, could determine which model describes what is actually underground. The possible range of depths is even greater than shown by the two models in this figure: The source may instead be a very thin layer that is very close to the surface; it may also be a very small magnetic feature at a depth of as much as 5 m. The interpreter must decide which the most-reasonable solution. The antiquity of the paleochannels in [Figure 13](#) is not known. At this site, the Salgir River is 1.5 - 2 m below the level of the fort. It is quite possible that the river has risen more than 2 m during floods, and the river may have then shifted its channel, even in historic periods.

details Figure 28: Each of the strongest anomalies along the river meander was approximated by the calculated anomaly of a spherical object; this analysis was done with the Potent program. If these were iron objects (with a relative magnetic moment of $0.017 \text{ Am}^2/\text{kg}$), their average mass would be 31 kg. However, the directions of total magnetization of these objects are usually far from the direction of the Earth's magnetic field. This suggests that these objects have a strong remanent magnetization and are more likely to be modern steel than old iron. If they were modern steel, their average mass might be about 3 kg.

details Figure 29: The contour interval and its range are the same in both the measured and the calculated maps. The magnetic high is 2763 nT, and the low to the north has an amplitude of -397 nT. The magnetic model is a monopole with a strength of -193.4 Am at E526.1, S144.8 and at a depth of 1.9 m (to the top of the feature) . A dipole model is inferior to this monopole. A vertical feature that is relatively thin (in depth extent, like a slab or plate) can have a dipolar anomaly; as the thickness (or bottom depth) of the feature becomes larger, the anomaly slowly changes from a dipole to a bipole and then to a monopole. The magnetic survey was done with a Gem GSM-19FG Overhauser magnetometer at a sensor height of 0.8 m in June 1992. A proton magnetometer was a base station. Traverses went east-west and the spacing between readings was 2.5 ft (0.76 m). This well was readily detected with conductivity measurements (Geonics EM38 and EM31), resistivity, and also with ground-penetrating radar. Self-potential (SP) measurements detected this well as an anomaly of -20 mV. An interpretation of those SP readings gives an estimate that the iron in the well is rusting at a rate of 0.13 kg / year (possibly part of this SP anomaly is caused by percolation of water into the well). The magnetometer detects the upper and lower ends of the magnetic matter in the well; the upper end is so close that it is detected strongly; however, the lower end is so far away that its weak anomaly is hidden by

the strong anomaly of the upper end. Further information about this survey is found in Bevan (2004a, Fig. B167).

details Figure 30: These measurements were made with a Suunto model KB-14 compass (which can be read to a precision of 0.1°). The survey was done in October 1992 and the compass was supported on a wooden rod. The magnetic model for the calculated anomaly is the same monopole that was created for [Figure 29](#). The difference between the calculated and measured curves may indicate a calibration error in the compass. This test is also described in Bevan (2004a, Fig. B20).

details Figure 31: This is a plot of the calculated directions from [Figure 30](#). The deflection angles are small, so they have been magnified here.

details Figure 32: This magnetic survey was done on 20-21 July 1987 with a Scintrex model MP-2 proton magnetometer. Measurement traverses were made in E-W directions. While the temporal change in the Earth's magnetic field was recorded, this map has not been corrected for that shift, for it was only 1 - 2 nT during the measurements on each line. The Earth's magnetic field at this site was about 54,950 nT at an inclination of 70° . Paired high and low anomalies can be recognized by their high lateral gradient (a close spacing of the contour lines) between the high and the low; there are perhaps two additional locations in this map where a magnetic high and low may be paired. The field work of this survey was done by Susan Fry, John and Cari Ravenhorst, and also John Thompson. This survey is described in a report by Bevan (1987). While a technical interpretation was not made, it appears that there could be over 500 kg of iron buried in this area.

details Figure 33: The authors mention that the map in their Fig. 4 shows their original measurements after they have been reduced-to-the-pole (RTP). Therefore, it is not known why there is such a distinct magnetic low on only one side of the magnetic high. However, even if the measurements were not completely converted to an RTP map, the analysis should allow a good estimate of the magnetic moment; this is because the inclination and declination of the intensity of magnetization will correct for an incomplete RTP conversion. This magnetic map was calculated with the Potent program.

details Figure 34: This building was at 101-111 Arch Street in downtown Philadelphia. This photograph is from the Philadelphia Historic Preservation Corporation. The dry reservoir where the facade was stored was in Fairmount Park (near the new Robin Hood Dell) on George's Hill. For more information on buildings that are like this, see "Cast-iron architecture" at Wikipedia, and an old book such as Pierce (1945) or Birkmire (1892).

details Figure 35: The magnetic survey was done with a Varian model 49-544 cesium magnetometer. Because of the huge amplitude of the magnetic anomaly, no magnetic base station was needed. The survey was done on 4 October 1980 by Diana Bermingham, Helen Schenck, and Michael Parrington, from the Museum Applied Science Center for Archaeology at the University of Pennsylvania. An initial reconnaissance of 2 hectares with the method of free search found only one location with a broad anomaly having a high amplitude. After the four corners of the survey grid were accurately located around that anomaly, measurements

were made at intervals of 2 m (as estimated by pacing) along lines of traverse that went alternately to the east and west. There is uncertainty about the background magnetic field, for the magnetic readings in the survey grid were high and irregular; the value for the Earth's field from IGRF version 13 (55,600 nT) was assumed for the analysis. This exploration is described in a report (Bevan 1980). This calculated anomaly was generated with the Potent program. Since the actual source of this anomaly is not important, no detailed magnetic model has been created.

details Figure 36: This magnetic survey was done in April 1992; the magnetic sensor was high (at 2.4 m) and the measurement spacing was wide (at 3 m) so that a large area could be explored quickly. An excavation at this anomaly found the trash to have a thickness of 0.75 m and a depth of 0.15 m; both are similar to the estimate from this magnetic model. Note that the magnetic low of the calculation is weaker than that of the measurements. This suggests that the iron was not magnetized exactly in the direction of the Earth's magnetic field. While remanent magnetization may cause this, it is also possible that self-demagnetization has reduced the direction from the Earth's inclination of 68° to a shallower angle of about 50° ; this result was found when the analysis with the Potent program allowed the direction of total magnetization to be changed for the best match between the measurements and calculations.

details Figure 37: These magnetic measurements were made on 14 December 2001 with a total-field Geometrics model G-858G cesium magnetometer operated in difference mode, with the upper sensor directly above the lower sensor and both were carried on a two-wheeled cart. Traverses went east-west and measurements were made at intervals of about 0.5 ft (0.12 m); the separation between parallel lines of traverse was 2 ft (0.6 m) (Bevan 2002b, Fig. 16). The Earth's field at this site was 52,300 nT at an inclination of 66.1° ; magnetic north is about 11° west of grid north. Divide the difference readings of this map by 1.13 to get the vertical gradient in nT/m. The current soil surface in this area is smooth because of the "no till" farming in this field; the soil is not now plowed for each new crop. The rather linear magnetic anomalies near the southwest corner of the figure are caused by the filled trenches of a sewage drainage field.

details Figure 38: This is a Lambert azimuthal equal-area projection. Each of the directions is that of a best-fitting dipole whose calculated anomaly matches the measurements in a small rectangular area in [Figure 37](#). Many anomalies are fit poorly by a dipole, and the error of their directions will be larger than wished. However, since so many anomalies are analyzed, the general trend of the pattern is probably accurate. This figure has been modified from Bevan (2002b, Fig. 76), and a different version is found in Bevan (2009). Further information about the interpretation of directions of magnetizations like this are found in that article, and its idea is from Schnetzler and Taylor (1984). A publication by Scheiblecker (2021) has noted that the orientations of magnetic anomalies can allow features to be distinguished.

details Figure 39: The magnetic lows were found by watching the readings of a

Scintrex MP-2 proton magnetometer that remained stationary at three different points. The drop in the measurements when a car or truck was passing was noted. It is possible to analyze the magnetic anomaly that is caused by an object that are entirely outside the area of survey. As long as about half of the anomaly is recorded within the area of survey, an analysis can approximate the location, depth, and mass of the object. This test was made in 1981 at an archaeological site in the state of New York, in the USA (Bevan 1981, Fig. 3).

details Figure 40: During magnetic surveys on 23-25 and 27 January, about a dozen trains passed the area of the magnetic survey and all of them caused distinctive drops of 1 - 2 nT in the magnetic field. The amplitude of each drop did not appear to correlate with the length of the train that passed. These surveys were made at the Petersburg National Battlefield in Virginia, USA, as part of a survey there (Bevan 1996, Fig. B27). In the coordinate system of that survey, the magnetic sensor was located at E499 S301, and the ground surface there was elevated about 10 m above the level of the trains, which traveled on an east-west track. Most of the trains were long enough and slow enough that they were detected on more than one measurement at the base station. This plot also shows the typical drop of the Earth's magnetic field near the time of local noon. The A-index at the magnetic observatory near the town of Fredericksburg, Virginia, was 3 (a low value) on this date, and magnetic changes were smoother than usual. The magnetic anomaly of a distant object at about the same elevation as the magnetic measurement is: $B_a = -100 \cdot m / r^3$, where m is the magnetic moment, and r is the distance. The magnetic moment of a passenger car is about 300 Am^2 ; a typical van has a moment of about 700 Am^2 , while the moment of a train may be about 10^5 Am^2 .

details Figure 41: This calculation was made with the Potent program from Geophysical Software Solutions, and the effect of demagnetization has been included. The plane of the calculation ($Z = 0$) is 10 m above the magnetic object; that object has an intensity of magnetization of 6000 A/m, in the direction of the Earth's field. Contours are drawn only in the low amplitude range of -10 to 0 nT; they would be extremely close together in the purple area if they were included there. The peak magnetic high is 35,300 nT directly over the object, the lowest value is -2600 nT at 20 m north of the middle of the sphere.

details Figure 42: This figure is a modification of Fig. B38 in Bevan (1996). The magnetic moment of 1000 Am^2 is about what is caused by a pair of cars.

details Figure 43: The curves are red wherever the angle will result in a positive anomaly; this anomaly reaches a peak of 200 nT. For magnetic lows, a blue line indicates the amplitude at a distance from the center of the circle, where the anomaly drops to -100 nT. This diagram is like a wheel with radial spokes; the magnetic object is at the axle, and magnetic calculations are made around the rim of the wheel. As an example, the magnetic anomaly 1 m north of the object and at the same elevation of the object would be about -100 nT; at an elevation of about 15° , the anomaly would be about 0. The curves will be similar for other locations, where the inclination of the Earth's field is different.

details Figure 44: This anomaly was mapped at Beale Air Force Base in California

(USA). The survey was done in 1989 with a pair of GeoMetrics G-856 proton magnetometers (one was a base station). The measurements were made at intervals of 20 feet (6.1 m) along north-to-south traverses that alternated with south-to-north traverses. Traverse distances were estimated by pacing. The beaded pattern at the southern edge of the plate is perhaps caused by errors in that pacing, for the lateral gradient is very high at that southern edge. The errors in the measurements prevent an accurate analysis of the magnetic map. There is a regular pattern of holes in the plate; these allow rainwater to drain easily. This large plate is constructed from a group of smaller plates that are joined together.

details Figure 45: The magnetic model for the steel plate had a thickness of 0.1 m, when its actual thickness was about 0.02 m. An approximate demagnetization was applied to both calculations; as noted on the left, the actual susceptibility of the steel appears to be about 90 (SI), although demagnetization lowers this to an effective value of 70 (SI). These calculations were made with the Potent program. If the remanent magnetization was strong and its direction was quite different from the direction of the Earth's field, the two maps could be very different. The direction of magnetization in the left map is that of the Earth, while the direction of total magnetization of the model on the right is at a different angle. The magnetic moment of this plate is roughly $300,000 \text{ Am}^2$. Further information about the magnetic anomalies of steel plates has been provided by Kristjansson, (1983); Rambabu and Sivakumar Sinha (1986); Eskola, Jokinen, Soininen, Tervo (1993), and Eskola, Puranen, and Soininen (2001). The analysis of the magnetic field of an iron plate (with reference to the hull of a ship) can be found in a paper by Chadebec +4, (2000).

details Figure 46: This survey was done with a Scintrex MP-2 proton magnetometer; because of the high anomalies, no base station was operated. For the initial mapping shown here, traverses went in an east-west direction. Later, when the initial map revealed the east-west orientation of the tanks, additional measurements were made along north-south lines, and these allowed two of the three tanks to be delineated better; a gradiometer survey would have been better for resolving the three tanks. This survey was done during 2 hours on 13 November 1987 for Albert Depman, and he assisted with the field work. The urban site was at a former gasoline station in an urban setting in the state of Pennsylvania, USA.

details Figure 47: The map in the left panel here is the same as the map on the left in [Figure 48](#). A proper analysis would have only the shell (the outside metal of the drum) magnetic, while the fill of the drum is non-magnetic. If the source is not known to be a magnetic shell, that detailed analysis would not be justified. This analysis was made with the Potent program; an approximate correction was made for demagnetization. The low Q ratio of this object can also be seen in [Figure 48](#): The direction of the remanent magnetization (R) appears to be close to the direction of induced magnetization (I). The drum may be modeled by assuming that both susceptibility and remanent magnetization can be combined to get the total magnetization; these values are 184 A/m for the upright drum and 136 A/m for the upside down drum. Therefore, $I + R = 184$ and $I - R = 136$ which can be solved to $R = 24 \text{ A/m}$ and $I = 160 \text{ A/m}$, for a Q ratio of 0.15, as derived from the analysis with this figure.

details Figure 48: In the USA, this is called a 55-gallon drum, and it is often applied to the storage of chemicals. The drum has a diameter of about 0.6 m and a height of 0.9 m; its interior volume is 0.34 m³. The mass of steel is 18 kg. The surveys were made on 1 January 1983 in a sand quarry where the Earth's magnetic field was 55,250 nT at an inclination angle of about 70°. The measurement spacing was about 1.5 m and the survey was done with a Geometrics model G-856 proton magnetometer. The survey and data are included in a report (Bevan 1983). The rotation angle (about a vertical axis) of the drum probably changed when it was turned upside down.

details Figure 49: For the magnetic anomaly with a difference magnetometer, the field at a sensor at a height of 1 m has been subtracted from the field measured at a sensor that is at a height of 1 m. Since the upper sensor is now closer to the magnetic feature, it causes a stronger anomaly that greatly reduces the resulting difference anomaly. Magnetic measurements may also be made on a vertical surface, perhaps this is the side of an excavated trench; if the site is in the northern hemisphere, magnetic lows will then be prominent at magnetic bodies.

details Figure 50: This was the site of an early battle (on 3 July 1754) of the French and Indian War in North America. The area of survey is about 10 m north of the reconstructed Fort Necessity. The magnetic survey was done with a pair of proton magnetometers, model G-856, manufactured by Geometrics. One instrument remained stationary as a base station (the background field was about 55,600 nT); the other magnetometer was carried around the area of survey. Measurements were made at intervals of 2.5 feet (0.76 m) along east-west lines that were 320 feet (98 m) long; the direction of traverse was unidirectional and toward grid north, rather than alternating. The spacing between the lines of traverse was 5 feet (1.5 m). The colored contour lines are plotted in the range of -200 to +200 nT; peak anomalies from the pipes are typically in the range of 300 to 2500 nT. Note that one pipe is just outside the northern edge of the map, and another crosses the left edge. These pipes were probably unused at the time of this survey, and their purpose is not known. This survey was done for David Orr (US National Park Service) on 29 - 30 May 1988; the survey and its analysis are described in a report (Bevan 1988). The history of the fort at the Fort Necessity National Battlefield is explained by Alberts (1975). While an electromagnetic conductivity survey (such as with a Geonics EM38) would also detect these pipes strongly, a resistivity survey would find little effect from the pipes. It is likely that each pipe segment has a length that is about the distance from the middle of one magnetic high to the middle of the adjacent low. Perhaps most of pipes were oriented in about the same direction during manufacture.

details Figure 51: The ground width of this map is 100 feet (30 m), and the pipe extends to the east outside the area of the grid by 3.3 m. The magnetic survey was done with a Gem model GSM-19FG Overhauser magnetometer, with a separate base station magnetometer. The location of this survey is about 60 m south of the area shown in [Figure 29](#). The magnetic map was analyzed with the Potent program, yielding an estimate of the

depth of the pipe of 0.5 m. Including the effect of demagnetization, the magnetic moment per unit of length of the pipe is 7 Am.

details Figure 52: This magnetic survey was done with a Varian model 49-544 cesium magnetometer that had a pair of sensors, connected by a coaxial cable. One sensor measured the magnetic map while the other was stationary (this was a base station and it corrected for the diurnal change in the Earth's magnetic field). The top of the grounding rod was at the surface of the soil; the diameter of the steel rod was about 1 cm. The rod was located at about E5.2 N7.0 in this map. This magnetic survey was done by Harold Spaulding and Diana Birmingham on 10 July 1978, as part of a large-area survey at Valley Forge that was done by MASCA (University of Pennsylvania Museum); this was part of grid M17 of that survey (Schenck 1978). Calculated models with neither a single dipole nor a single monopole gave a good match to the measurements. However, a model with two monopoles did allow a magnetic map that was similar to the measurements. The upper monopole had a strength of $S_1 = -30$ Am and was at the surface ($Z_1 = 0$); the lower monopole had a strength S_2 of +30 Am at it was at a depth of $Z_2 = -0.5$ m. It would have been reasonable if this Z_2 depth had been to the bottom of the rod, which was a length of 1.5 m. The reason for this shallow monopole is not known. The archaeological pit was 2 m in diameter and 0.8 m deep and it contained a variety of historic refuse.

details Figure 53: These measurements are described in a report (Smekalova and Bevan 2015, Fig. 8). Except for the storm on the 17th, the sky was clear on the other two days. The temporal anomalies were always toward lower magnetic field; this has also been found at other sites and times during thunderstorms. The cause of lows, rather than highs, has not been determined. A magnetic survey at a site in Virginia (USA) in 1992 detected 10 measurement spikes with anomalies of about -38 nT during a thunderstorm; two other spikes were positive anomalies (Bevan 2004, Fig. B34 details). The instrument was a Geometrics G-856AX proton magnetometer. During another survey at this site in a storm, 17 one-point anomalies with amplitudes of about 4 nT were detected (Bevan 2004, Fig. B48 details). During an experiment near Denver, Colorado (USA), a pair of GeoMetrics G-856 proton magnetometers were separated by a distance of 16 km and the instruments were recording time-synchronized measurements to a precision of 1 s; a thunderstorm at one of those locations detected magnetic spikes of about -3 and -8 nT, while the other magnetometer (not in a storm) detected no spikes (Bevan 1993, p. 2). A magnetic survey in Virginia (USA) detected magnetic low spikes of about 50 nT that were caused by a buried electrical power cable at a distance of about 5 m (Bevan 2000, Fig. 23). Four different magnetometers (3 proton and one cesium) were tested to see if they differed in their detection of changes in the magnetic field due to nearby electrified trains or buses (Smekalova and Bevan 1993, p.21); all four magnetometers detected this noise identically.

Equally-magnetic

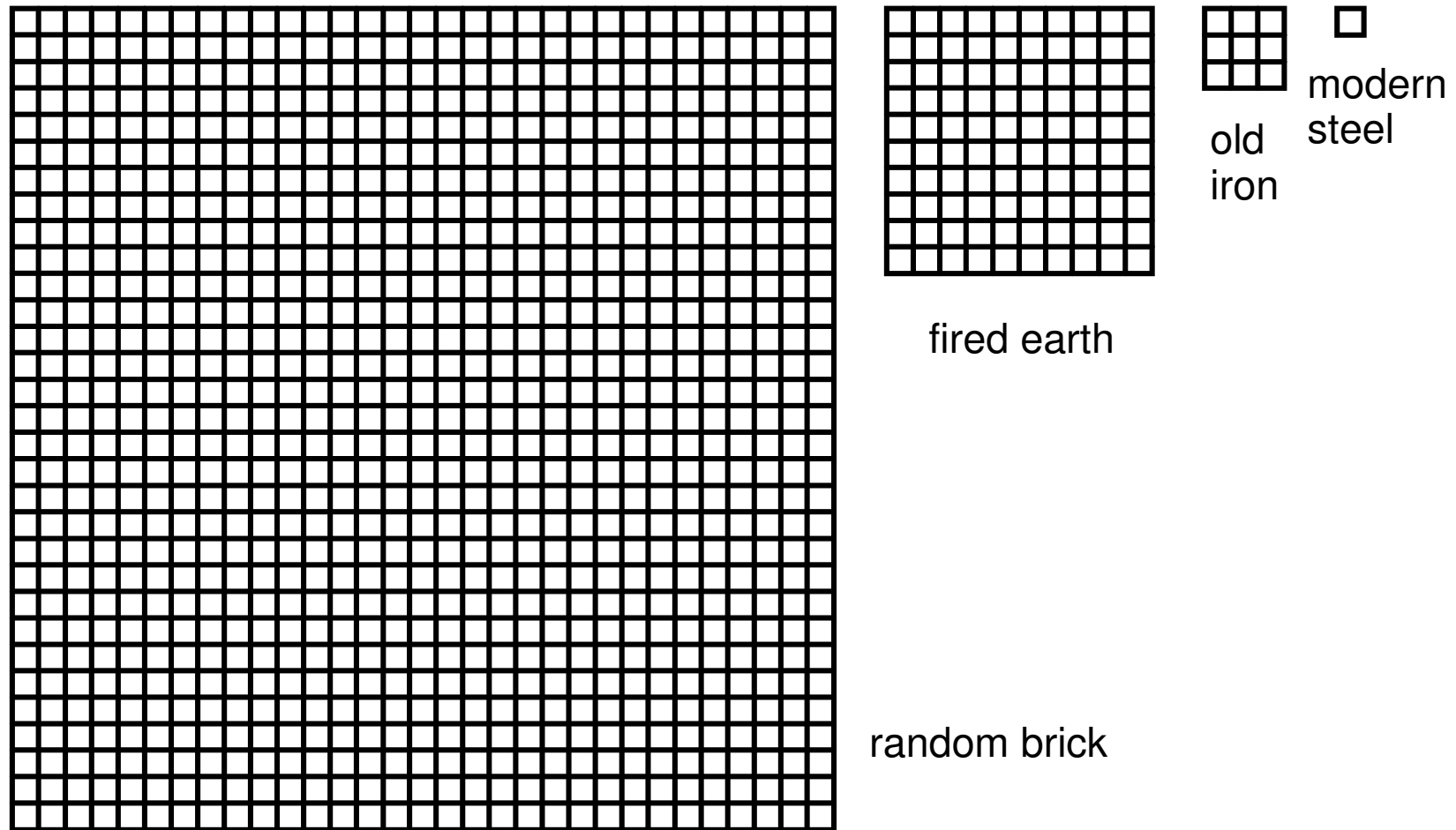


Figure 1: A comparison of magnetic features and artifacts. The number of small squares indicates the quantity of magnetic material that causes each of the four materials to be about equally magnetic. As shown, it takes a huge amount of broken bricks or pot sherds to equal the magnetic effect of a modern steel object. [details](#) (further information)

The relative magnetic moment and mass of some iron objects

The unit of magnetic moment is milliampere-meter-squared per kilogram and both induced and remanent magnetization are added

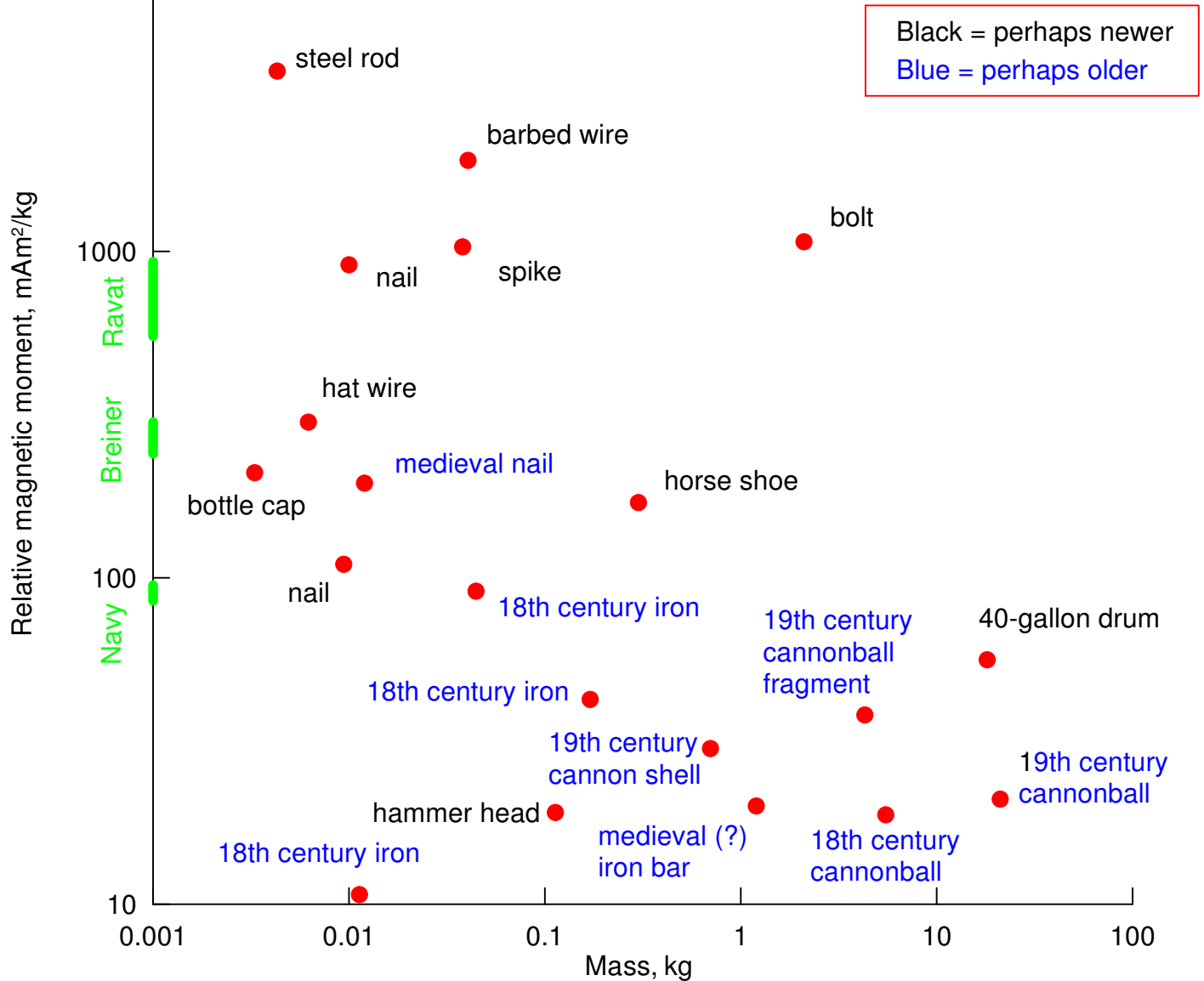


Figure 2: The magnetic moments of iron objects. The red circles mark the measurements of relative magnetic moment and mass for different artifacts. Black text marks modern objects from the 20th century. Blue text marks objects that are earlier; note that these older objects are usually less magnetic than the modern artifacts. The green bands on the left side of the graph show estimates of relative magnetic moment that have been made by other investigators. [details](#)

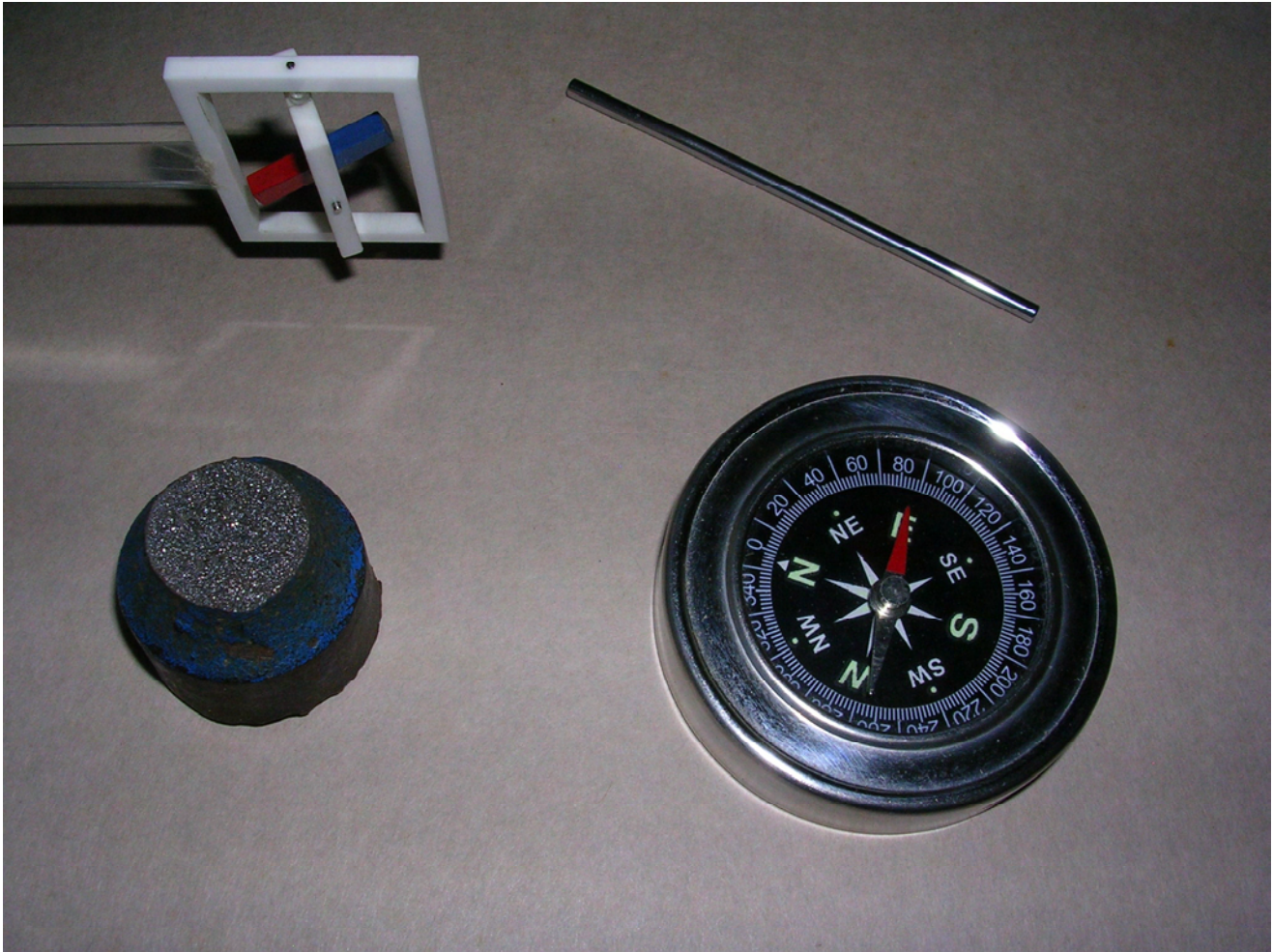


Figure 3: Simple tests on iron objects. A gimbaled bar magnet is at the upper left; this is a magnetic probe. The red-blue bar is free to rotate in any direction; in the northern hemisphere, the red end points downwards in about the direction of the Earth's magnetic field. Put an iron object near to that rotatable magnet to see whether the red or blue end of the bar magnet moves toward the iron. Then, rotate the iron object by 180° and see if the same or the opposite end of the magnet approaches the iron. If only one end of the probe magnet is attracted toward the iron, that iron object has induced magnetization. If one end and then the other end of the probe magnet are attracted to the iron object as the object is rotated, the object has remanent magnetization. While iron can be checked by a touch of a hand magnet, it may be better to test for induced and remanent magnetization. [details](#)

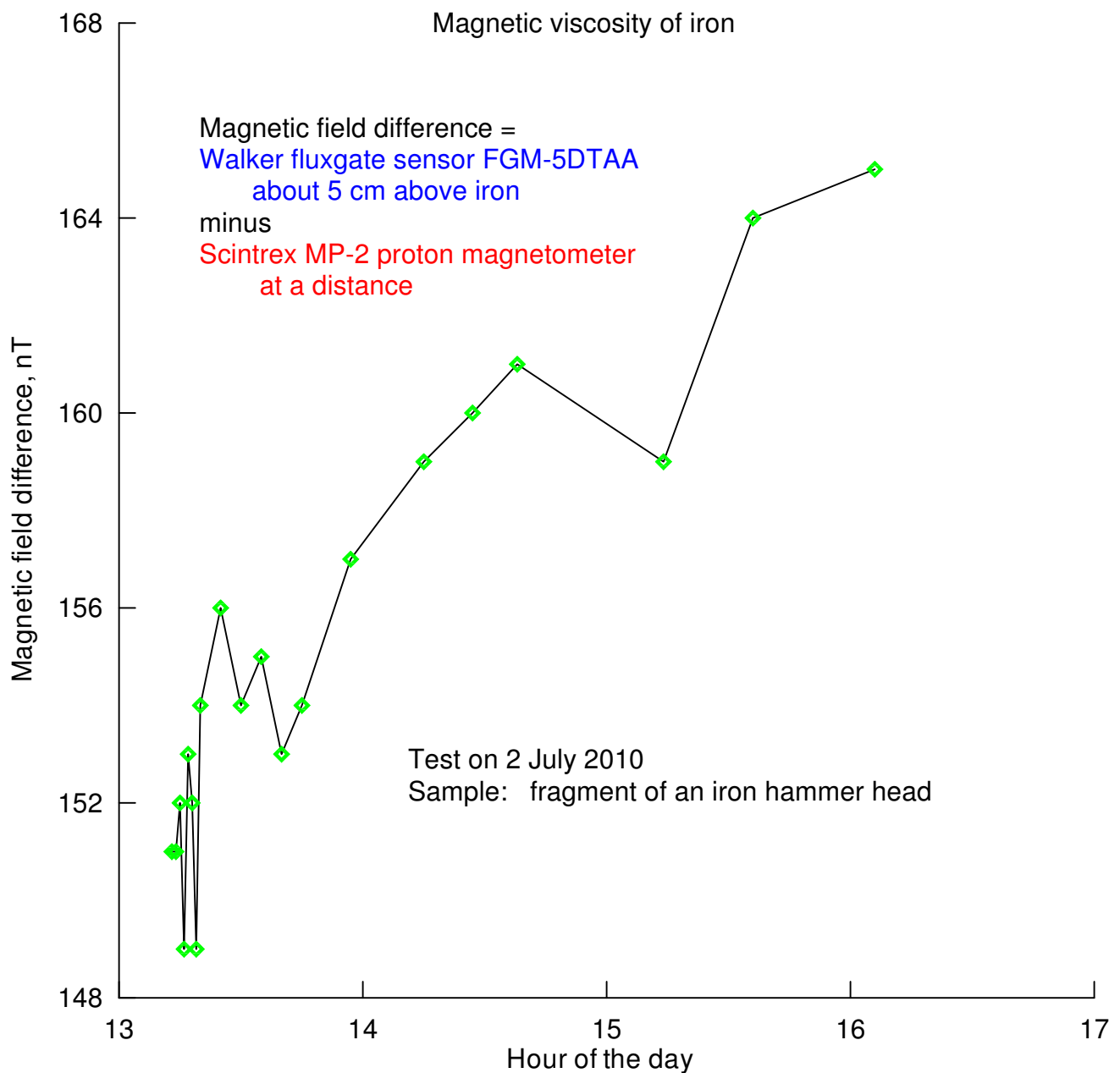


Figure 4: The magnetic viscosity of iron. The magnetic field increased by about 15 nT in three hours, apparently due to magnetic viscosity. The temporal change in the Earth's magnetic field (monitored at a distant magnetometer) was subtracted from the magnetic measurements that were made with a sensor that was close to the iron object. [details](#)

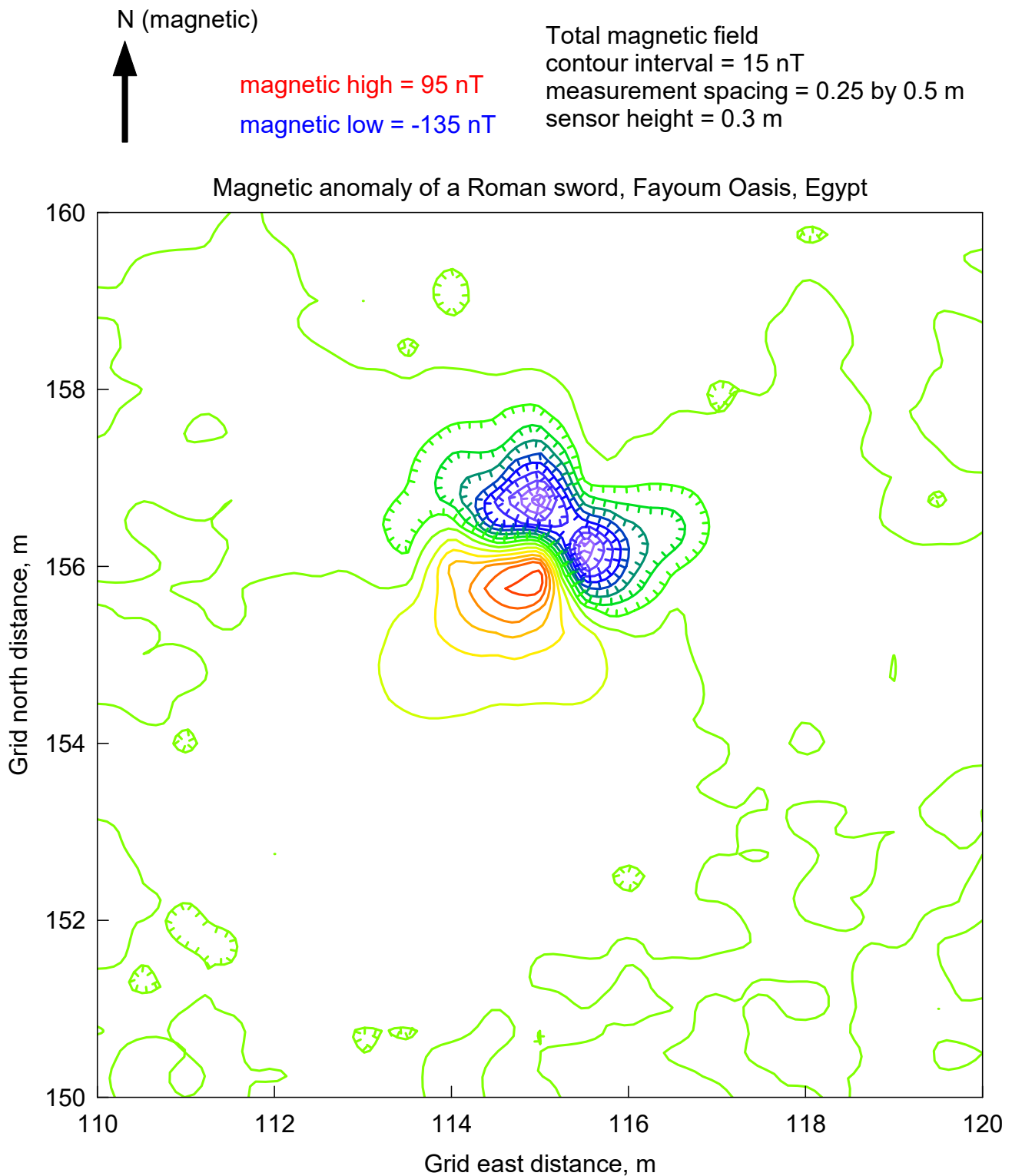


Figure 5: The magnetic anomaly of a Roman sword. A later excavation revealed the sword at a depth of 0.8 m. The magnetic low of this dipolar anomaly is toward the north. The magnitude of the low (-135 nT) is stronger than the companion high (95 nT); this strong low is probably caused by the low latitude of the site (30°), and by induced magnetization in the sword. The magnetic low is also unusual, for it is elongated into two separate and adjacent lows. [details](#)



Figure 6: The exploration, excavation, and cleaning of a Roman sword that is somewhat less than 1 m long. The upper photo shows the site at Dimai (Egypt). The middle photo illustrates the rusty scabbard (case or sheath) of the sword that was detected by the magnetic survey. The lower photo shows the sword after the fragments of rust from the scabbard were removed from the well-preserved iron of the sword. [details](#)

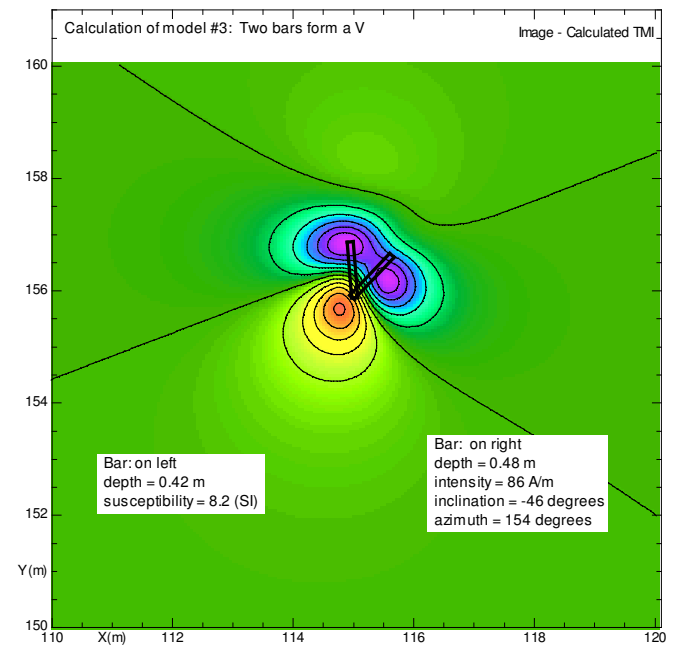
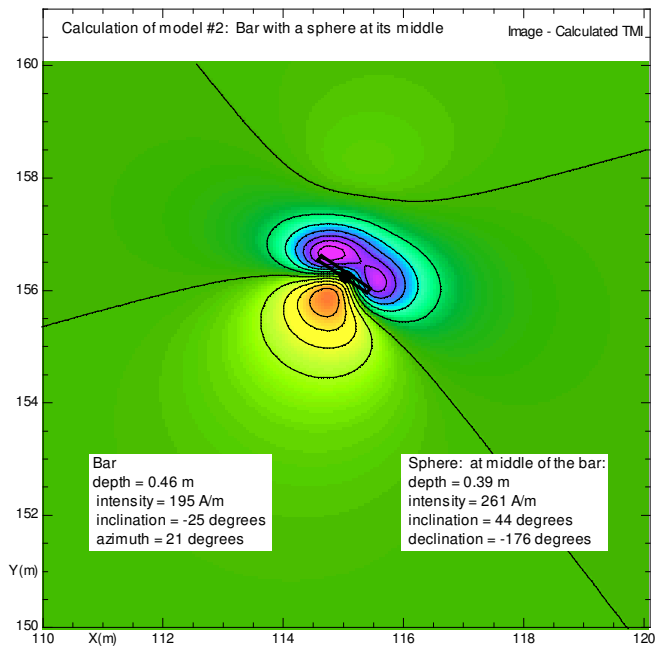
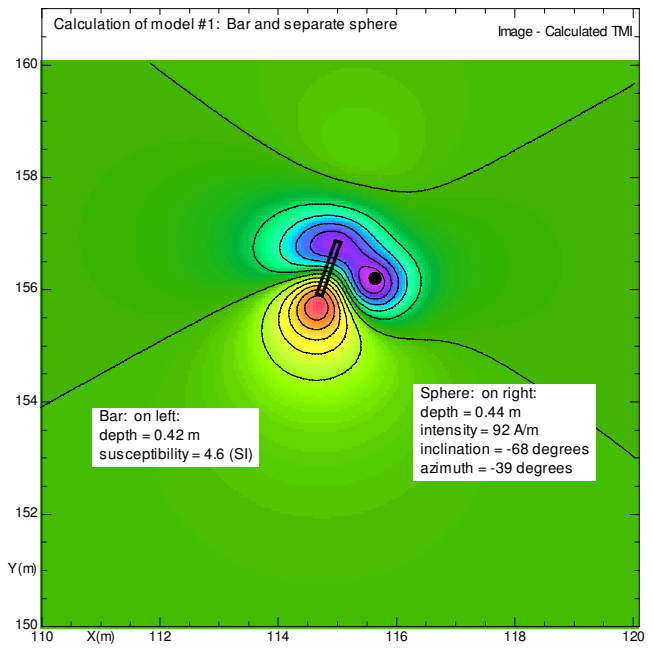
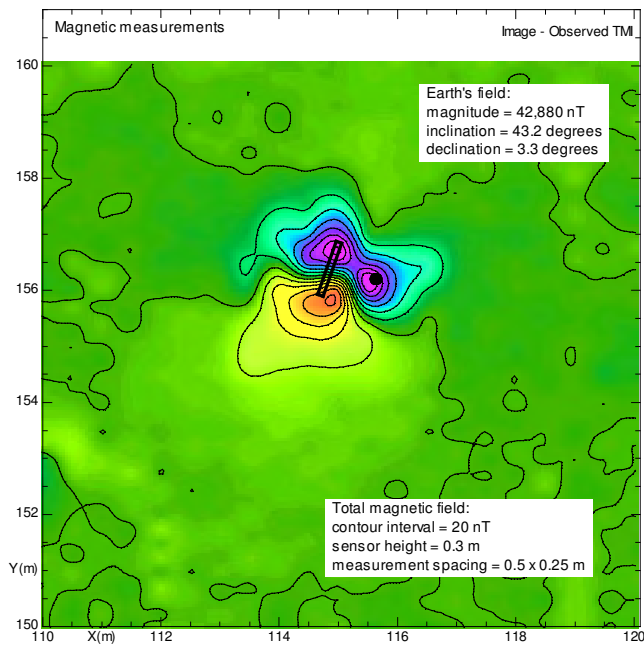


Figure 7: Three different magnetic models whose calculations approximate the measurements that are plotted at the upper left. The most reasonable model is #1, at the upper right. It has a magnetic bar (located with a thin black rectangle) that is 1 m long; this approximates the anomaly of the sword. A separate spherical body on the right (a black circle) provides a good model of the magnetic low on the right; the radius of this sphere is 0.1 m. [details](#)

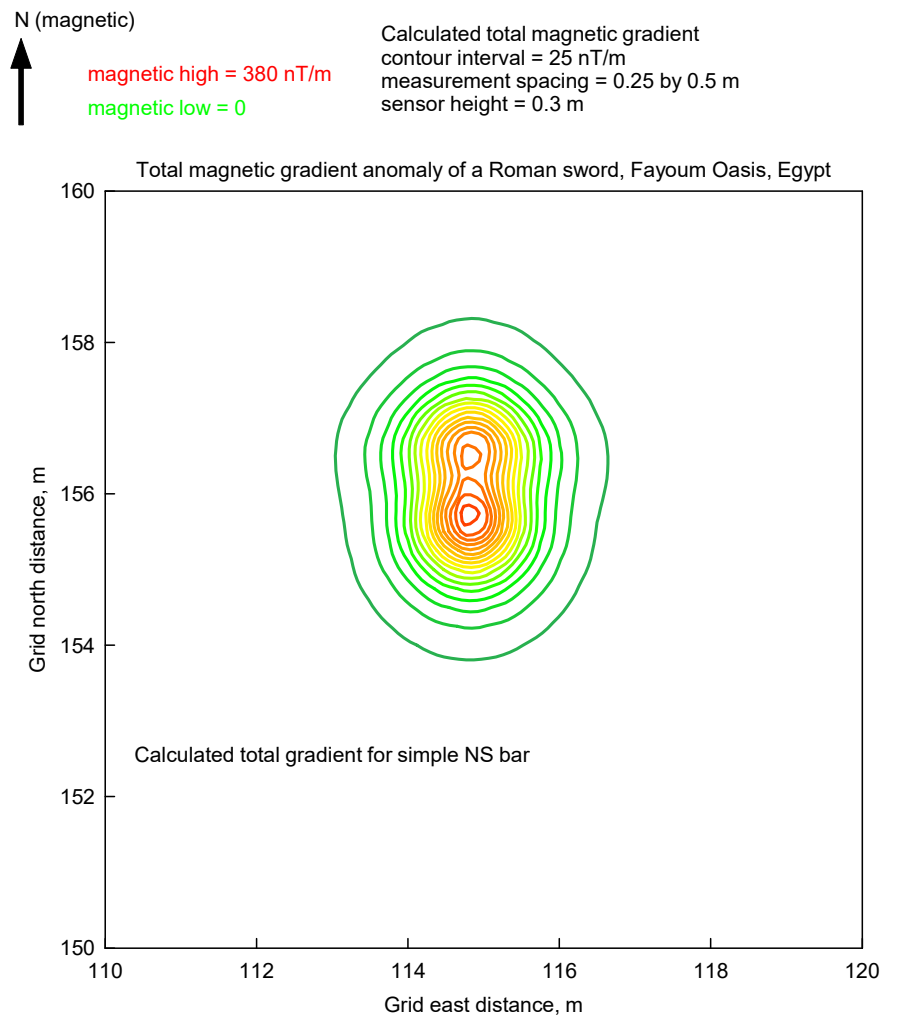
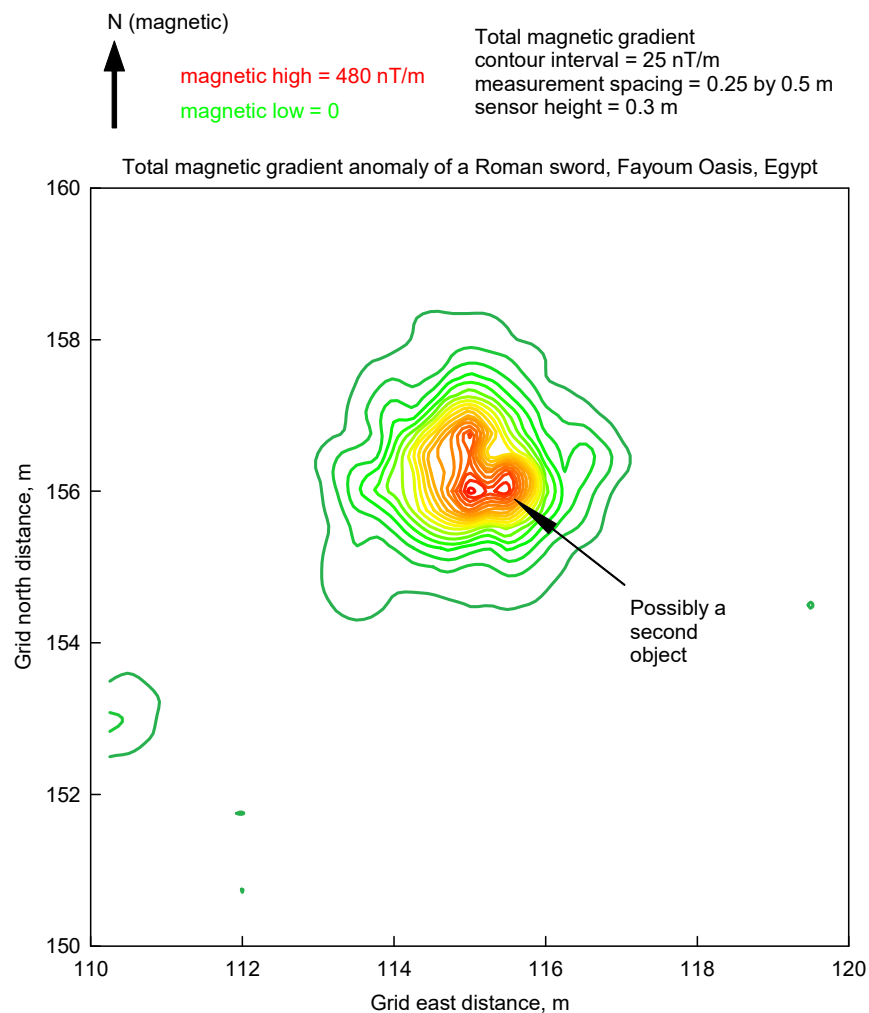


Figure 8: Maps of the total gradient of the magnetic field. While the measurements at this site were made with a total-field magnetometer, rather than a gradiometer, the magnitude of the gradient can be calculated as shown here. The total gradient of the measurements in [Figure 5](#) is plotted on the left, while the total gradient of a simple bar feature (the model for a sword that is 1 m long) is on the right. Both maps have a pair of highs that are 1 m apart. The map on the left has an extra high that could be caused by a small magnetic object at that location. [details](#)

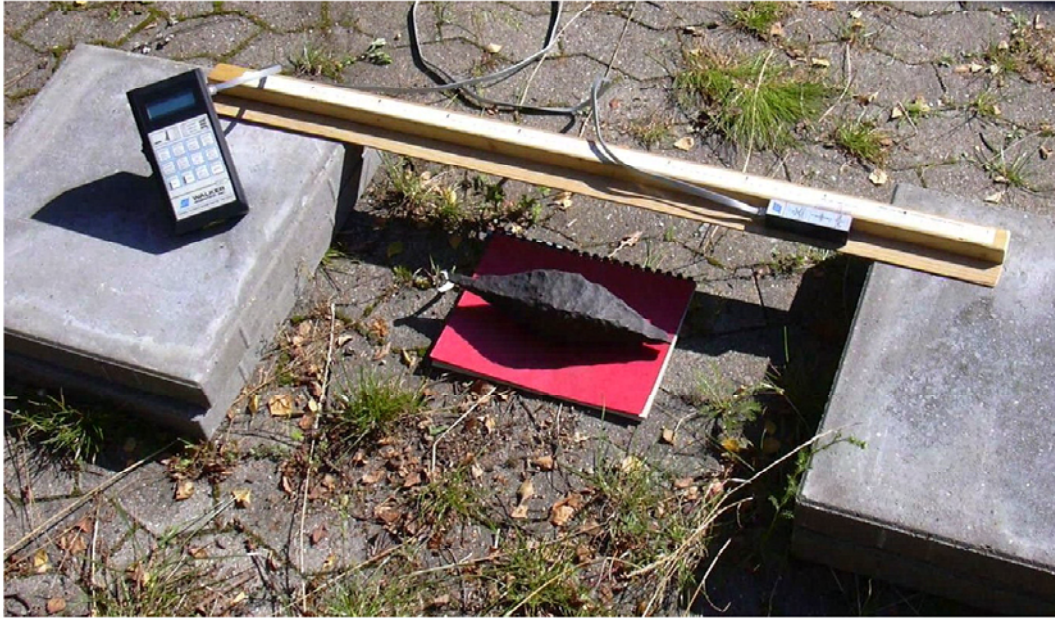


Figure 9: The lower photo shows a bar of old iron that was found in Denmark. It is about 30 cm long and 7 cm in diameter. The magnetic character of this bar was measured with the equipment shown in the upper photo. A single line of measurements was made along the length of the bar; see [Figure 10](#). For the measurements, the sensor of the fluxgate magnetometer moved steadily along the 1-m length of the traverse that was defined with a wooden board. The measurements were recorded in the control unit for the magnetometer, shown on the left. [details](#)

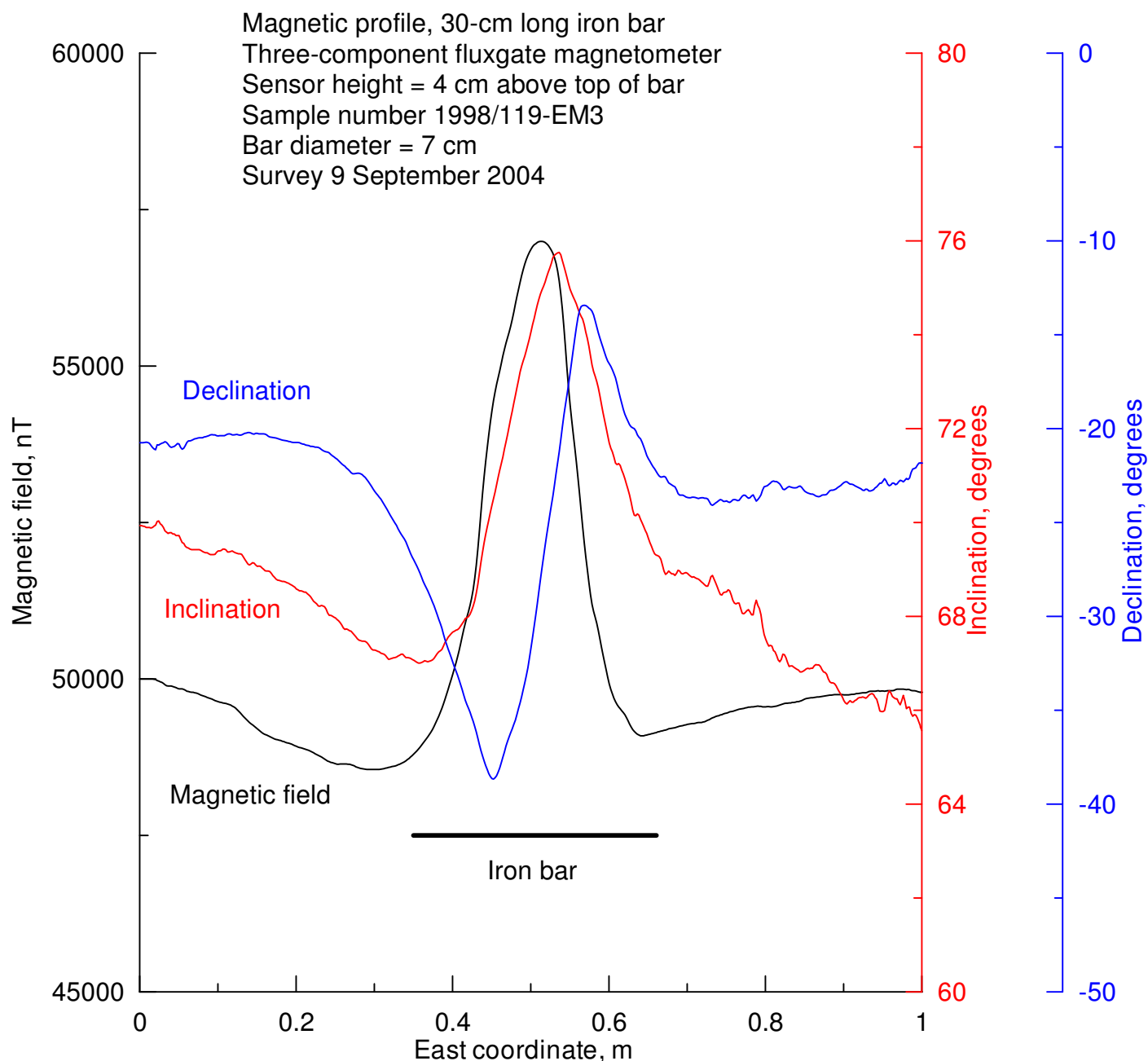


Figure 10 Vector magnetic measurements that were made along the length of an iron bar. The peak magnetic anomaly that was measured at a height of 4 cm above the top of the bar was about 6000 nT. The inclination of the magnetic field changes by about 10° and the declination changes by 20° along the line of the measurements. A broad line below the curves marks the span of the iron bar. [details](#)

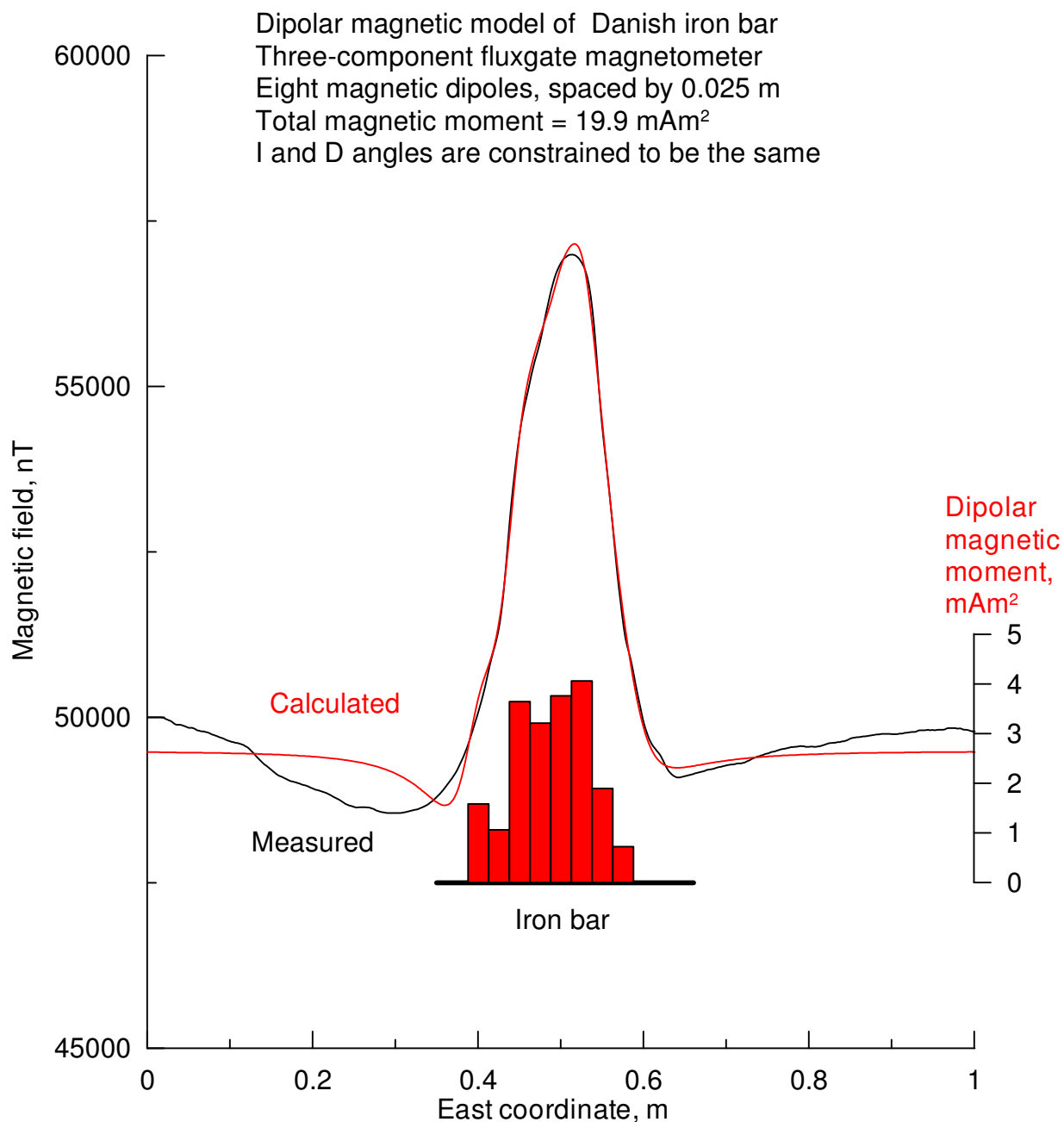


Figure 11: Comparing measured and calculated anomalies. There is a good match between the magnetic high measurements and the calculation of a multi-dipole magnetic model. This analysis suggests that the magnetic moment of this Danish iron block is about 20 mA/m². The bar graph at the bottom plots the magnetic moment of each of the eight dipoles that are models along the mid-line of the iron. [details](#)

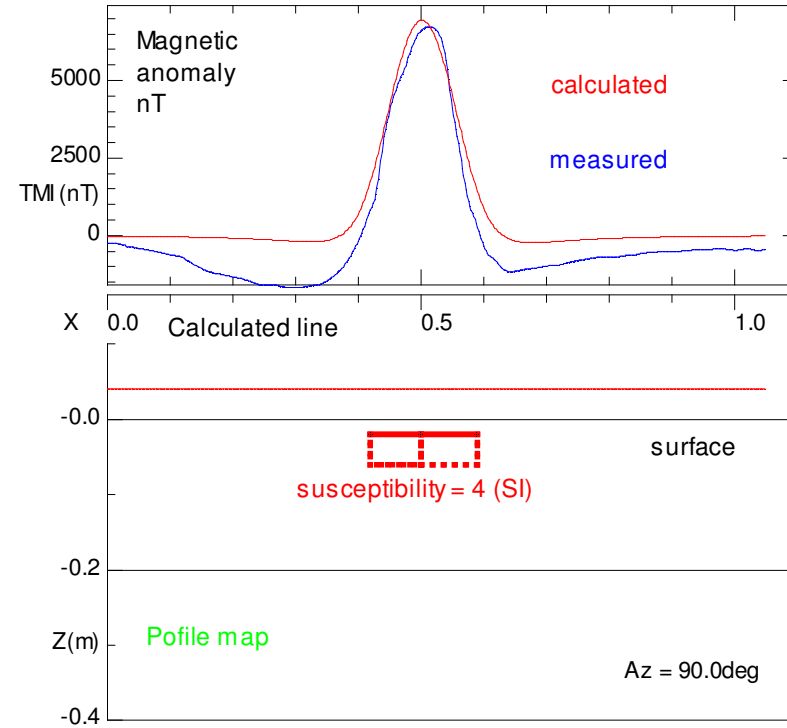
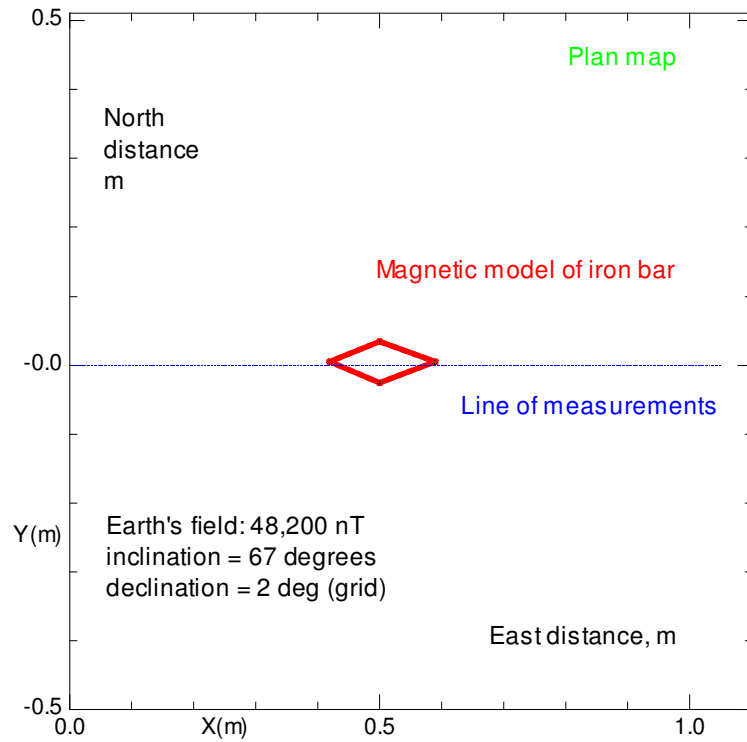


Figure 12: Another magnetic model of the bar of iron. This yielded a total magnetic moment of 29 mA/m^2 , higher than the moment of 20 mA/m^2 that was determined with the analysis of [Figure 11](#). The map on the left shows a plan view of the magnetic model, outlined with red. A profile of the magnetic model is on the right, along with the measured field (blue curve) and the calculations (red curve). [details](#)

Magnetic map, Salgir fort (1772-1784), Crimea

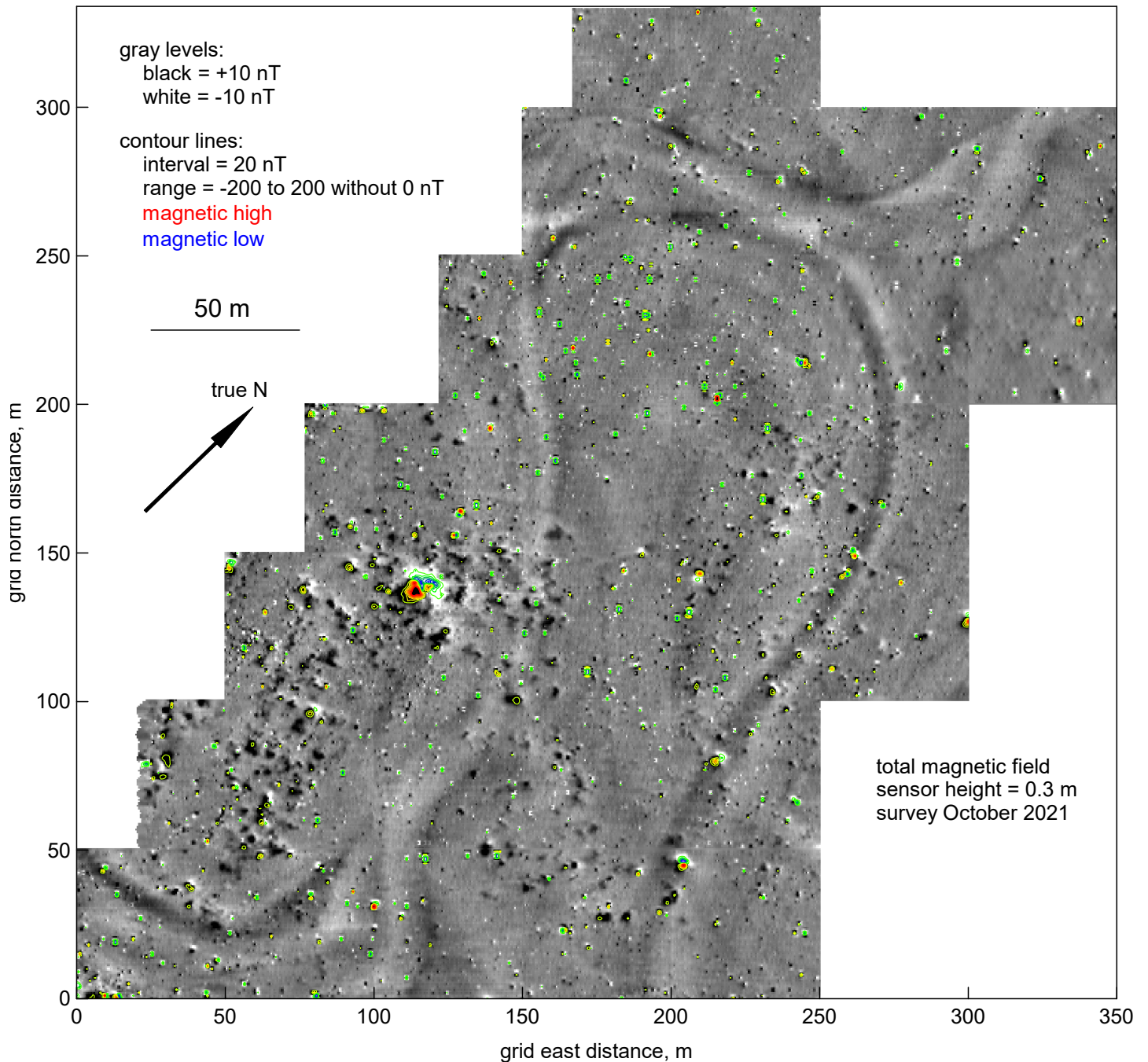


Figure 13: The magnetic map that located the fort on the Salgir River. The strongest magnetic anomaly was caused by a group of several hundred cannon balls. This 250-nT anomaly is indicated with red and yellow contour lines near E100 N150. An enlargement of this part of the map is found in [Figure 14. details](#)

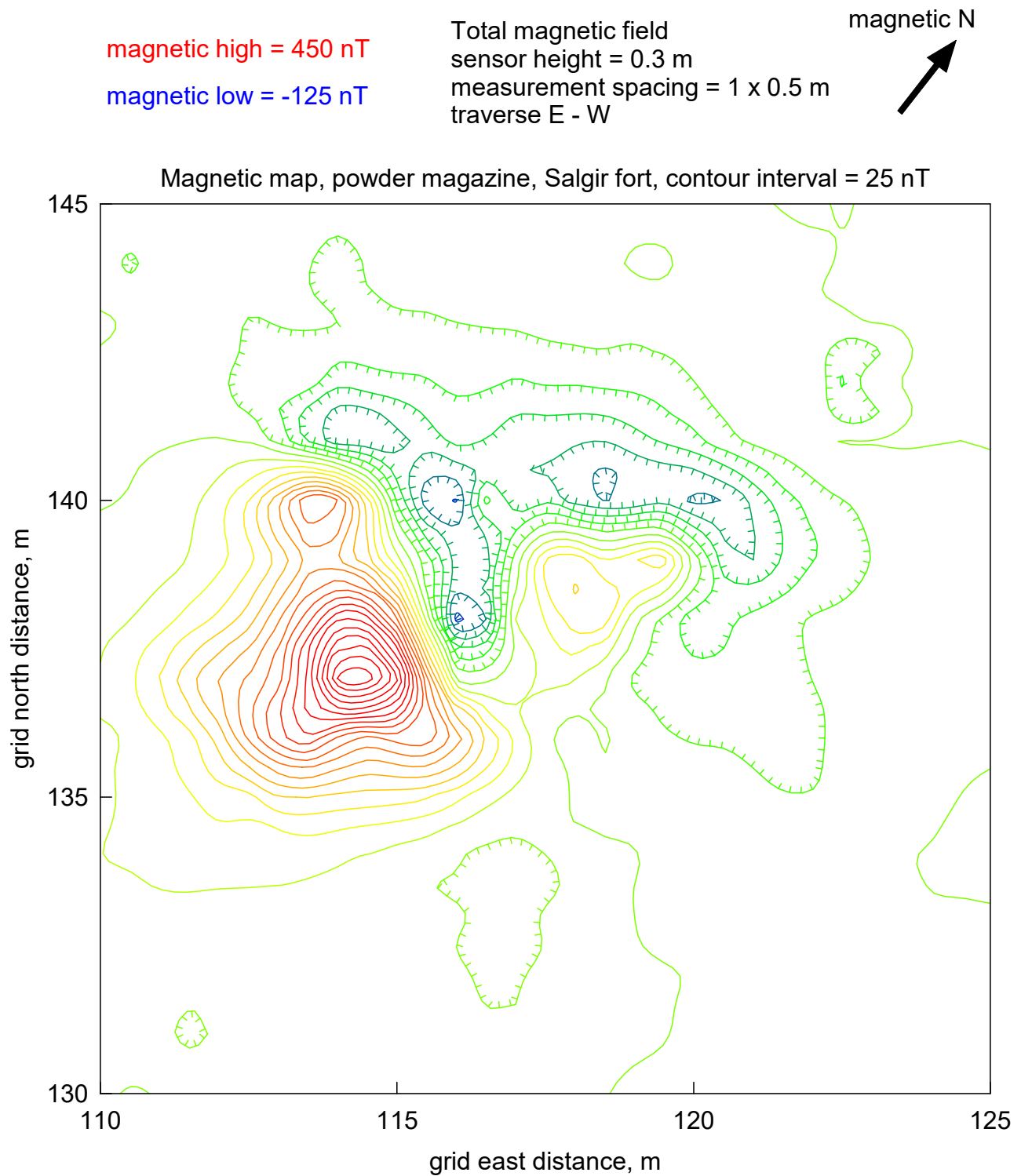


Figure 14: An enlargement of the major magnetic anomaly at the fort on the Salgir River. As usual, magnetic lows (blue and green) are toward magnetic north from the magnetic high (red and yellow contour lines). The contour lines of magnetic lows have hachures (perpendicular tick marks) along their length. [details](#)

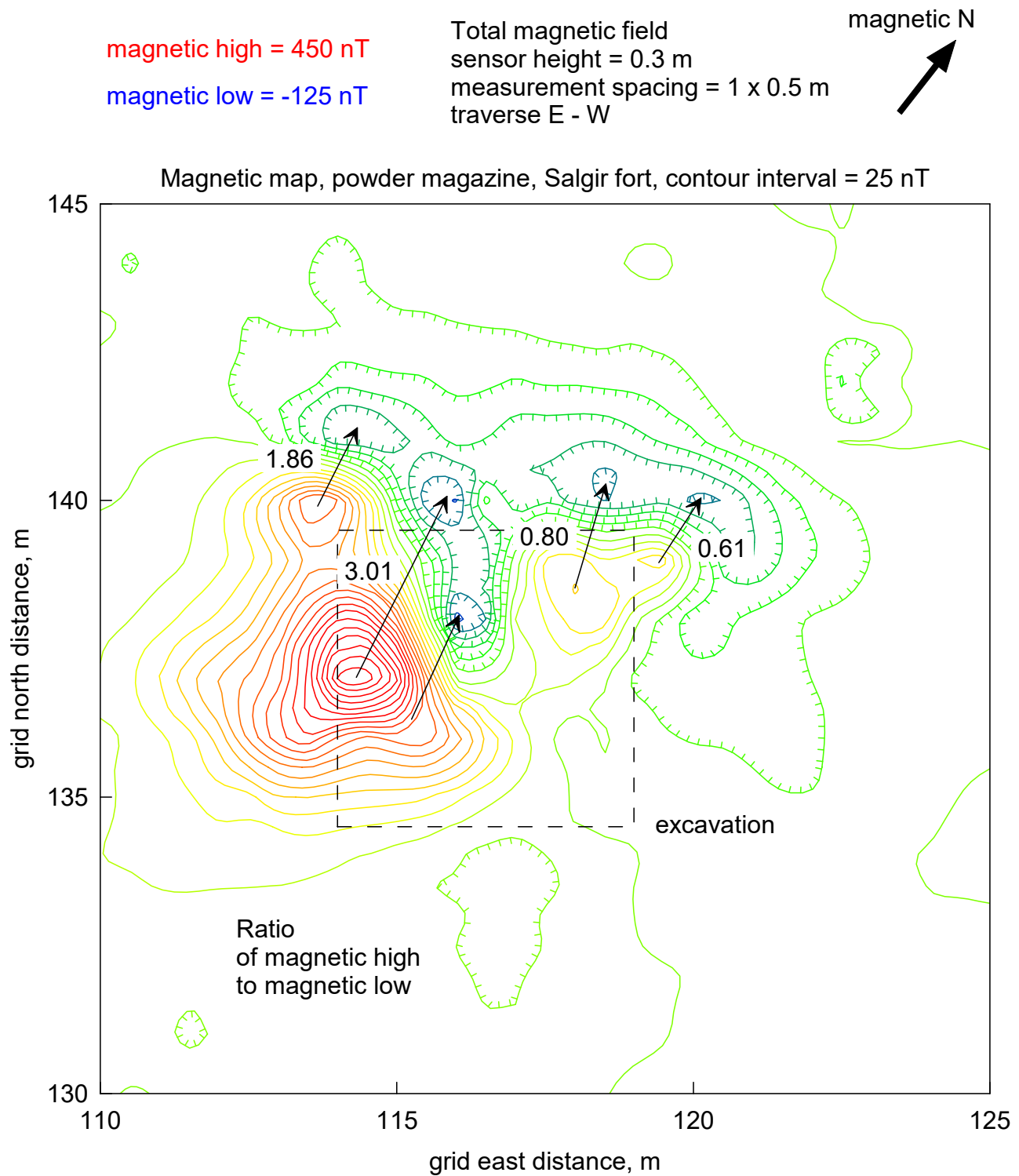


Figure 15: A graphical analysis of the major magnetic anomaly at the fort on the Salgir River. Black arrows extend from each magnetic high toward the magnetic low that appears to be associated. Black numbers list the ratio of amplitudes of the magnetic high to the absolute value of the low. The 5-m dashed-line square locates the later excavation at the powder magazine. [details](#)

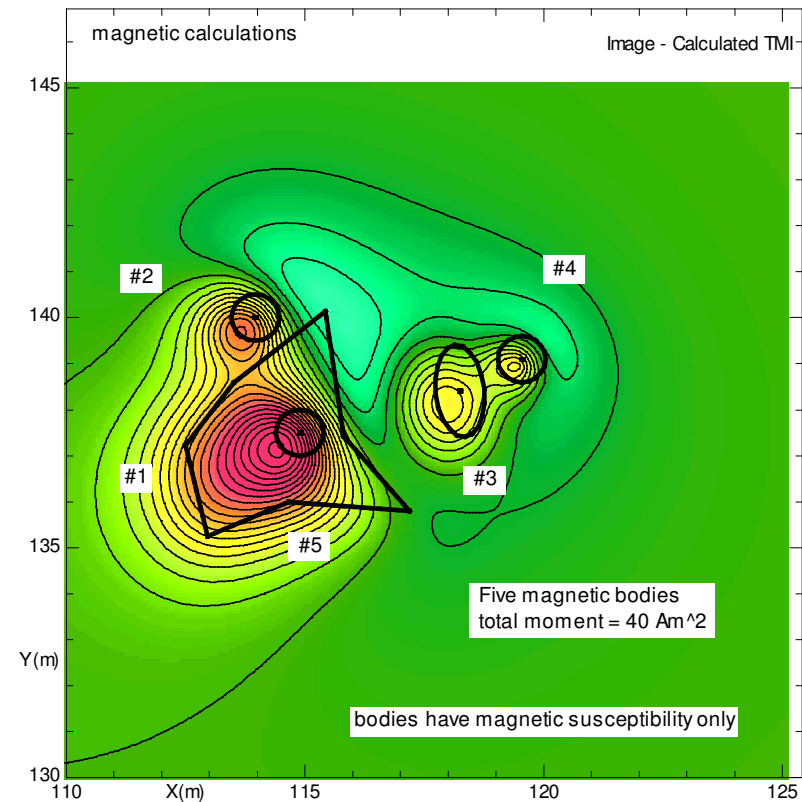
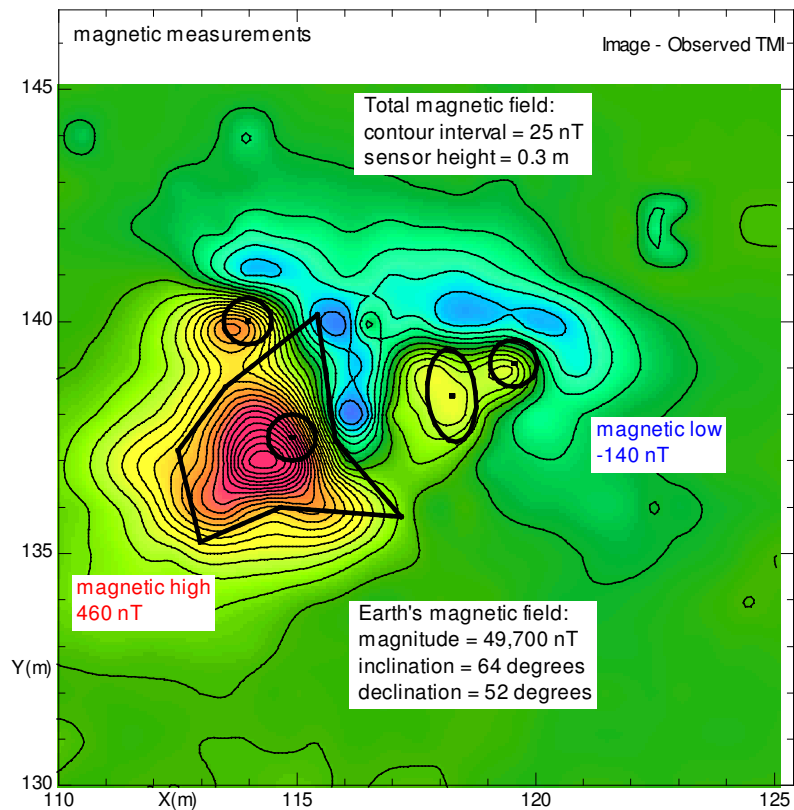


Figure 16: The first analysis of the strong anomaly in the magnetic map of [Figure 13](#). This study was done before an archaeological excavation located a large mass of cannon balls here. The magnetic measurements are plotted on the left, and the calculated anomaly of five magnetic bodies (outlined with thick black lines) is on the right. The goal of the analysis is to create a magnetic model whose calculated anomaly is very similar to the measurements. [details](#)

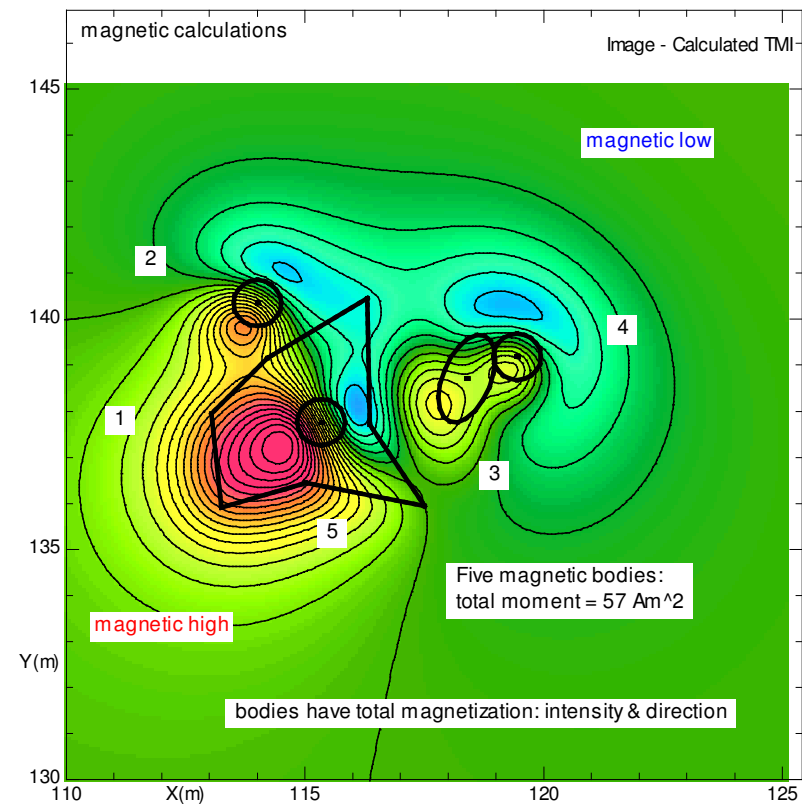
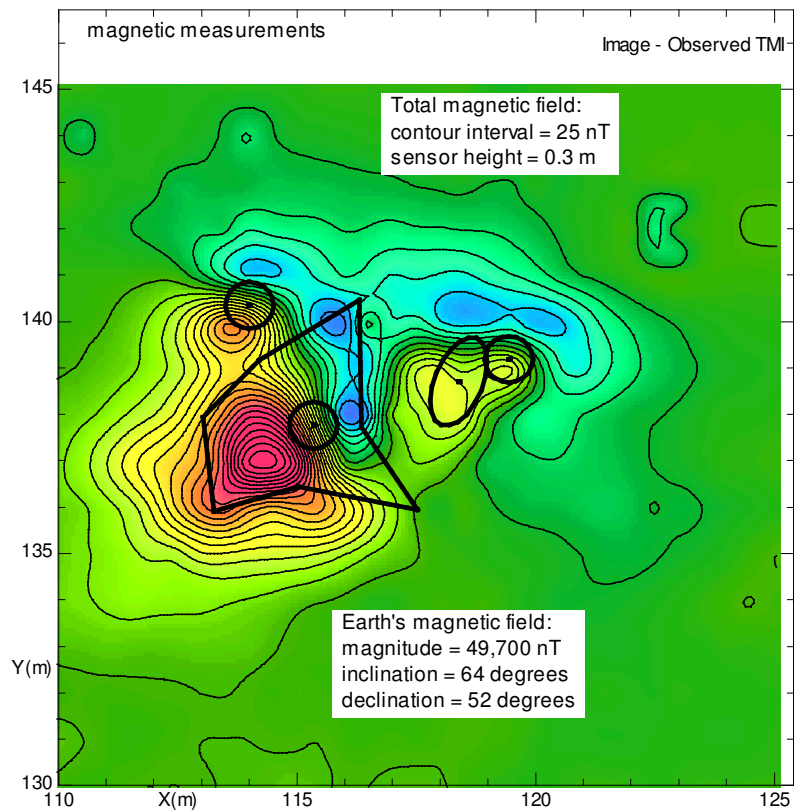


Figure 17: An improved magnetic model. Notice that these calculated lows are now stronger than those in [Figure 16](#). For this analysis, the angle of inclination of the magnetization of the bodies was allowed to change. In [Figure 16](#) the inclination angle was that of the Earth magnetic field (64°); for this calculation, the inclination angle of the most magnetic bodies were much lower (body #3 has an angle of 10° , while body #5 has an angle of 13°). [details](#)

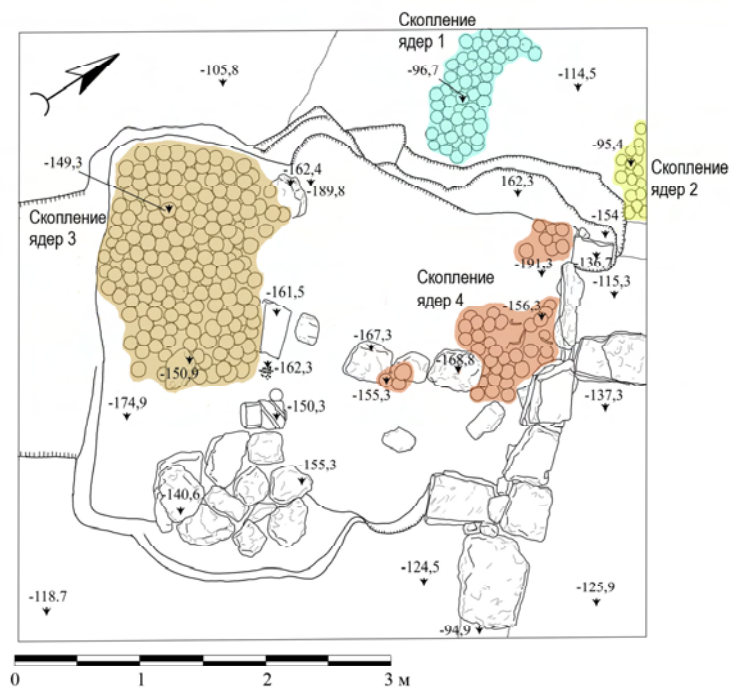


Figure 18: Cannon balls that were found in an excavation at the Salgir fort. Clusters of spherical cannon balls are visible at several locations in the photo (at the top). In the lower panel, elevations (underground and therefore negative) to the tops of clusters of cannon balls are indicated, in cm. Depths range between 0.6 to 1.9 m underground. [details](#)

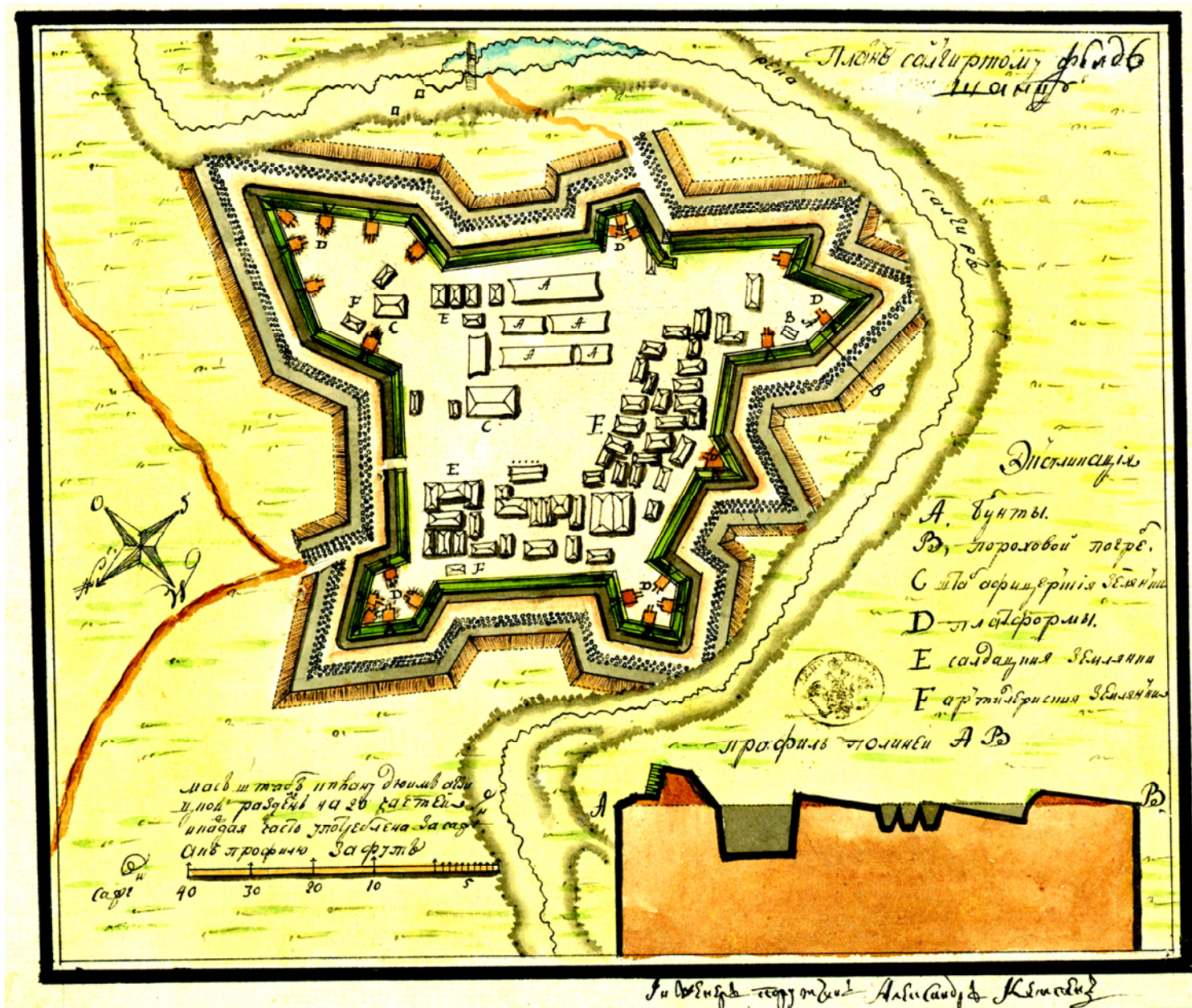


Figure 19: A detailed map of the Salgir fort. This map was prepared in about 1778. The map locates two powder magazines which are marked as roofed buildings with the letter F; these are near the lower left (magazine #1) and the upper left (magazine #2) sides of the fort. The length of the scale bar at the lower left is 50 Russian sazhen, which is 106.5 m. The north direction is toward the lower left in this orientation of the map. The Russian equivalent of "powder magazine" is "artillery cellar", which is артиллерийских погребов and noted at the lower right hand side this map. [details](#)

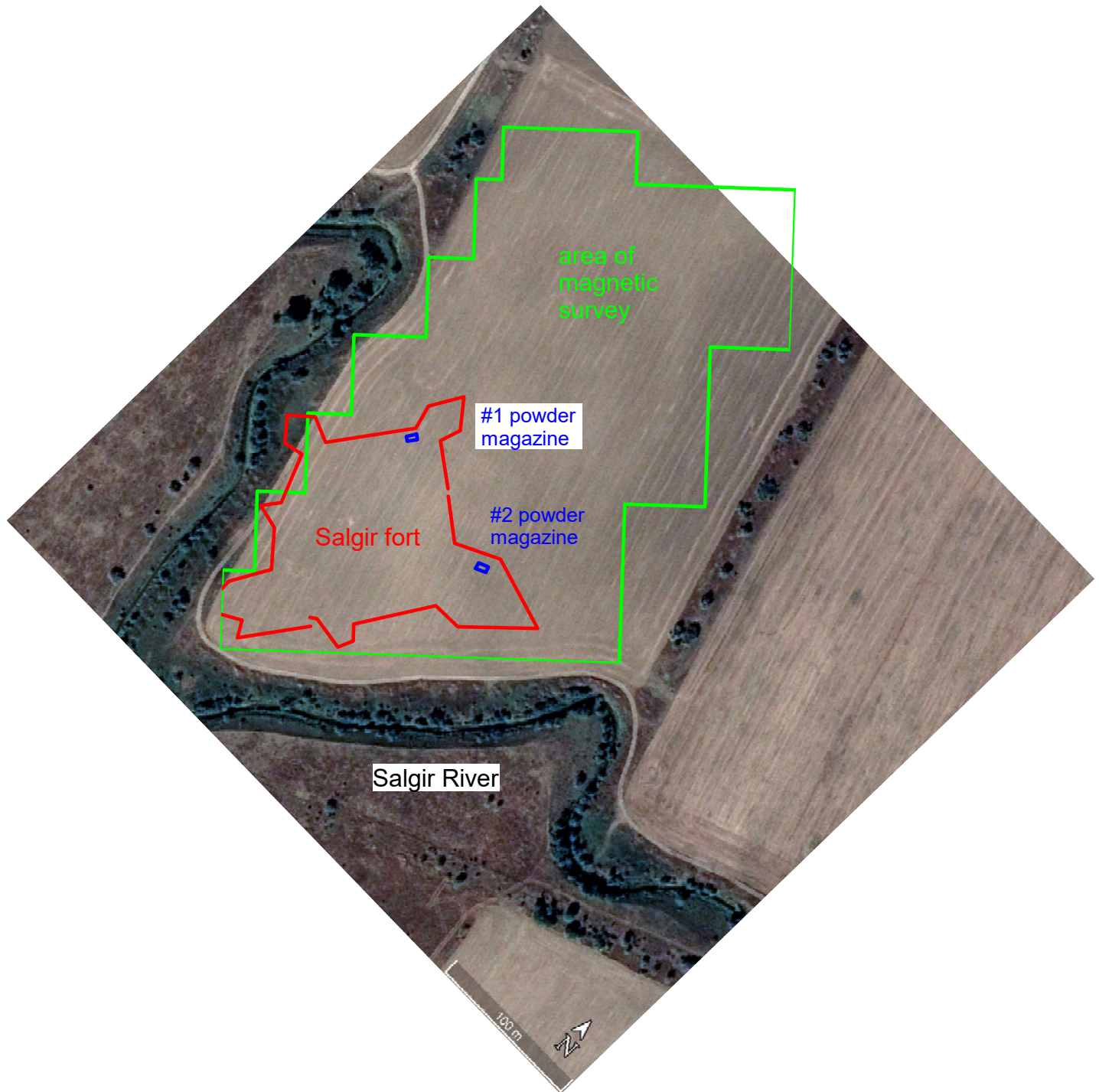


Figure 20: The location of the Salgir fort. A red line traces the ridge of the earthwork of the fort; Nothing unusual is seen along this line at the ground surface. Blue rectangles locate the two powder magazines; only the anomaly for powder magazine #1 can reasonably be placed at the strong magnetic anomaly. The path of the Salgir River is seen along two sides of the fort; this river also constrains the location of the fort. [details](#)

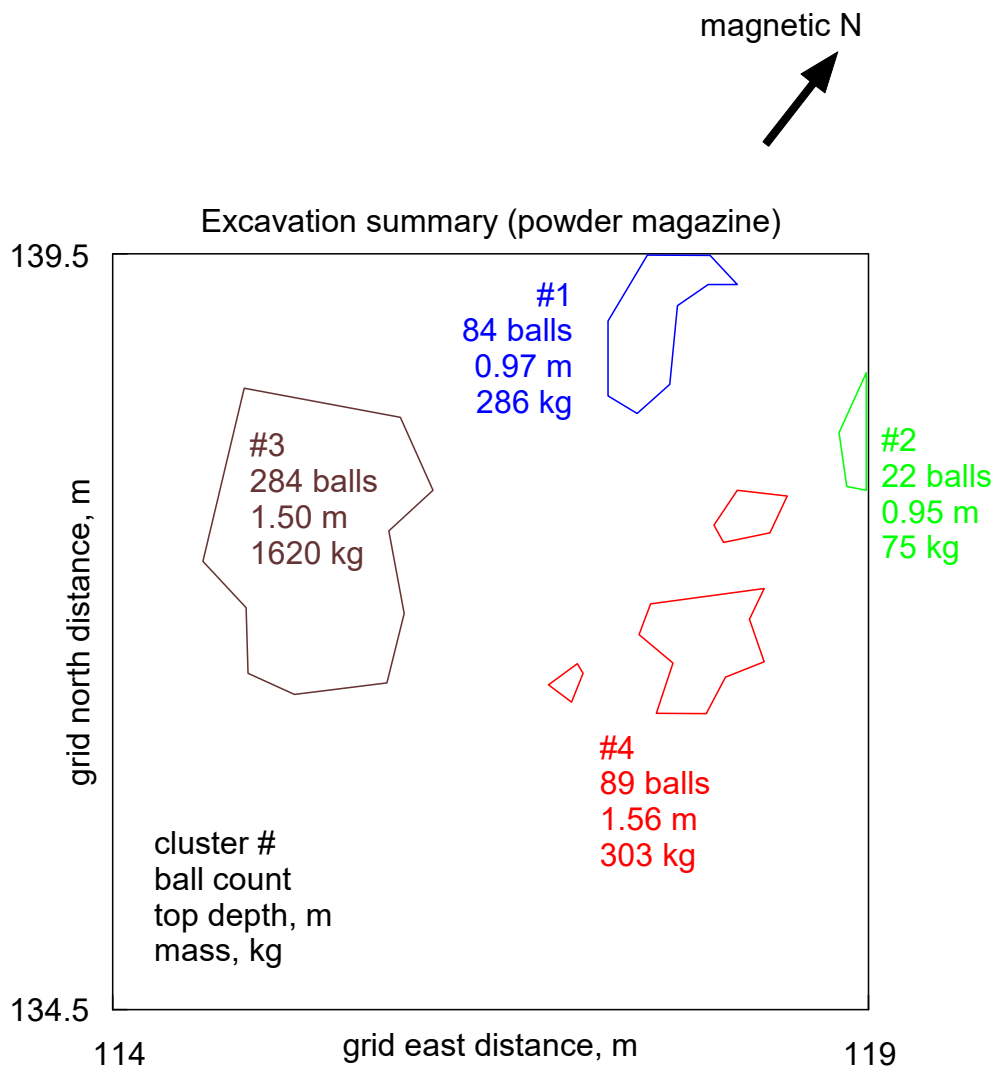


Figure 21: An approximation of the findings (in [Figure 18](#)) of the archaeological excavation of the strong anomaly. Four separate clusters of cannon balls were found in the excavation; these are labeled here as #1 through #4, and these are the same identifications as those in [Figure 18](#). Text at the lower left side of the square defines the four parameters. The quantity of iron and its depth here were the basis for calculating the magnetic anomaly of the cannon balls in this excavation. [details](#)

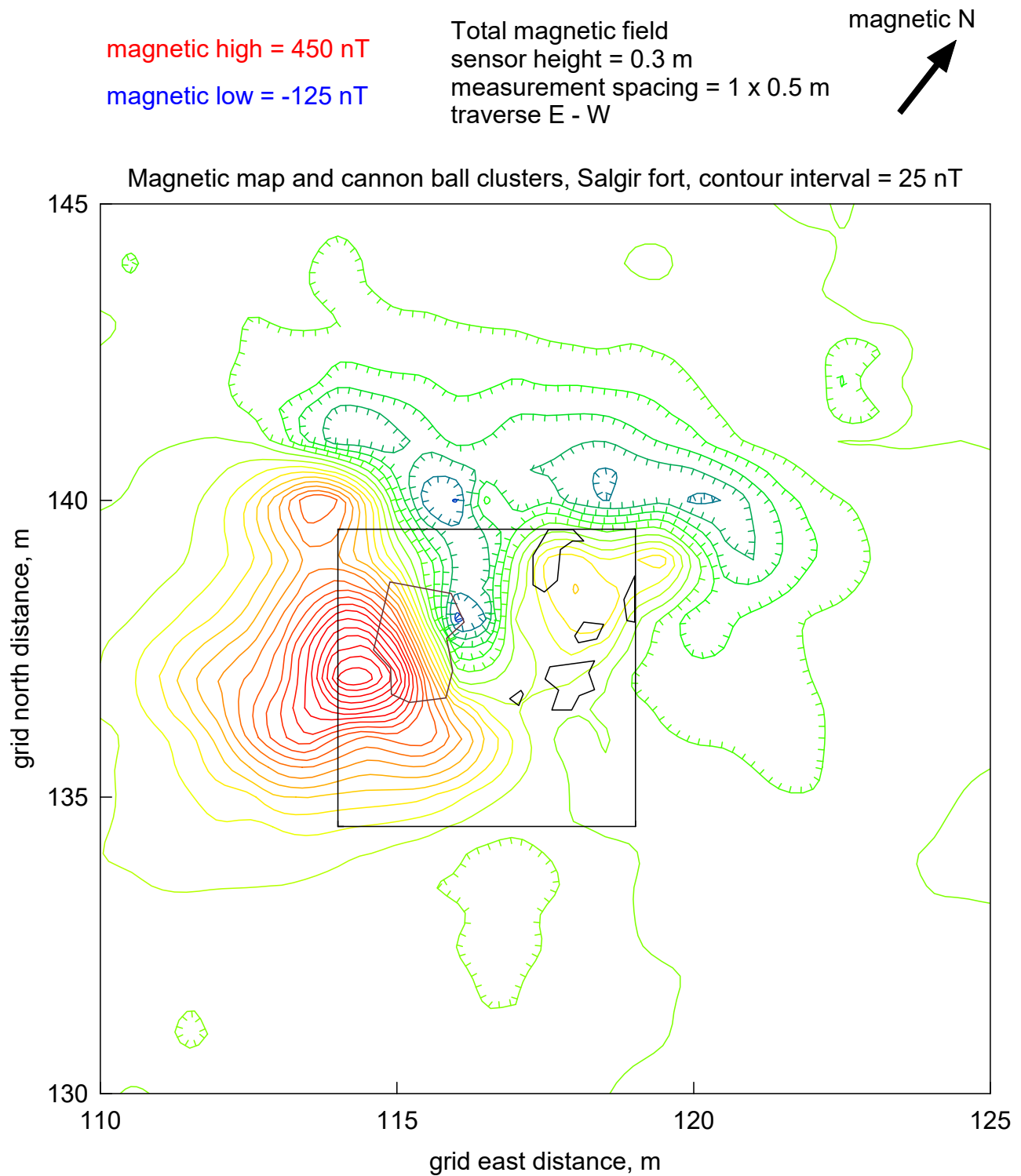


Figure 21a: The magnetic map of the powder magazine along with the clusters of cannon balls. The clusters are outlined with black. The largest cluster (#3 on the left side of the excavation square) clearly causes the greatest magnetic anomaly. The other clusters create a weaker anomaly, and its contour lines are yellow here. The excavation (5 m on a side) is marked with a black square. [details](#)

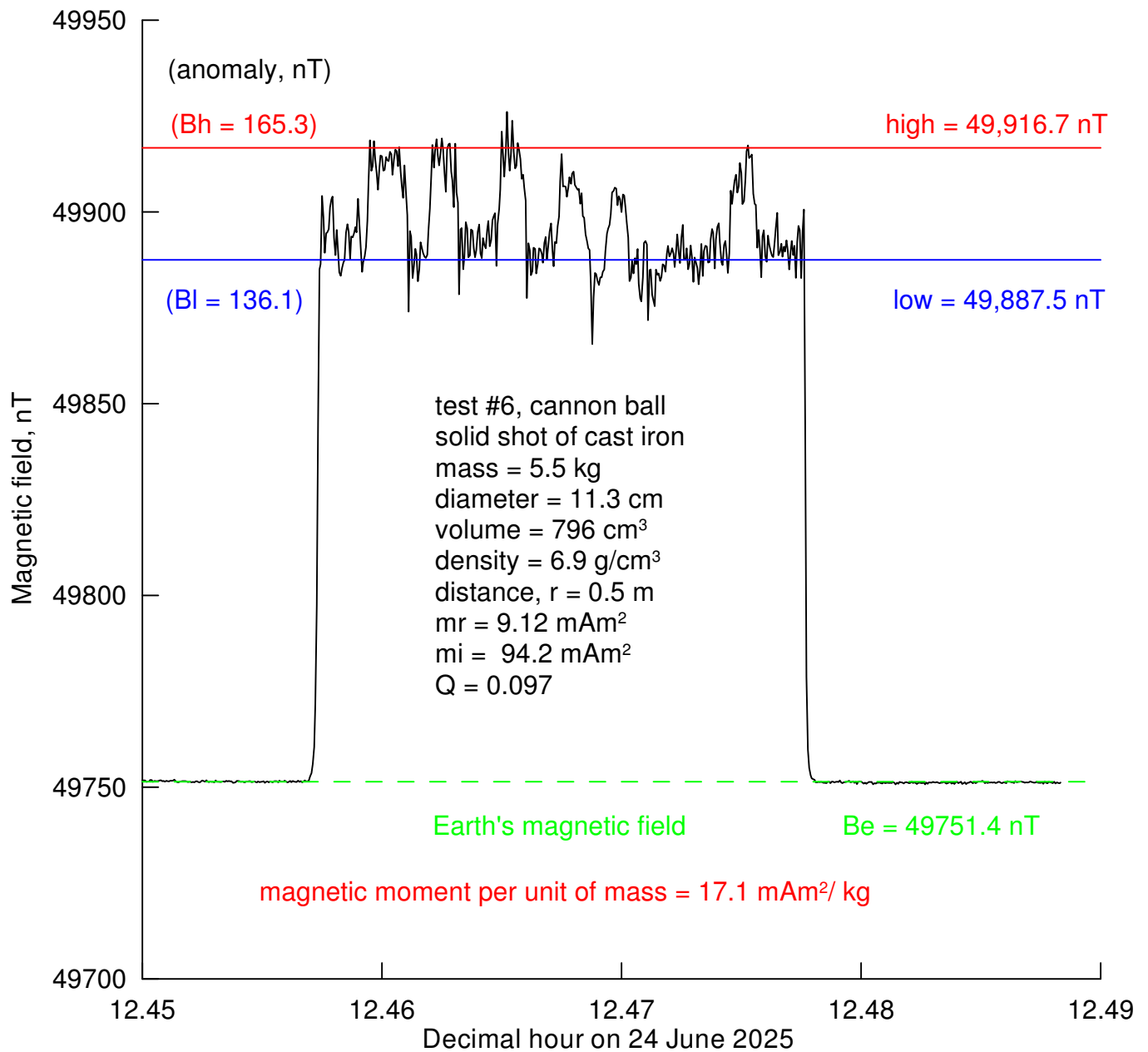


Figure 22: Measuring the magnetic properties of a cannon ball. This graph shows the measurements of a ball that was randomly rotated at a distance of 0.5 m between the middle of the ball and the middle of the magnetic sensor. The red line approximates the peak readings during rotation, while the blue line indicates an estimate of the lowest readings. The text on the right side of the graph lists the total magnetic field of the Earth (49,751 nT). On the left, that value of the background Earth's field has been subtracted, resulting in the two anomalous readings that are placed between parentheses. [details](#)

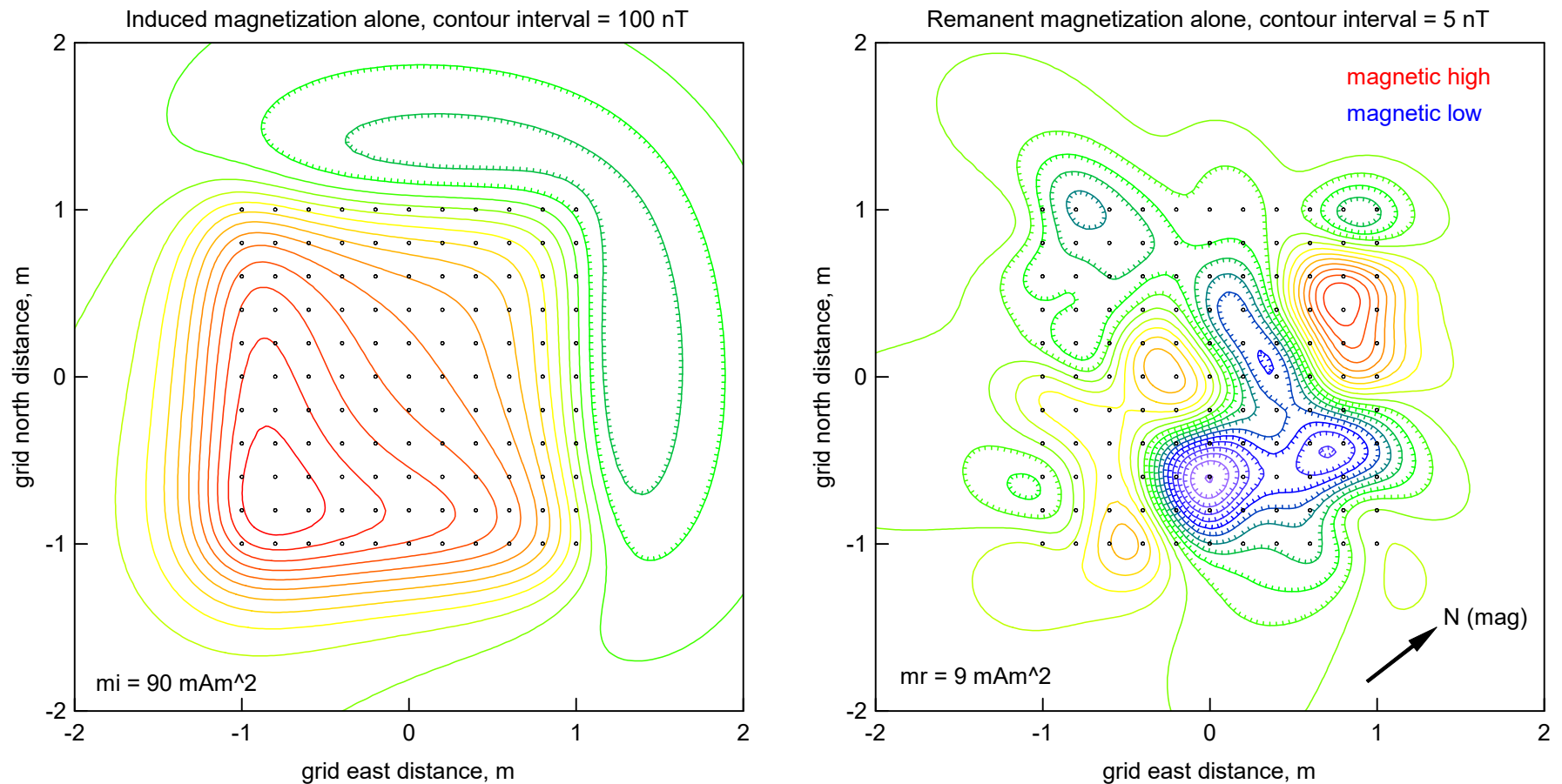


Figure 23: The calculated magnetic anomaly a group of 121 cannon balls. The small circles locate their centers, without showing their size. On the left, each ball has only induced magnetization, and a simple anomaly is created. On the right, the map shows the anomaly caused by random remanent magnetization; note that the contour interval for this map is much smaller than that on the map of induced magnetization. Since the remanent magnetization is one-tenth of the induced magnetization ($Q = 0.1$), the complex remanent pattern will cause only small changes as compared to the map of induced magnetization. [details](#)

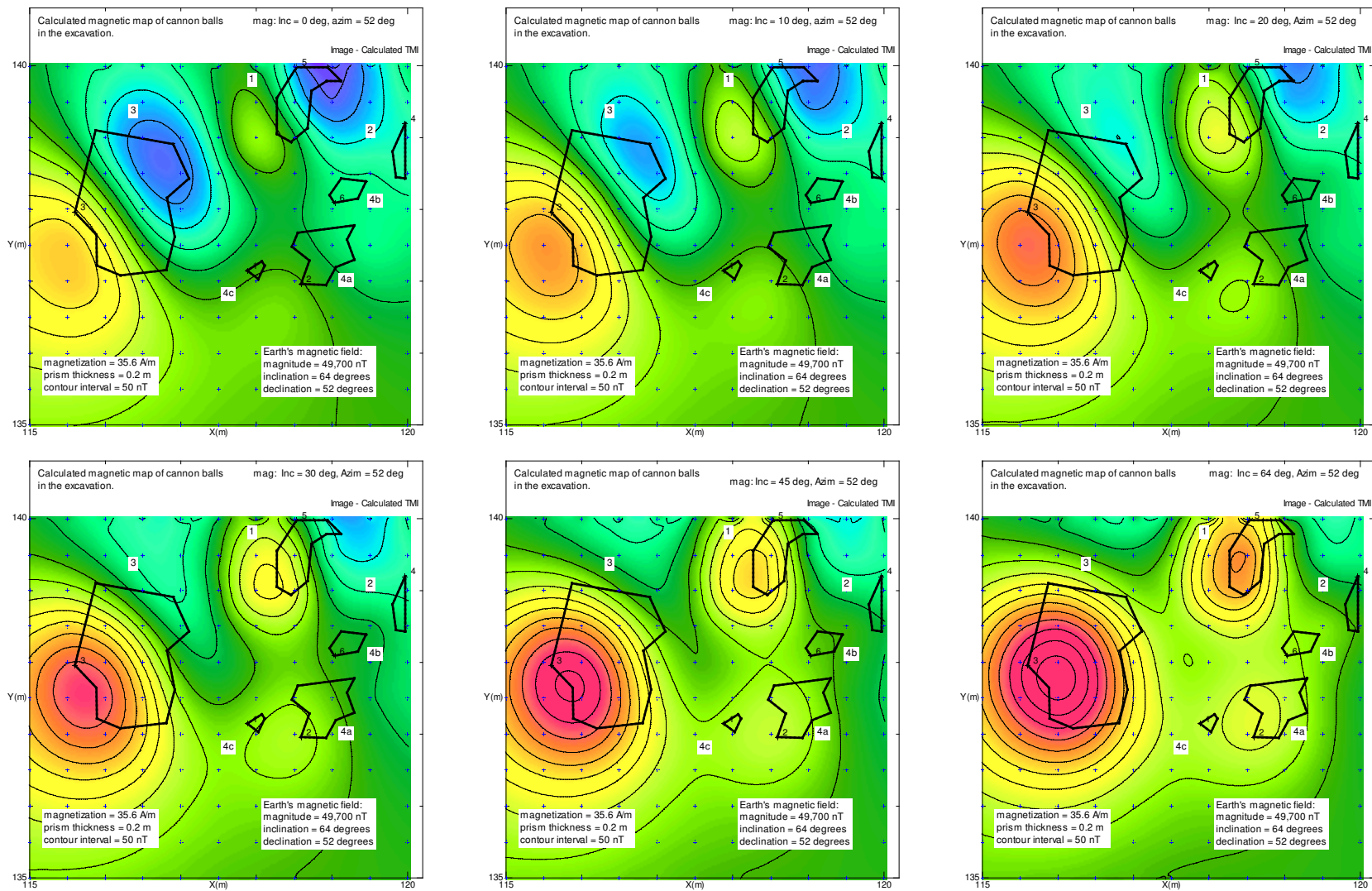


Figure 24: Versions of the calculated magnetic map of the known and excavated features. These maps show the effect of changes in the inclination of total magnetization; see the value for "mag: Inc" near the upper right corner of each panel. The directions that are calculated here vary between 0 (horizontal, at the upper left) and 64° (Earth's field, at the lower right). Notice how the magnetic highs become stronger and the lows become weaker as the inclination increases. [details](#)

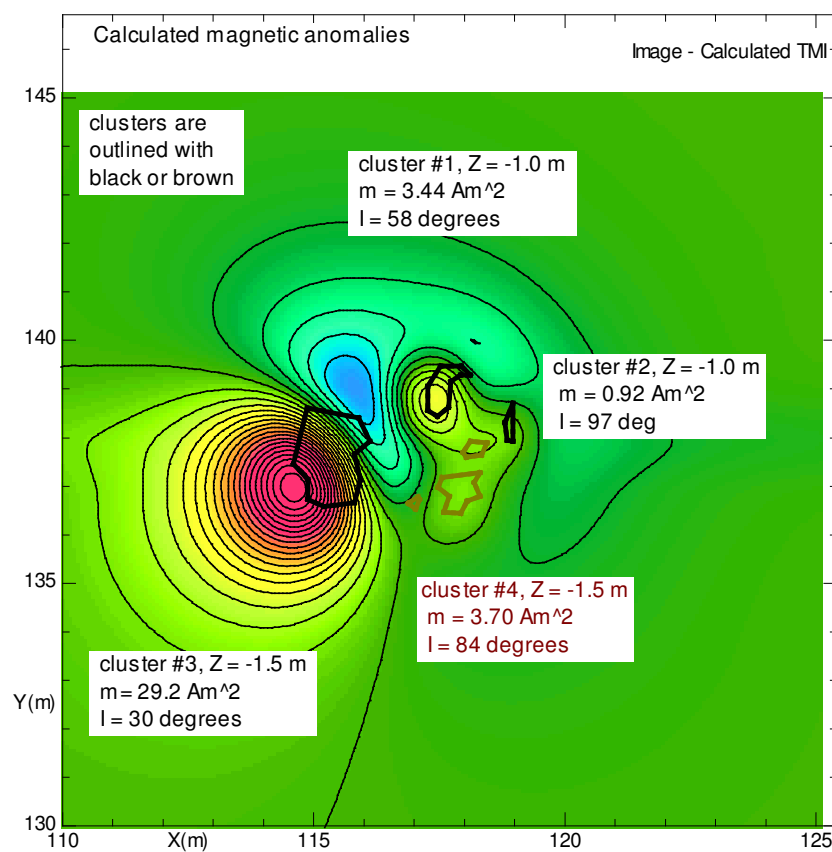
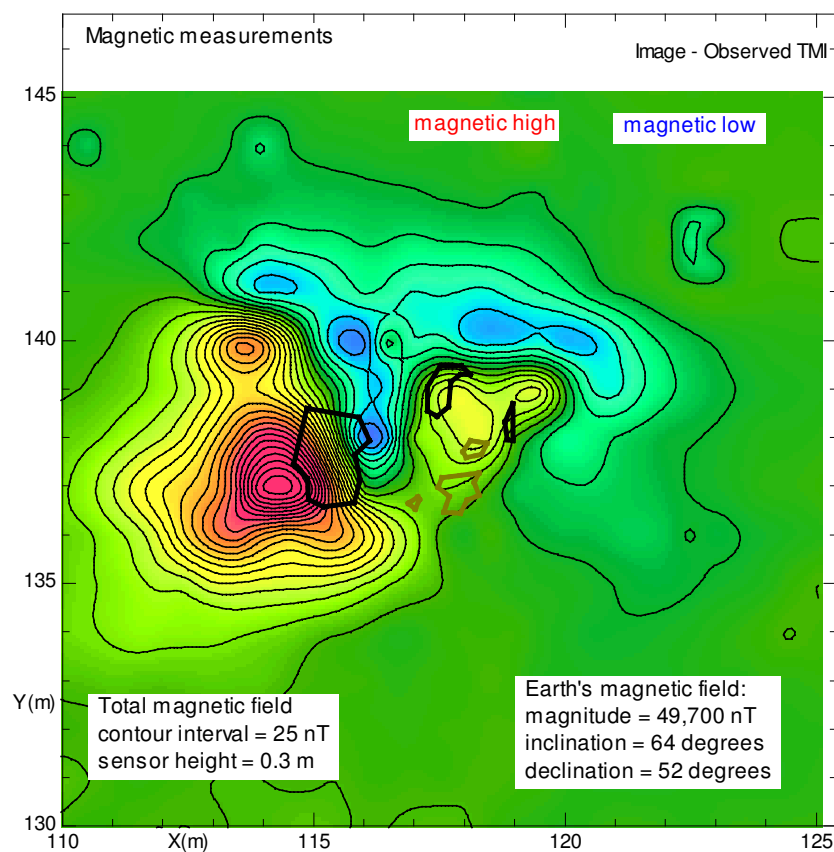


Figure 25: An important comparison at the powder magazine. The magnetic measurements that were made before the excavation are on the left, while a calculation of the magnetic anomalies of the clusters of cannon balls that were revealed in the excavation is plotted on the right. Note the inclination angles of magnetization for each cluster; the large cluster #3 has an angle of only 29°, much less than the inclination of the Earth's magnetic field (which was 64°). This is an indication that the magnetic feature is probably rather flat and horizontal. [details](#)

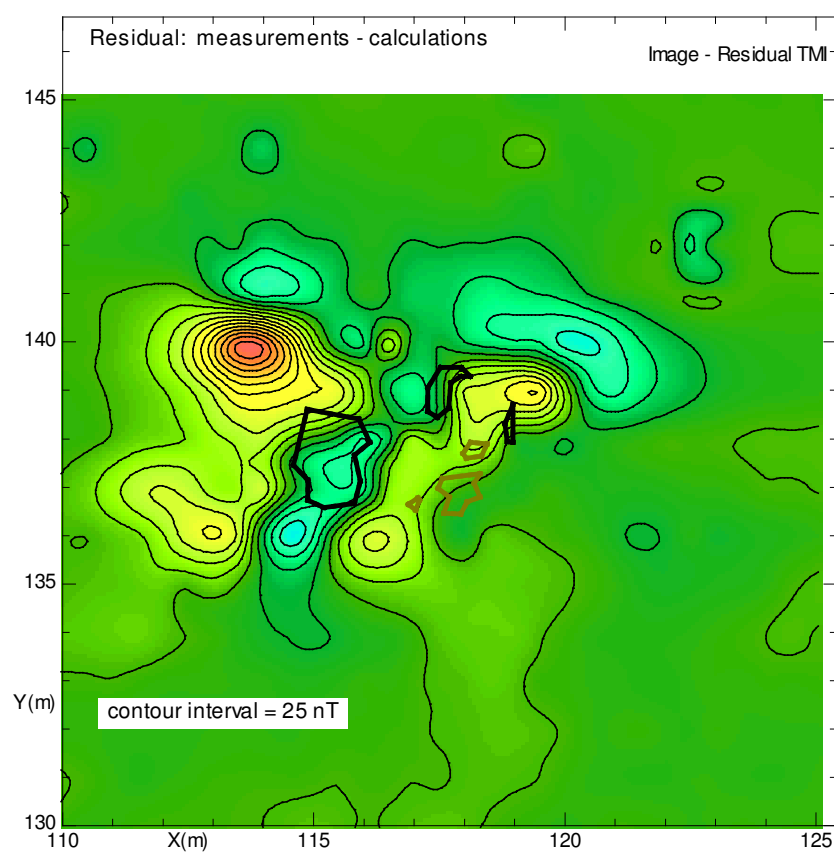
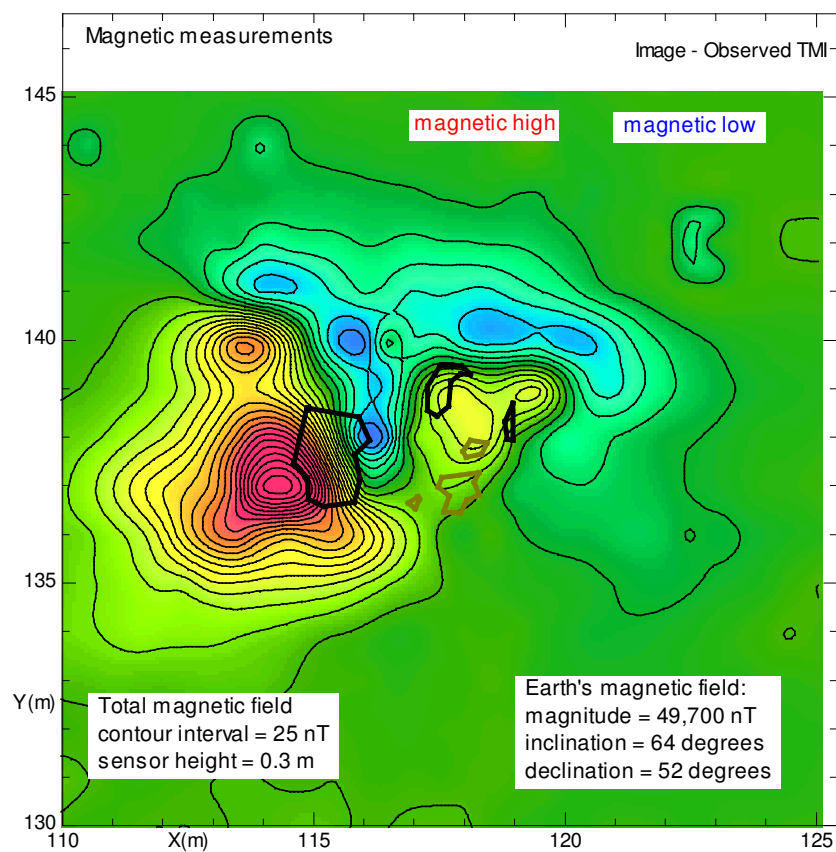


Figure 26: A direct comparison between the measurements and calculations at the powder magazine. The magnetic map that was measured before the excavation started is on the left. The map on the right shows the difference after the calculations (on the right side of [Figure 25](#)) have been subtracted from the measurements. The anomaly on the left has been reduced, but not eliminated. [details](#)

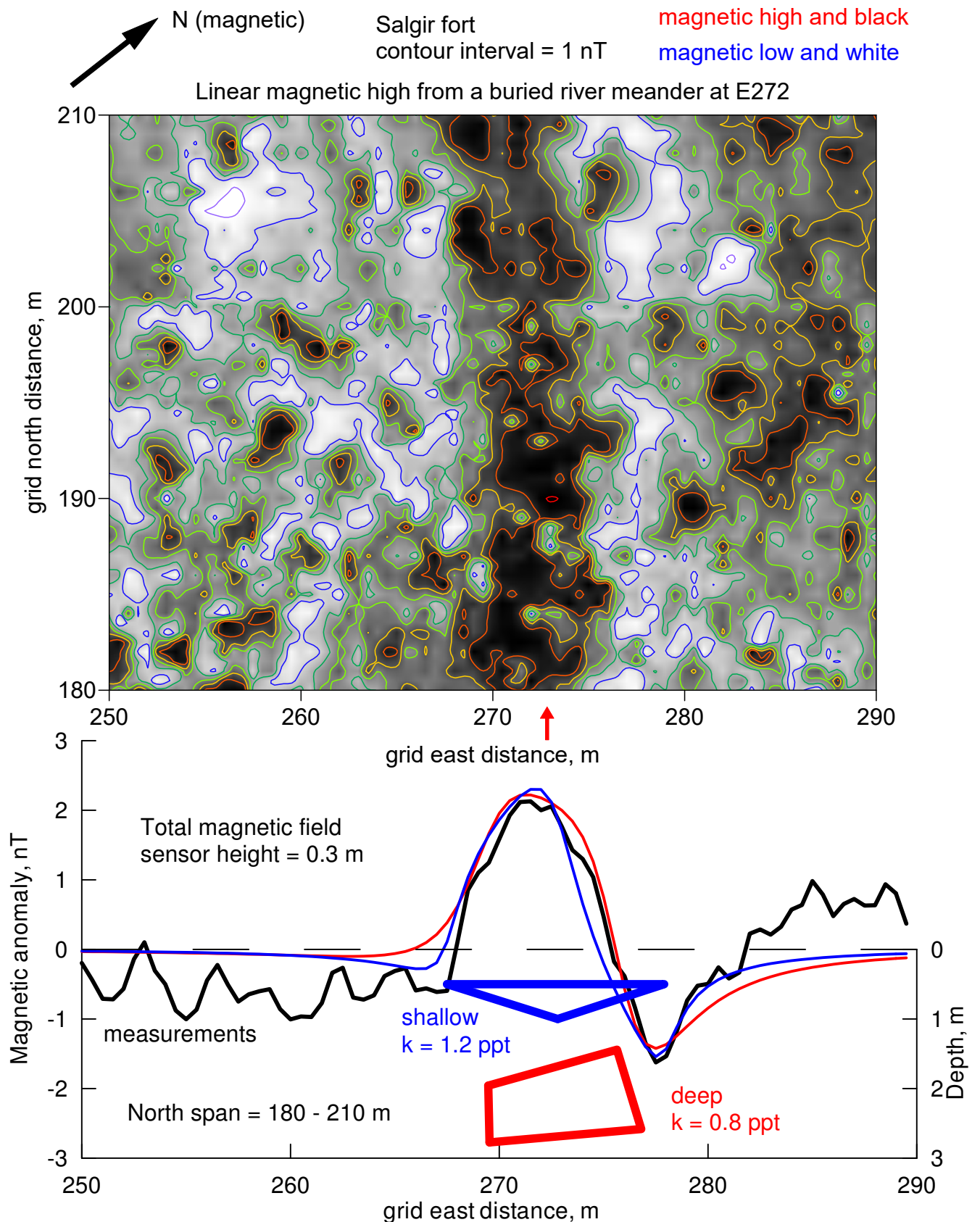
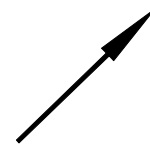


Figure 27: A segment of a now-buried meander of the Salgir River. The magnetic map in the upper panel shows it as a dark band (magnetic high) that is vertical. The magnetic calculations in the lower panel indicate two possible cross-sections, with either 3 sides (a blue triangle) or 4 sides (a red quadrilateral). [details](#)

gray levels:
black = +10 nT
white = -10 nT

contour lines:
interval = 20 nT
range = -200 to 200 without 0 nT
magnetic high
magnetic low

true N



Part of the Salgir magnetic map

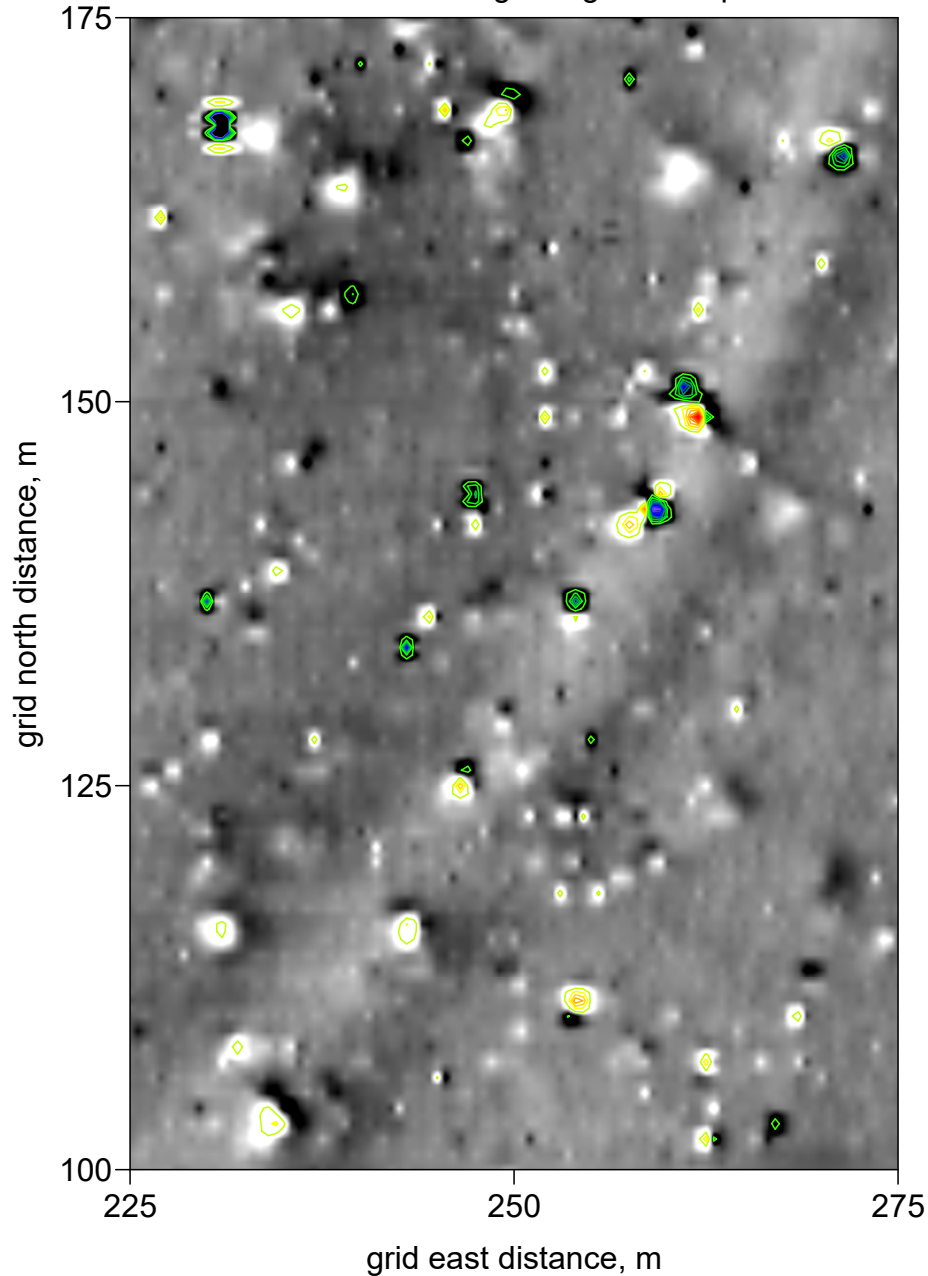


Figure 28: An enlargement of the right-hand side of the magnetic map of [Figure 13](#). This is a continuation of the paleochannel shown in [Figure 27](#). Several magnetic anomalies are along the magnetic band that reveals a river meander. Eight of these were analyzed, and the typical depth of the features was estimated to be 0.6 m. While these are deeper than plowing would have gone, it is most likely that these are relatively-modern steel objects.

[details](#)

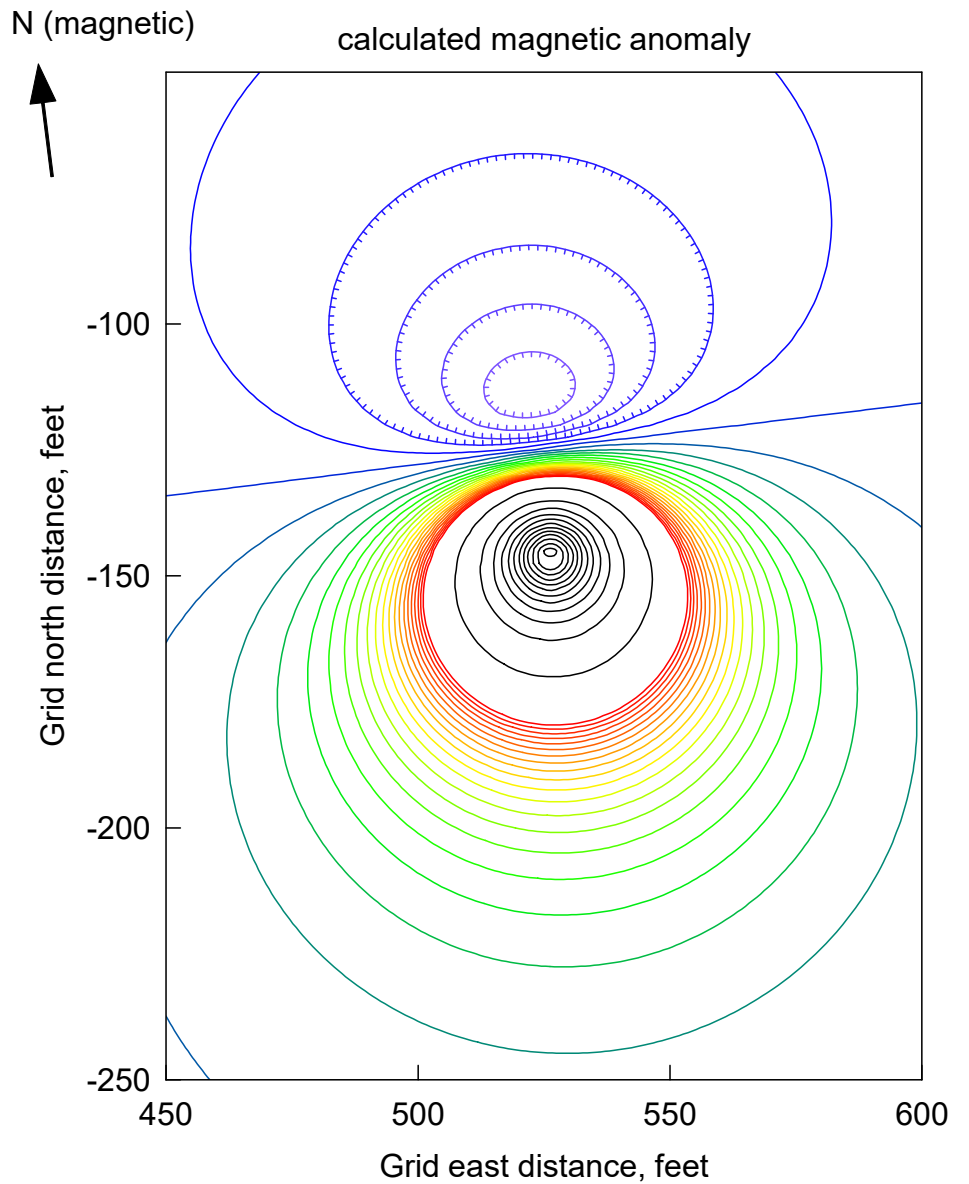
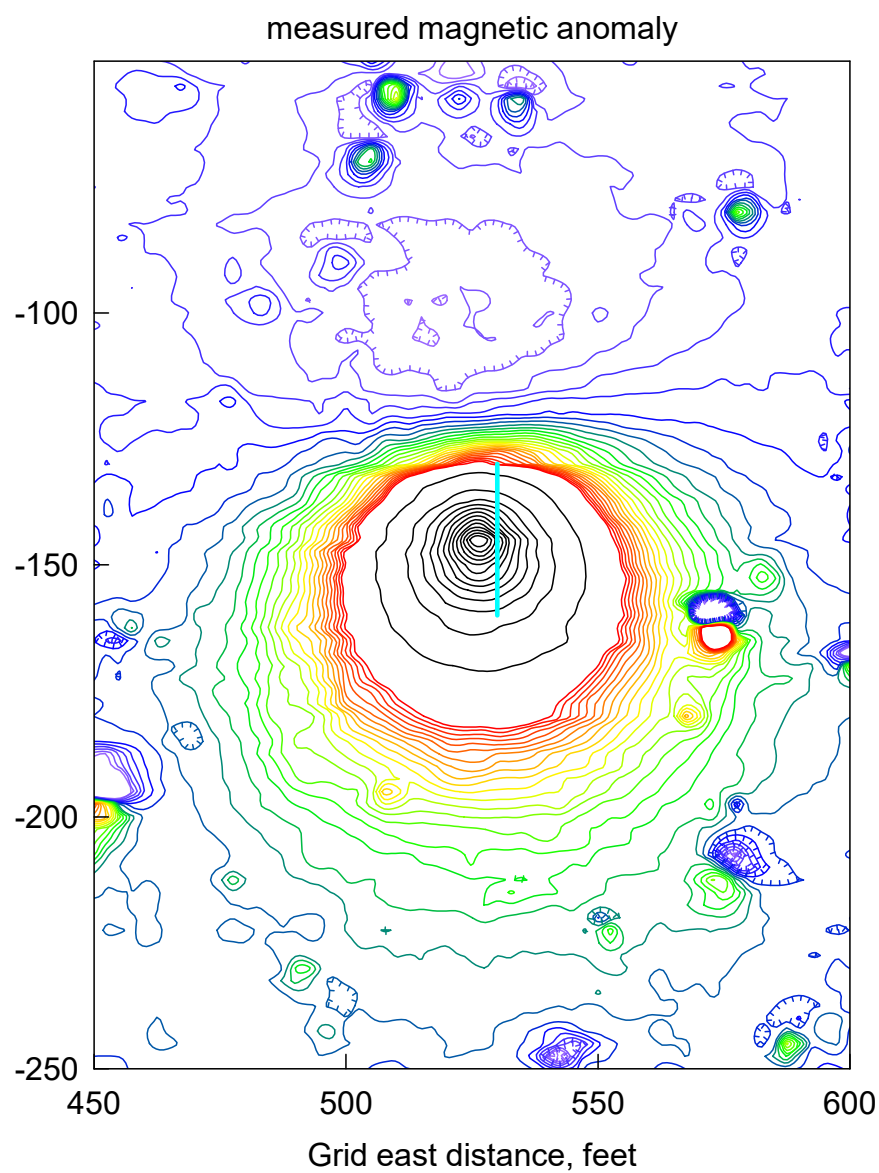


Figure 29: The magnetic anomaly of an iron-filled well that is not visible at the surface. The measurements on the left reach a peak anomaly of almost 2800 nT. The ground width of this map is about 46 m. The calculations on the right are for a magnetic monopole at a depth of about 2 m. Colored contour lines are at intervals of 5 nT; at an amplitude of 100 nT and greater, contour lines are black and at intervals of 100 nT. [details](#)

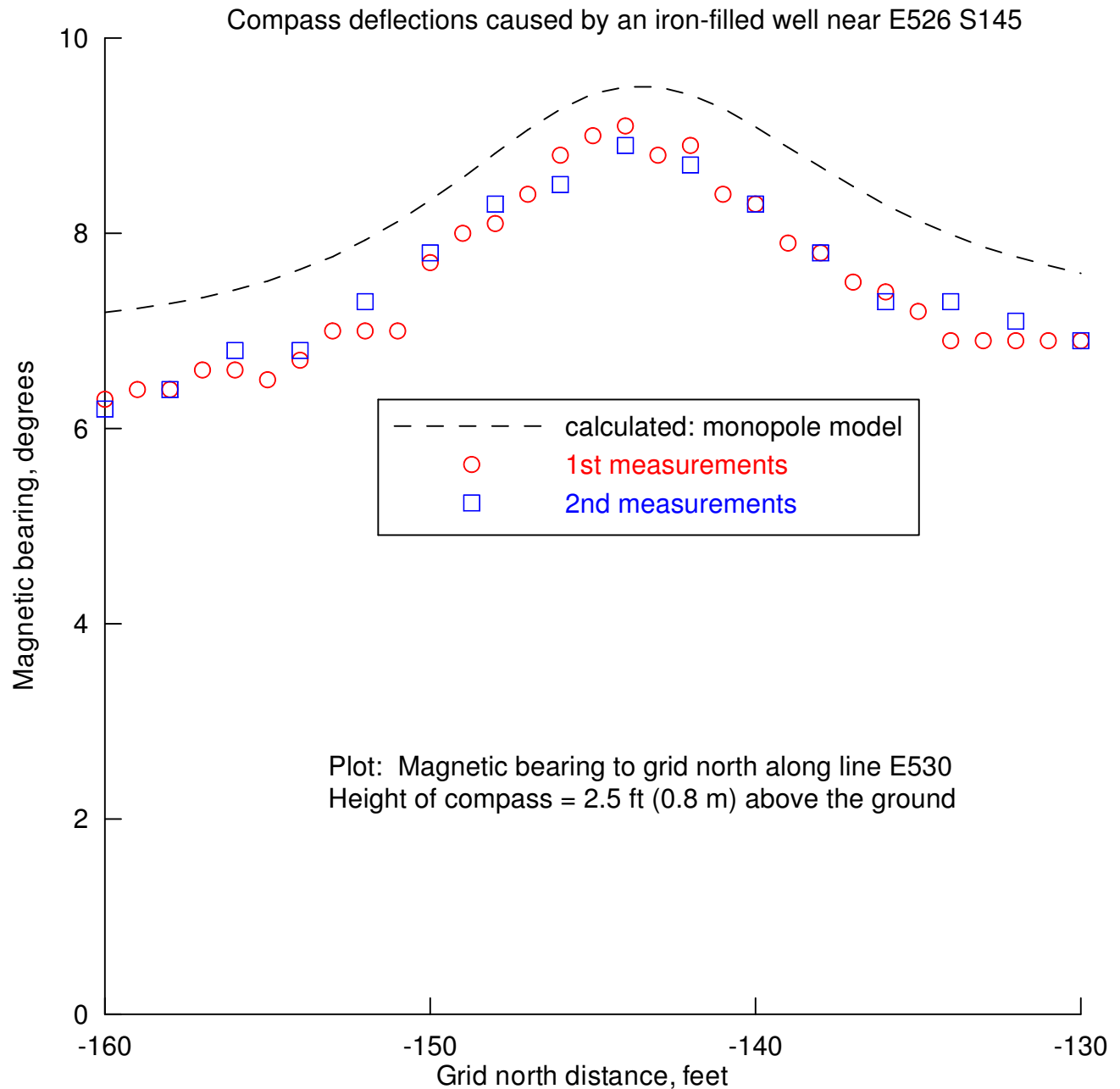


Figure 30: The deflection of the needle of a magnetic compass near the well. It swings to the right (greater declination) by about 2.5° when it is near the well. The measurements were repeated, and the second values are the same as the first test. Simple measurements like this have also been used to detect ships that have sunken and may be either underwater or underground. However, a magnetometer is both faster and more sensitive. [details](#)

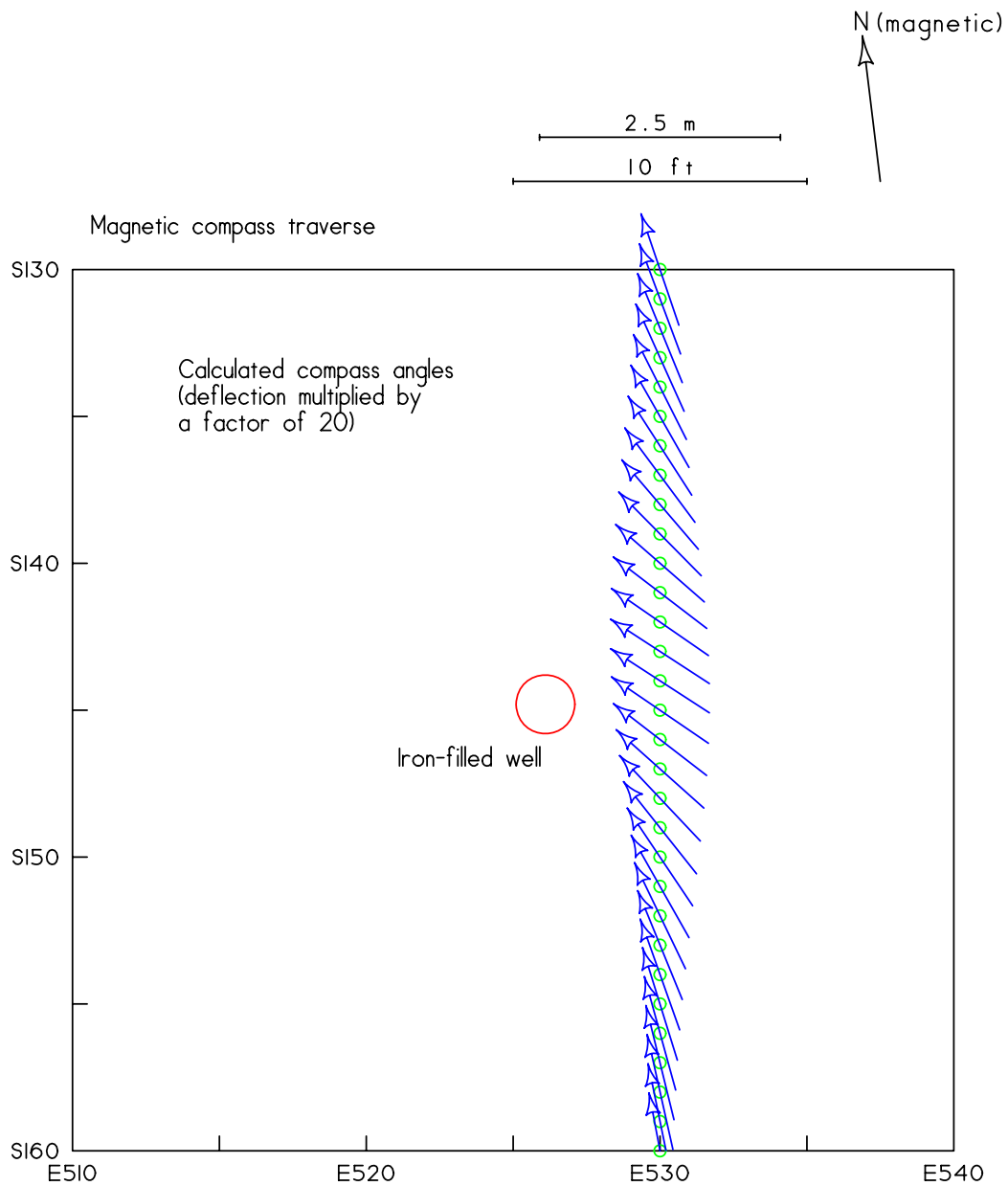


Figure 31: Another view of the changes in direction of a magnetic compass. This shows how the north end of the compass will swing toward the magnetic feature, and the maximum swing just measured when the compass was next to the well. [details](#)

Contour lines:
black -80 to +80 at 20 nT
color -1800 to +1200 nT at 100 nT

magnetic high
magnetic low

Total magnetic field:
sensor height = 3 feet (1 m)
measurement spacing = 5 feet (1.5 m)

Magnetic map, Virginius Island, Harpers Ferry, West Virginia, USA

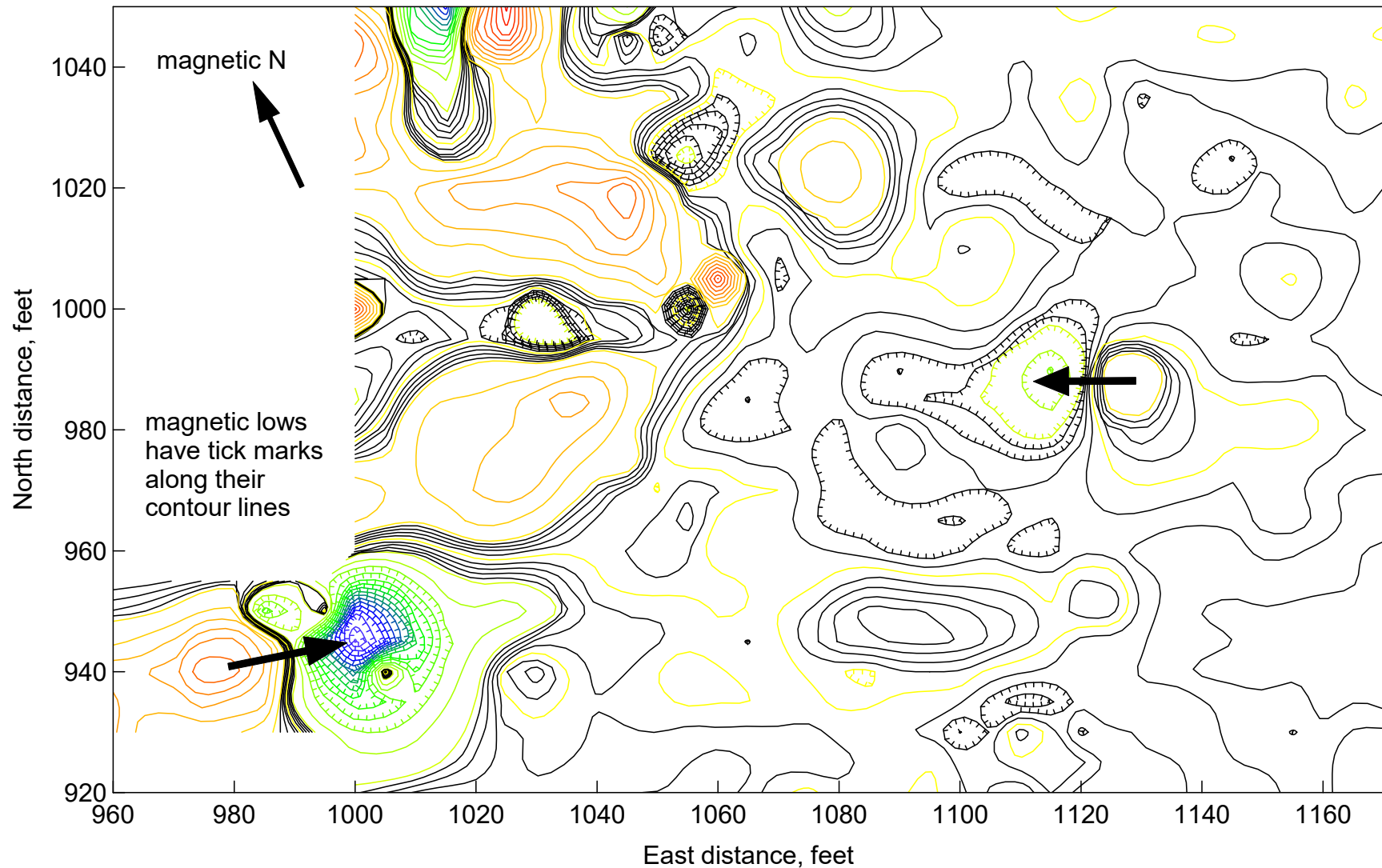


Figure 32: Masses of now-buried iron in an industrial area. The magnetic anomalies can be greater than 1000 nT, and the sources are probably deeper than 1 m. The ground width of this map is 64 m. Two bipolar anomalies (each having a high and a low) are marked with black arrows; there is probably a single object at both locations. [details](#)

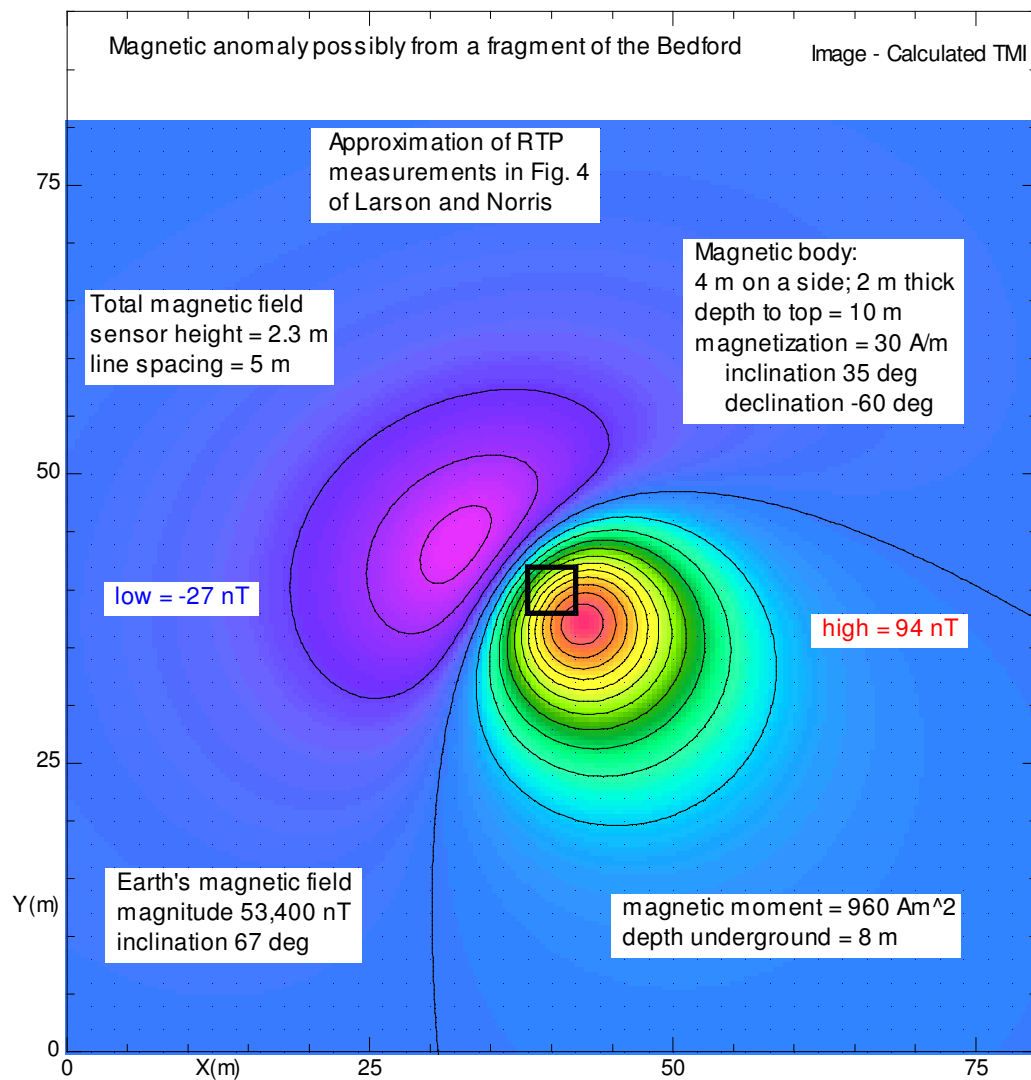


Figure 33: A calculated magnetic anomaly that is similar to a measured anomaly. It is possible that this anomaly has been caused by a part of the steamboat Bedford (82 tons = 75 Mg) that was sunk in 1840 on the Missouri River in the US. The spatial size, pattern, and amplitude of this rather circular pattern are about the same as those shown on the map of magnetic measurements. This calculation suggests that the depth of the feature is about 8 m. [details](#)

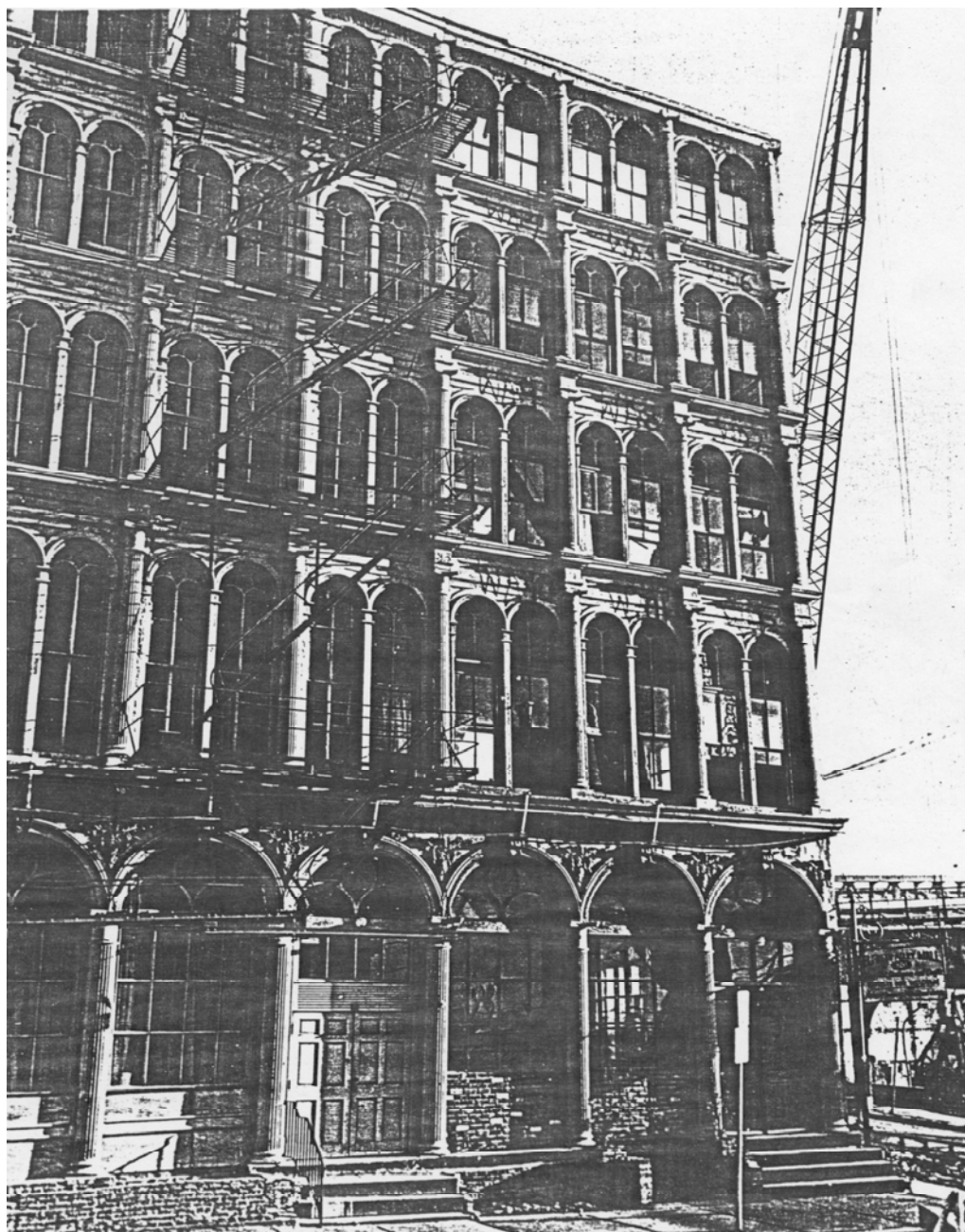


Figure 34: Saving an old building. The cast iron facade (made in the 1800s) of this building in Philadelphia (USA) was carefully dismantled and removed for storage in an empty water reservoir. That reservoir was later filled with soil, covering the facade with 2 - 3 m of earth and stone; the location of the facade was lost. [details](#)

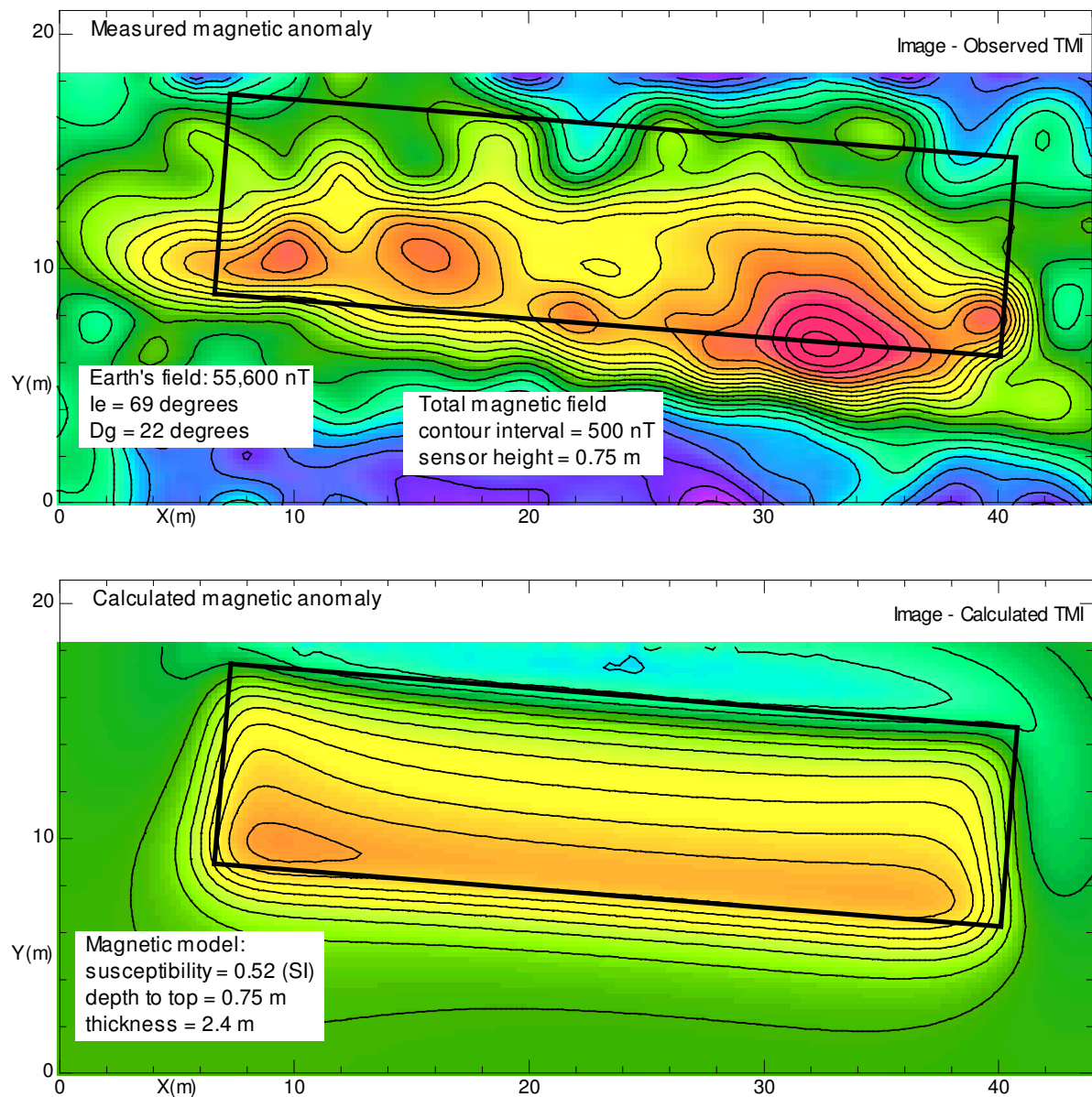


Figure 35: The measurements of a magnetic anomaly (at the top), and the calculation of a simple magnetic model (at the bottom). A black rectangle outlines the magnetic slab in both maps. The high anomaly (red) in the measurements has an amplitude of about 7000 nT. The approximate model for this calculated anomaly has a magnetic moment of 16,000 Am².

[details](#)

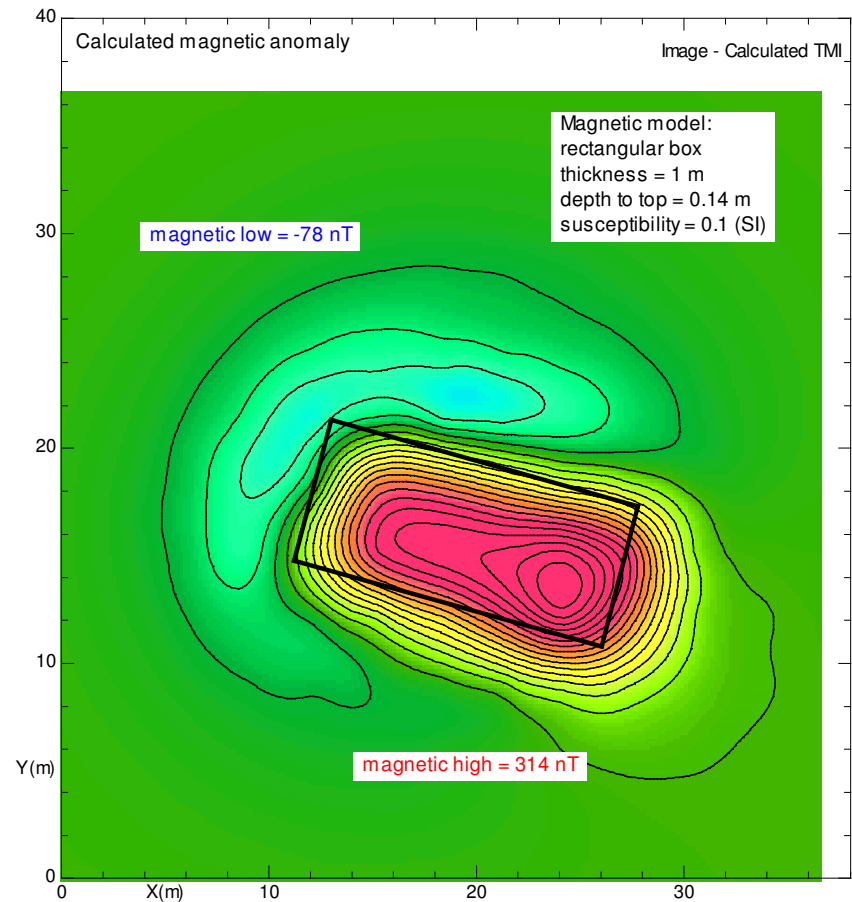
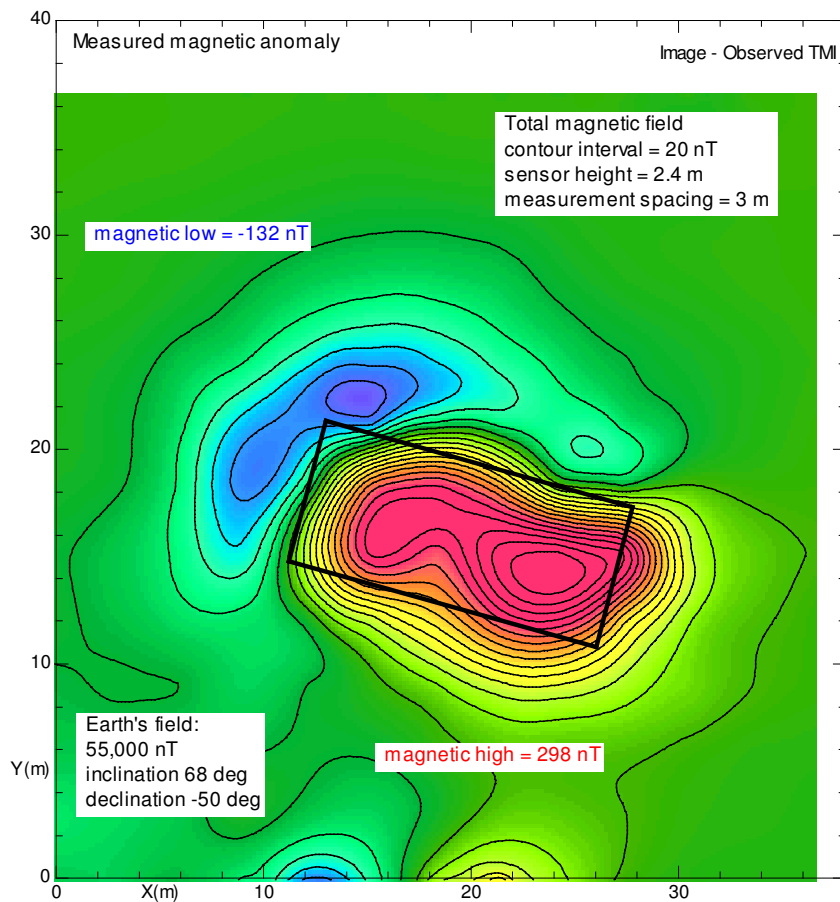


Figure 36: The magnetic map of a large mass of buried iron. The measurements are plotted on the left, and the magnetic high near the iron is colored red. The map on the right has been calculated for a rectangular body at a shallow depth; it is outlined with black in both panels. The volume of this model body was $V = 104 \text{ m}^3$ and its contrast in its magnetic susceptibility was $k = 0.10 \text{ (SI)}$. The Earth's magnetic field at this site was $B_e = 55,000 \text{ nT}$, so its intensity of magnetization was $H_e = B_e / 1257$ or 44 A/m . Therefore, its magnetic moment was $m = V * k * H_e = 460 \text{ Am}^2$. Assuming that the relative magnetic moment of iron is $0.1 \text{ Am}^2 / \text{kg}$ (see [Figure 2](#)), the mass of buried iron could be 4600 kg. [details](#)

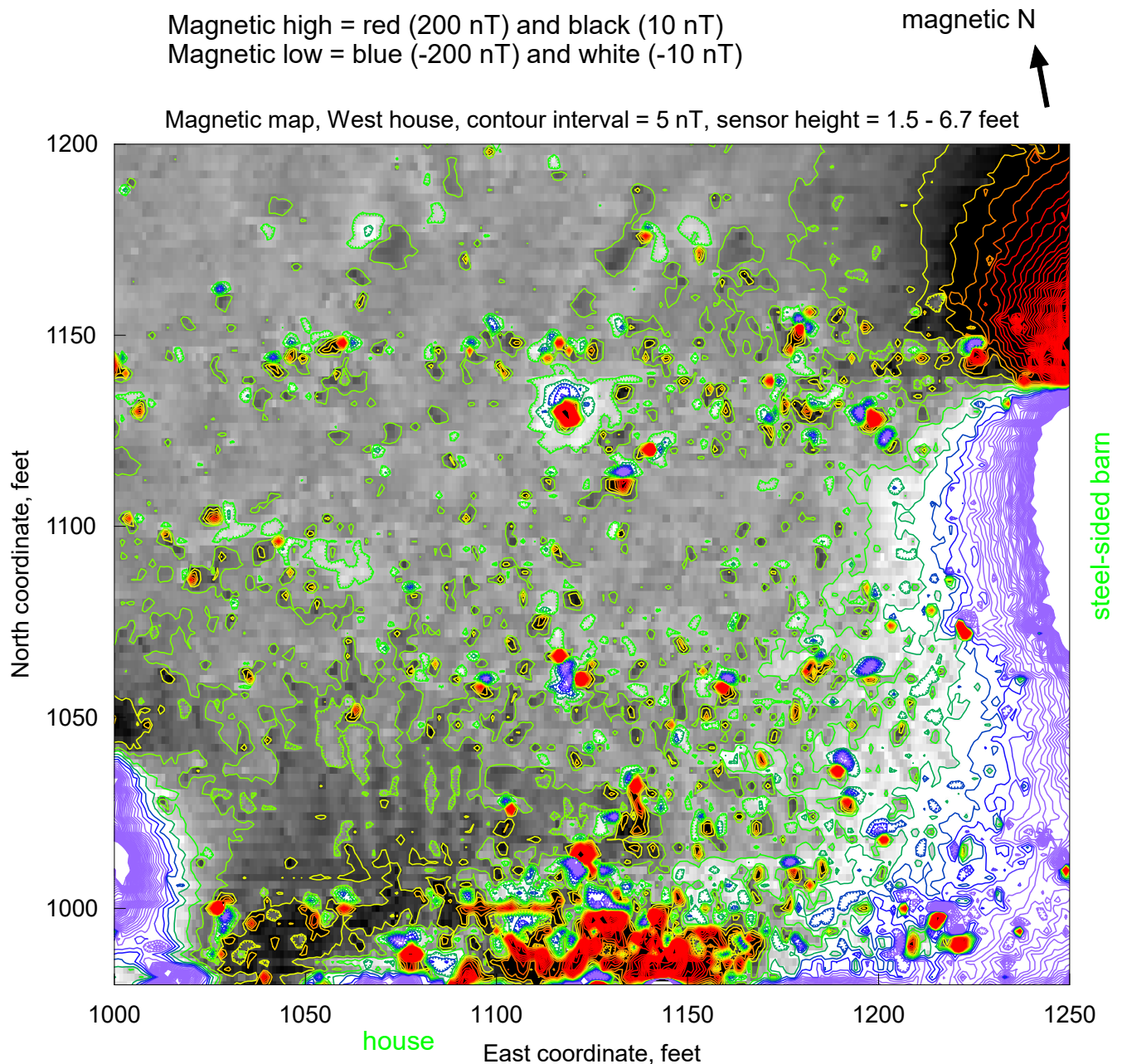


Figure 37: The total-field magnetic map of an area that is 76 m wide. The map was measured in the USA state of Virginia, and the area has long been farmed. Broad and strong anomalies are caused by unimportant structures that are just outside the area of the map: A metal-sided barn is at the east side, and a wood-framed house toward the south. The polarity of the anomaly from the barn is opposite from normal (the magnetic high is north of the low); this is because the major source of the anomaly is the steel roof of the barn, which is at a greater elevation than the magnetometer's sensors. These magnetic sensors were at heights of 1.5 feet (0.45 m) and 5.2 feet (1.58 m). The reading from the upper sensor has been subtracted from that of the lower sensor to create this map. Colored contour lines are drawn at intervals of 5 nT, between a range of -200 to +200 nT. A gray-scale map reveals weak anomalies, with a gray range that is spread between -10 (white) and +10 nT (black). [details](#)

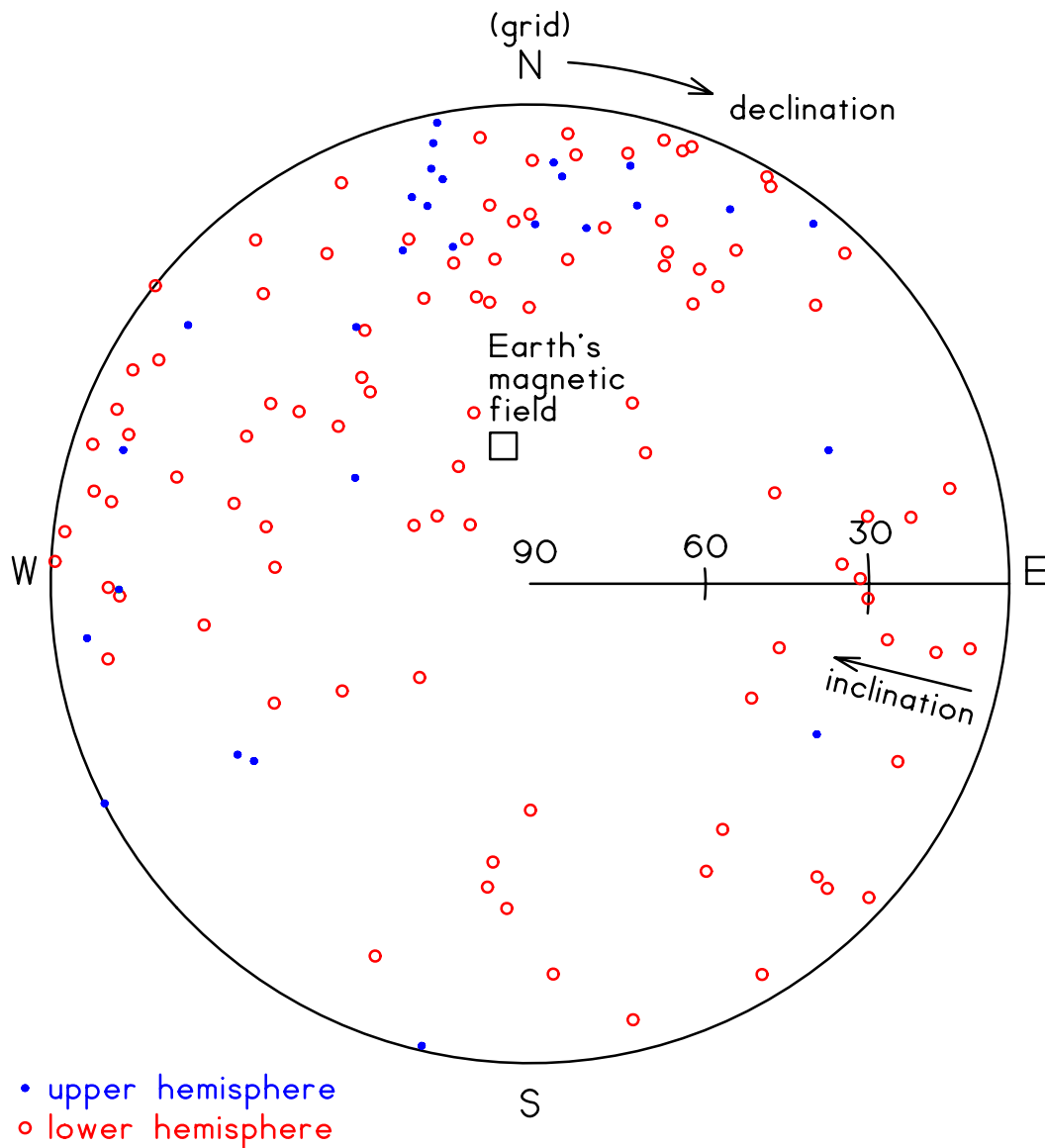


Figure 38: Estimates of the direction of total magnetization of 125 objects that create bipolar anomalies in [Figure 37](#). If a magnetic direction is horizontal, it will be marked along the outer circle; if any direction is vertical and downward, it would be marked at the middle of the circle (at 90° inclination). The larger circles (red) mark directions for anomalies that have a positive inclination (point downwards, therefore are in the lower hemisphere), while small blue circles indicate anomalies whose magnetization points upwards (negative inclination and plotted in the upper hemisphere). The average of the angles of inclination here is 18° . The black square indicates the direction of the Earth's magnetic field at this site, where it has an inclination of 66° . This angle is much greater than the average inclination of the objects.

[details](#)

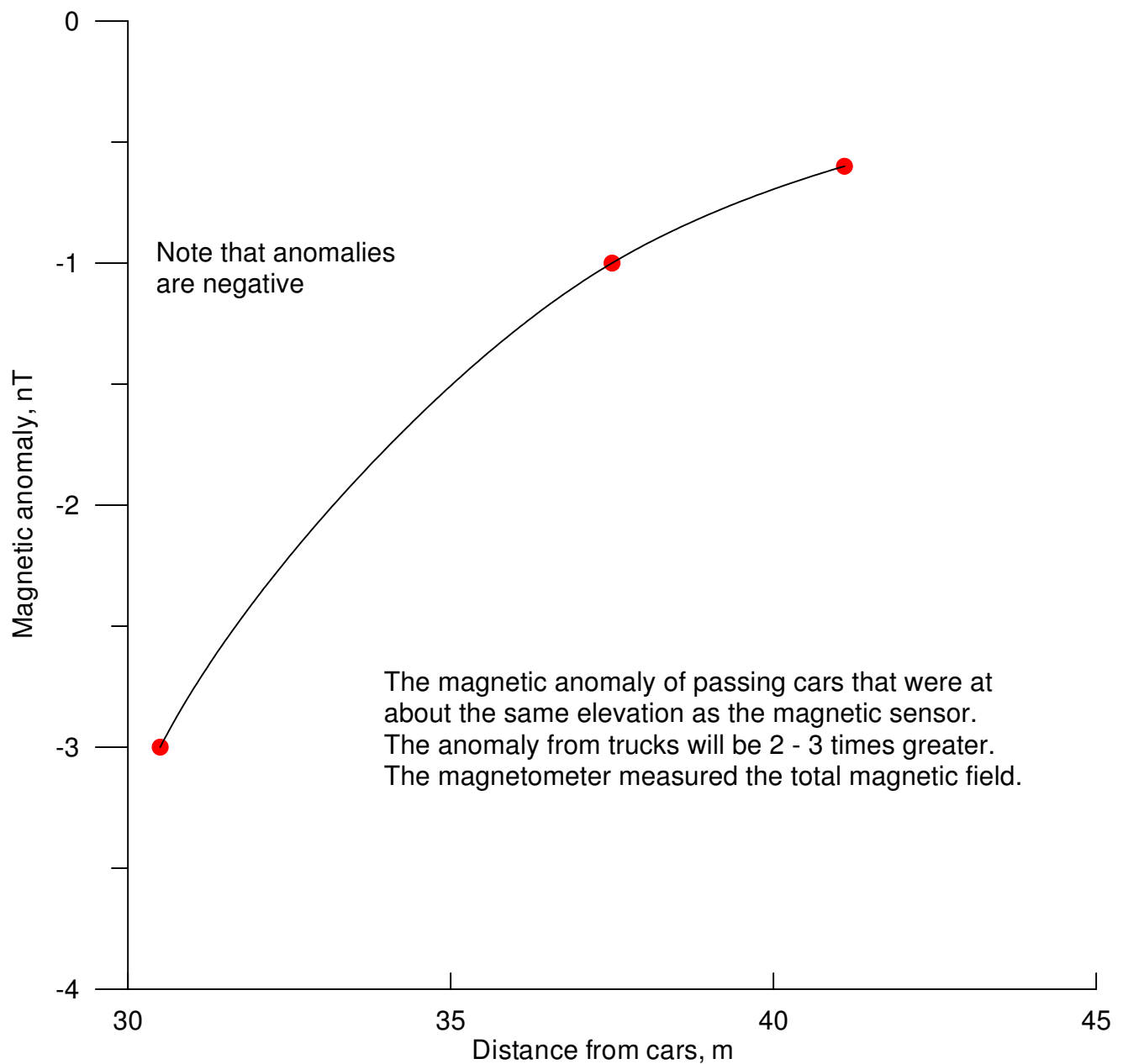


Figure 39: The magnetic anomaly of cars passing at three distances from a nearby road. The magnetic lows are the result of the elevation of the cars being about the same as that of the magnetic sensor. The cars create magnetic lows because the magnetic flux of the Earth is concentrated in the cars; therefore, the flux must be lower at a distance from the cars.

[details](#)

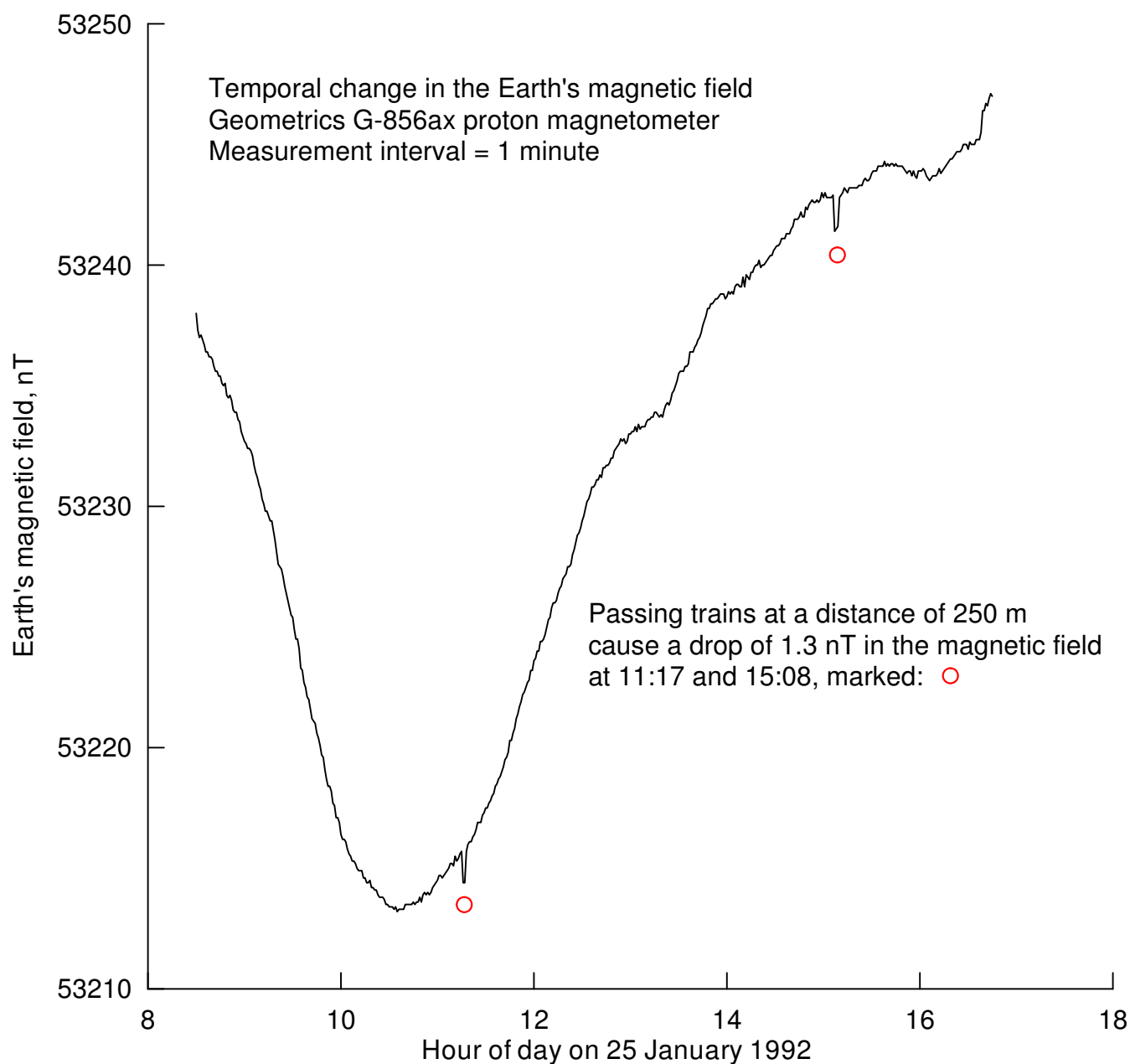


Figure 40: The detection of a distant train in the measurements of a magnetic base station. The magnetic sensor remained at a fixed location. A pair of small dips in the readings are caused by two freight trains that passed by at a distance of 250 m. [details](#)

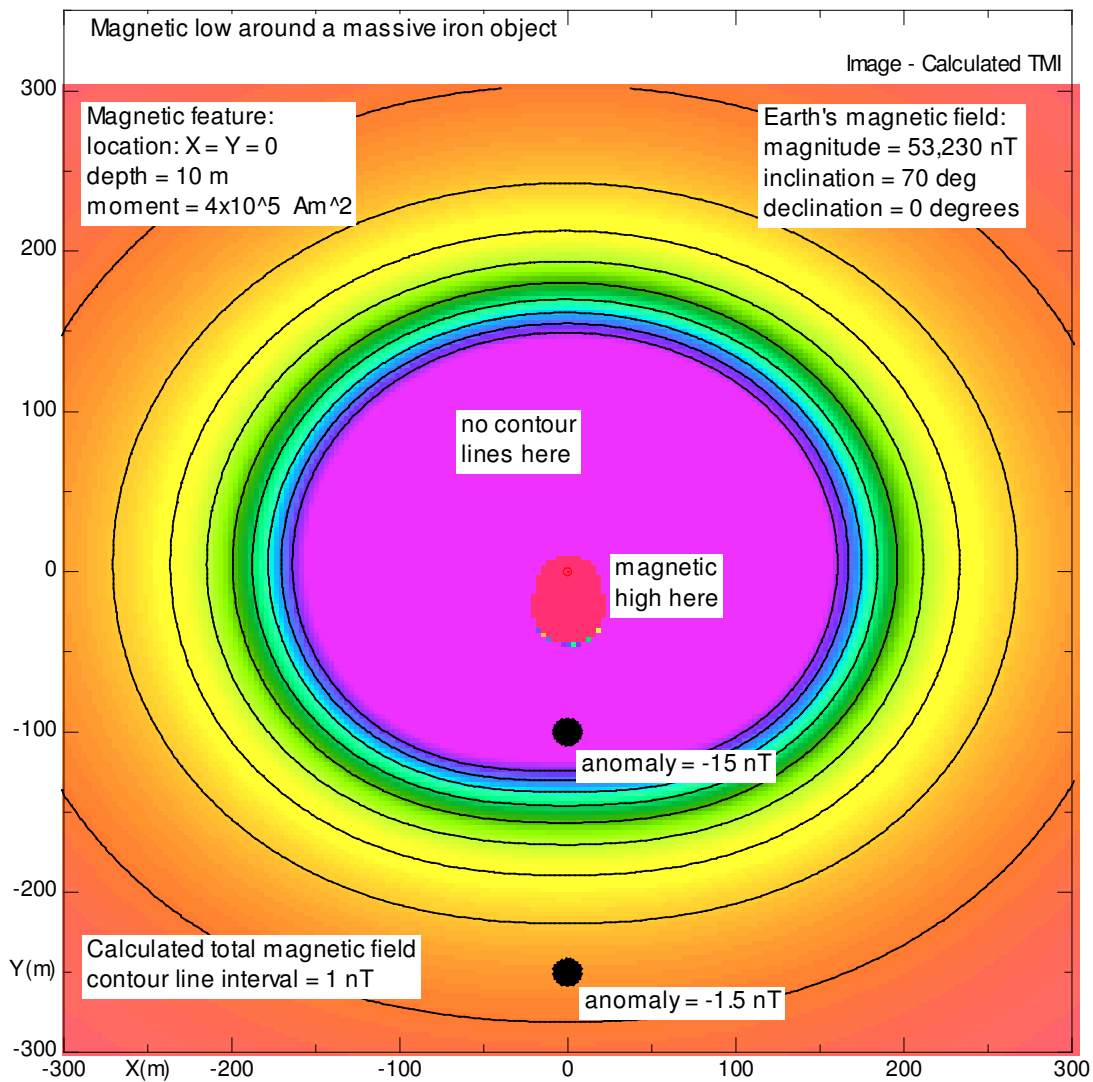


Figure 41: The calculated map (600 m on a side) around an intensely magnetic iron object. That object is a magnetic sphere with a diameter of 5 m. It is located at the center ($X = 0$ and $Y = 0$) of this map. Positive magnetic anomalies are found in the oval area that is red at the middle of the map. Everywhere else, the anomaly is negative. Filled black circles locate two points: At a distance of 100 m south of the object, the anomaly is -15 nT, and at 250 m south, the anomaly has been reduced to -1.5 nT. [details](#)

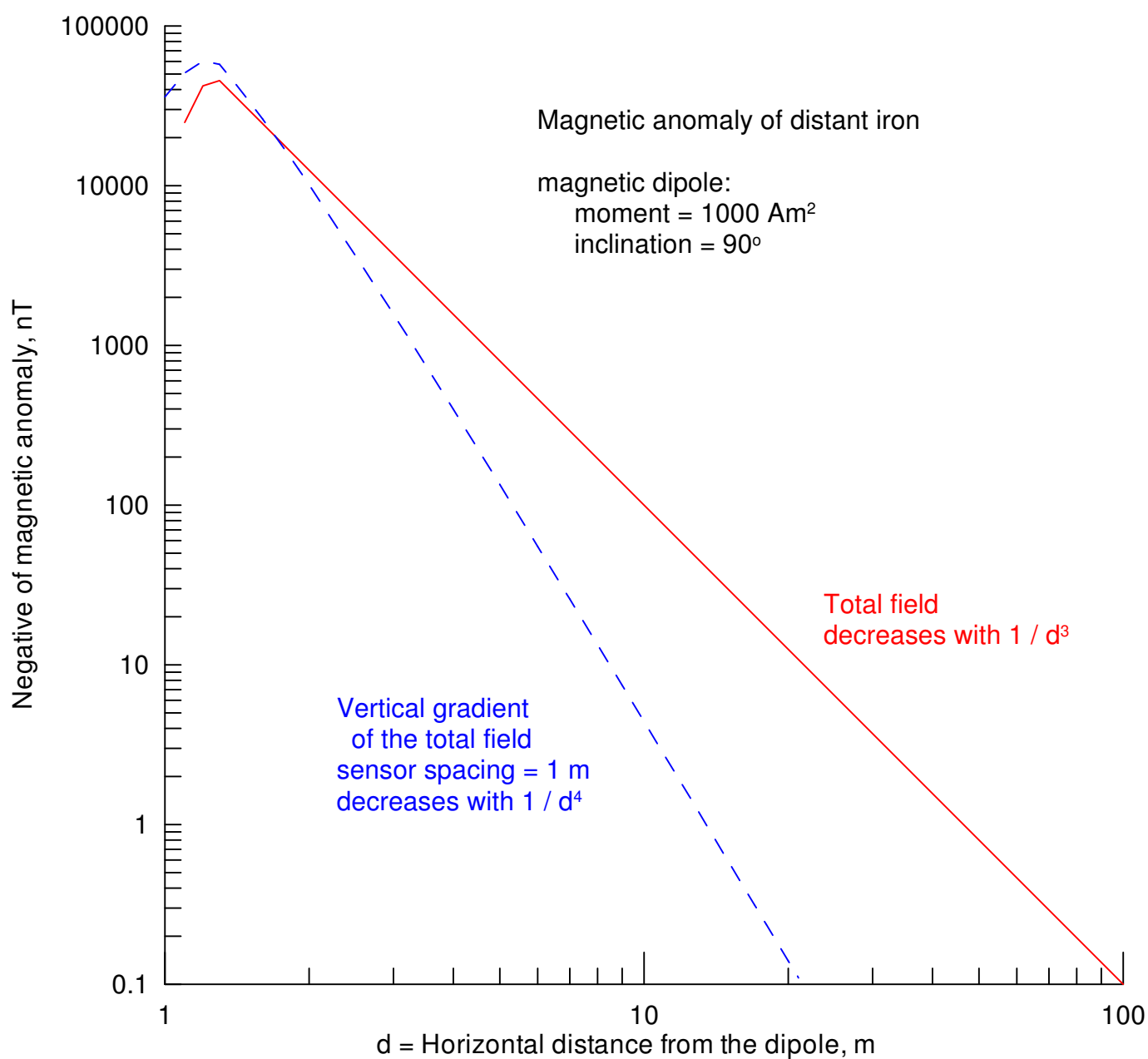


Figure 42: The effect of distance on a magnetic anomaly. The amplitude decreases with the inverse cube of distance for a total field magnetometer. With a gradiometer, the amplitude decreases faster; therefore distant objects will be detected only faintly, and this is often an advantage. Note that all of the anomalies on these curves are actually negative values; they are plotted as positive numbers for convenience. [details](#)

The circle is in a vertical north-south plane and it has a dipole at its middle. Calculations are made at a distance of 1 m from the magnetic dipole. The inclination of the Earth's magnetic field is 70°.

The magnetic anomaly as it changes with the vertical angle to the source

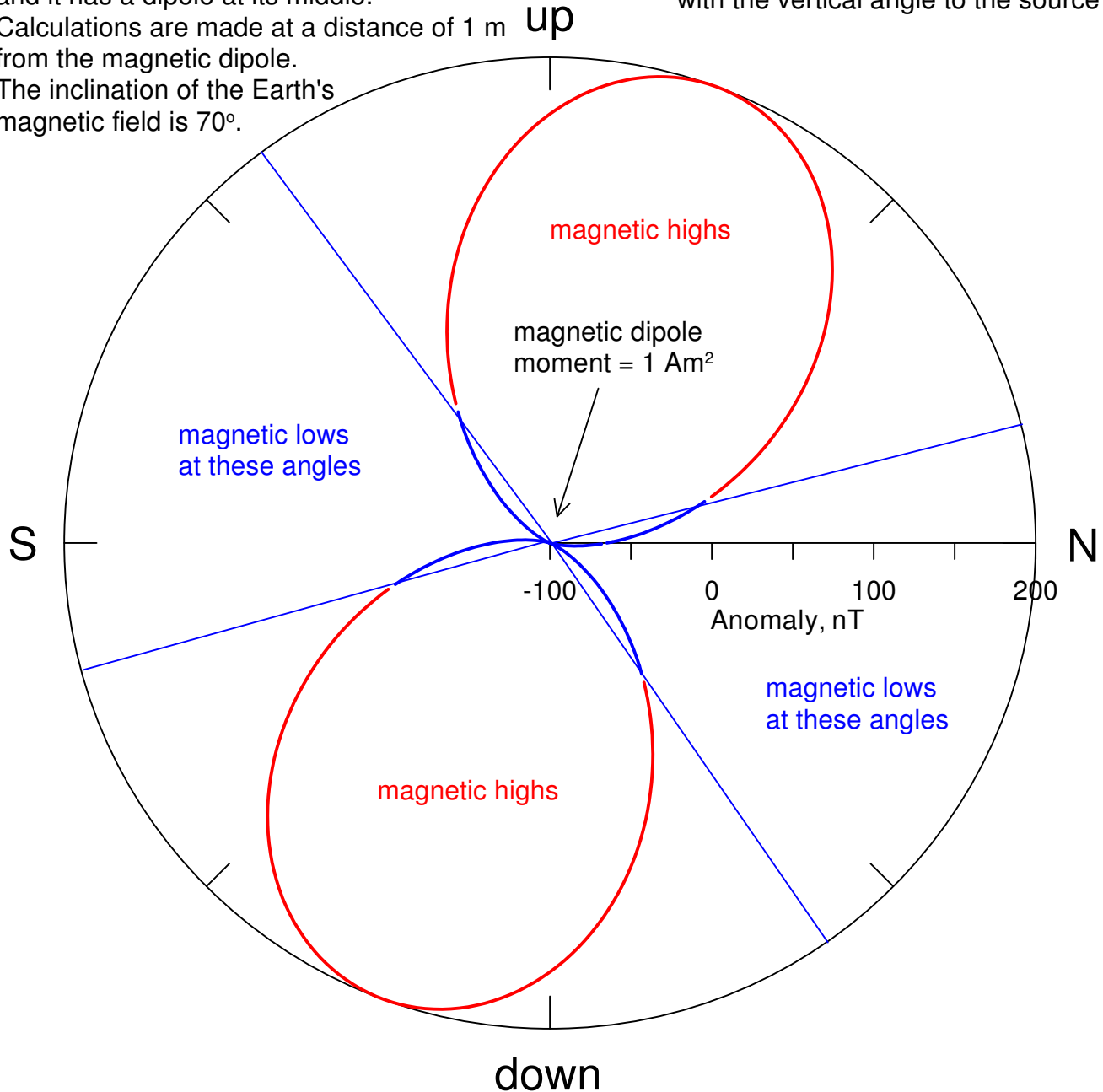


Figure 43: Some unusual calculations. They are made along the circumference of a vertical circle that has a magnetic object at its center. The 8-shaped curve reveals two lobes with magnetic highs; these are drawn with red lines. One high will, as usual, be measured above a magnetic object, but there will also be high readings below the object. It is important to note that there will be magnetic lows (shown as blue) to the north and south of the object at a nearly horizontal angle (that is, at about the same elevation as the object). [details](#)

Total magnetic field, sensor height = 8 ft (2.4 m)
Traverse N - S, measurement and line spacing = 20 ft (6.1 m)
Earth's field = 51,400 nT; inclination = 63 degrees

N (magnetic)



Magnetic anomaly, perforated steel plate, contour interval 500 nT

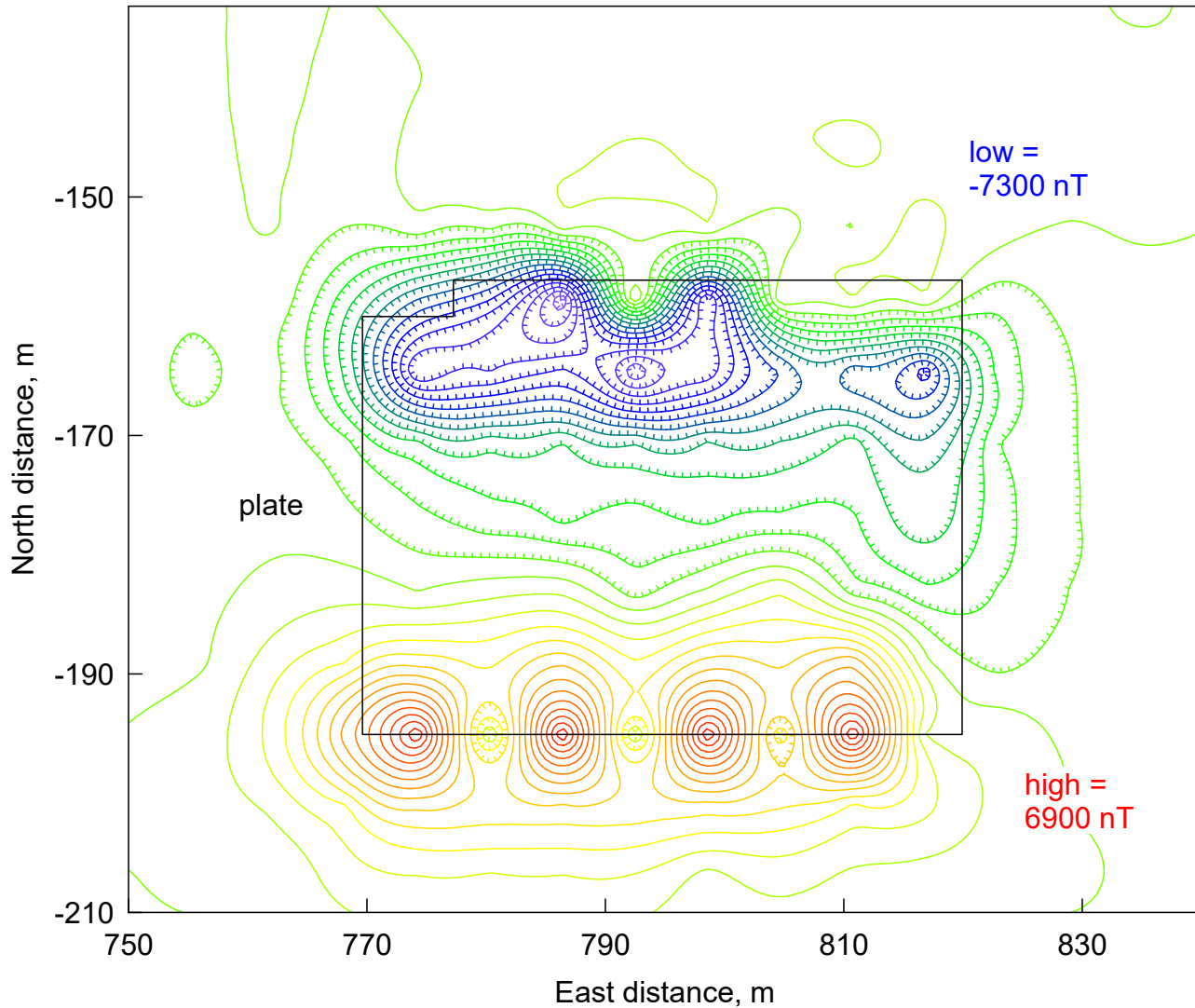


Figure 44 The magnetic anomaly of a large and flat steel plate. This rectangular feature is created by a group of steel plates that have been joined together to make a hard and weatherproof surface that may be used for a quickly-built airport runway. The black line defines the edge of this steel plate. [details](#)

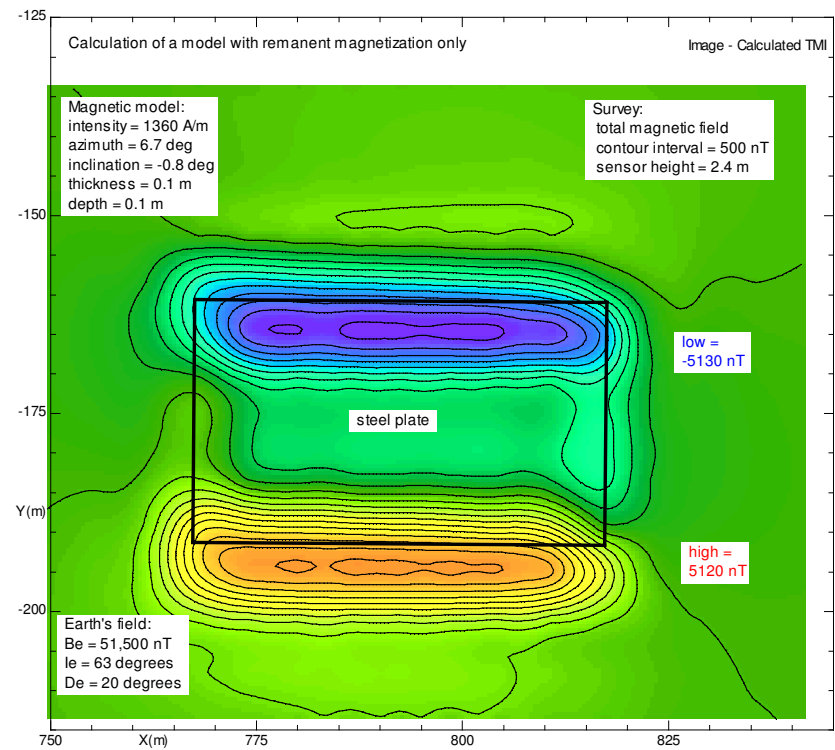
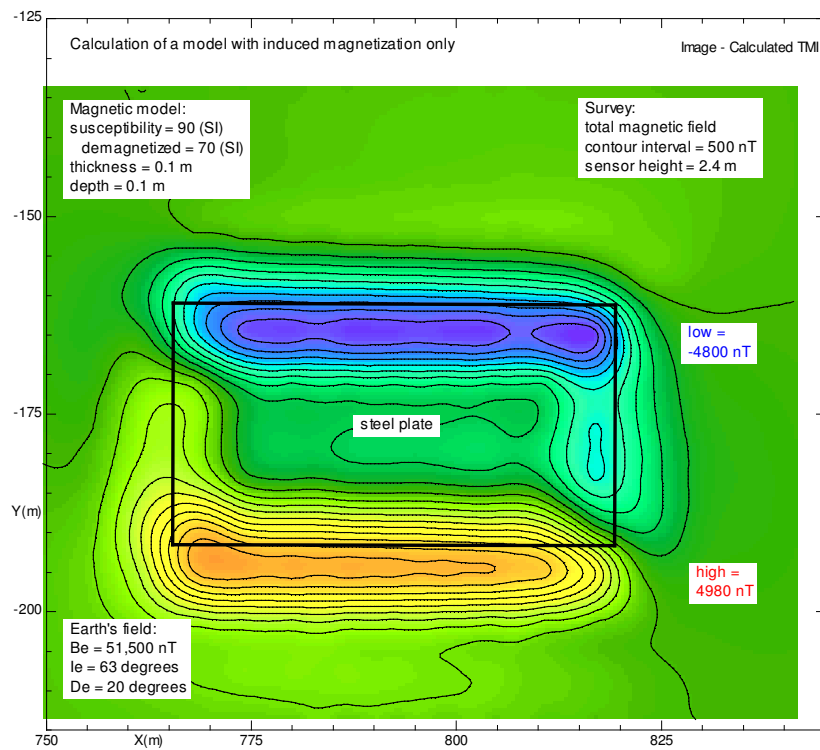


Figure 45: The calculated maps of two rectangular magnetic models for the steel plate in [Figure 44](#). The calculations on the left assume that the plate had only induced magnetization; however, the map on the right assumes that the plate had only remanent magnetization. The two maps are very similar. [details](#)

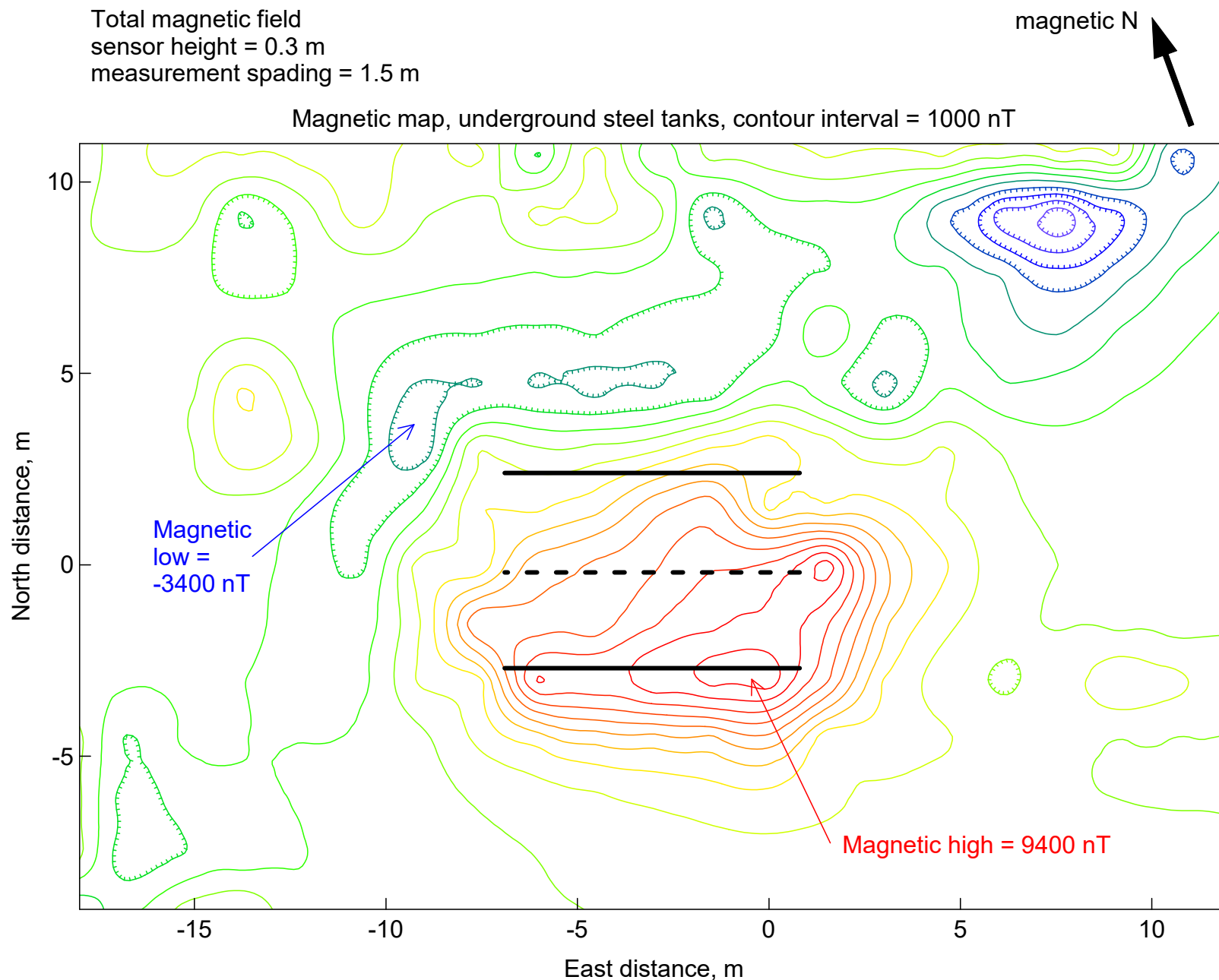


Figure 46: The magnetic anomaly of three buried tanks for storing fuel. The three horizontal lines approximate the span of peak magnetic anomalies along these tanks. The southern line is the most distinct. The northern line was delineated when further lines of measurement were made at a closer spacing. The peak anomaly of the middle tank, which was located along the third dashed line, was barely detected. [details](#)

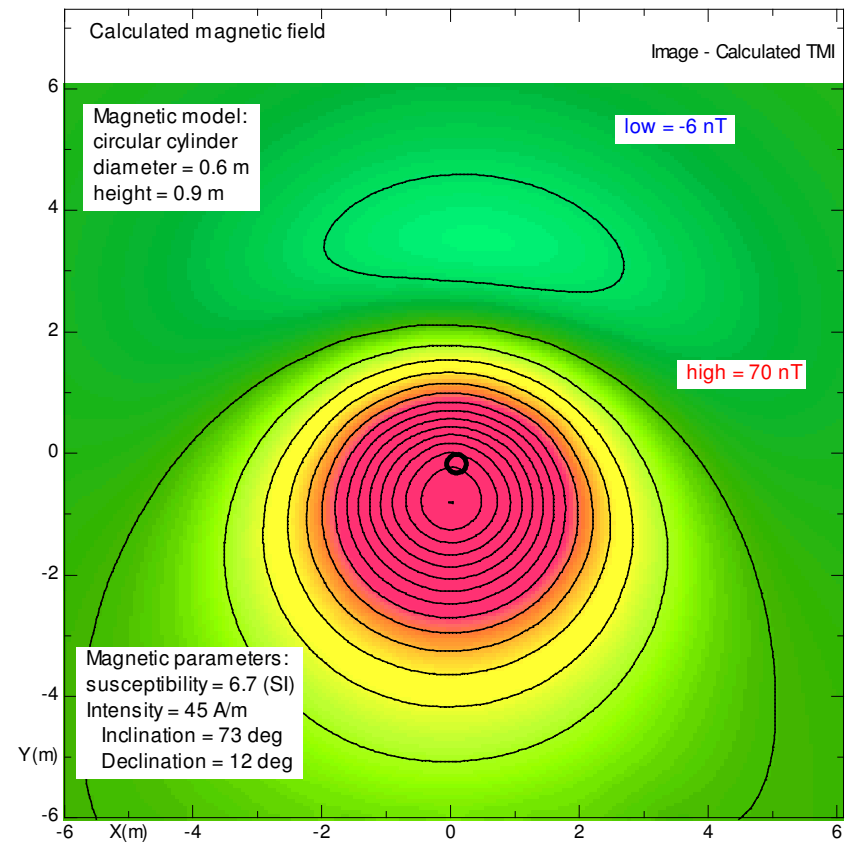
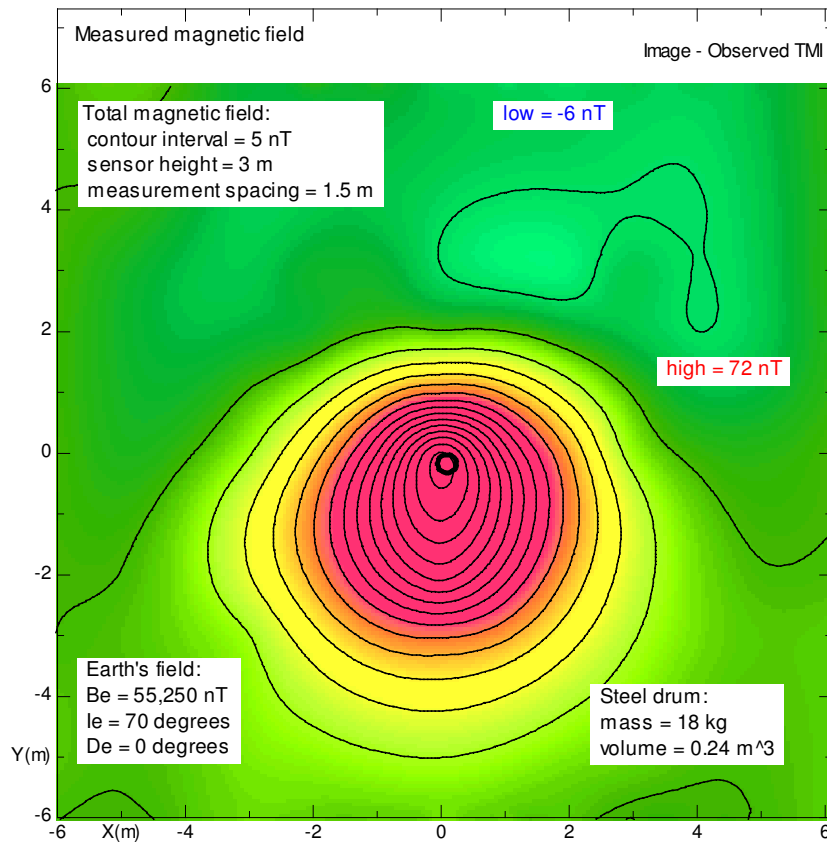


Figure 47: Analysis of the magnetic map of a steel drum. The measurements are on the left and the calculated field is plotted on the right. At first, the drum was assumed to have only induced magnetization. Material with a susceptibility of 11.1 (SI) that filled the volume of the model of the drum provided a good match to the measurements. Next, remanent magnetization was assumed to add to the induced magnetization. This model is shown on the right, with a susceptibility reduced to 6.7 (S), and an intensity of remanent magnetization increased from 0 to 45 A/m improved the model (see the parameters at the lower left of the panel on the right). [details](#)

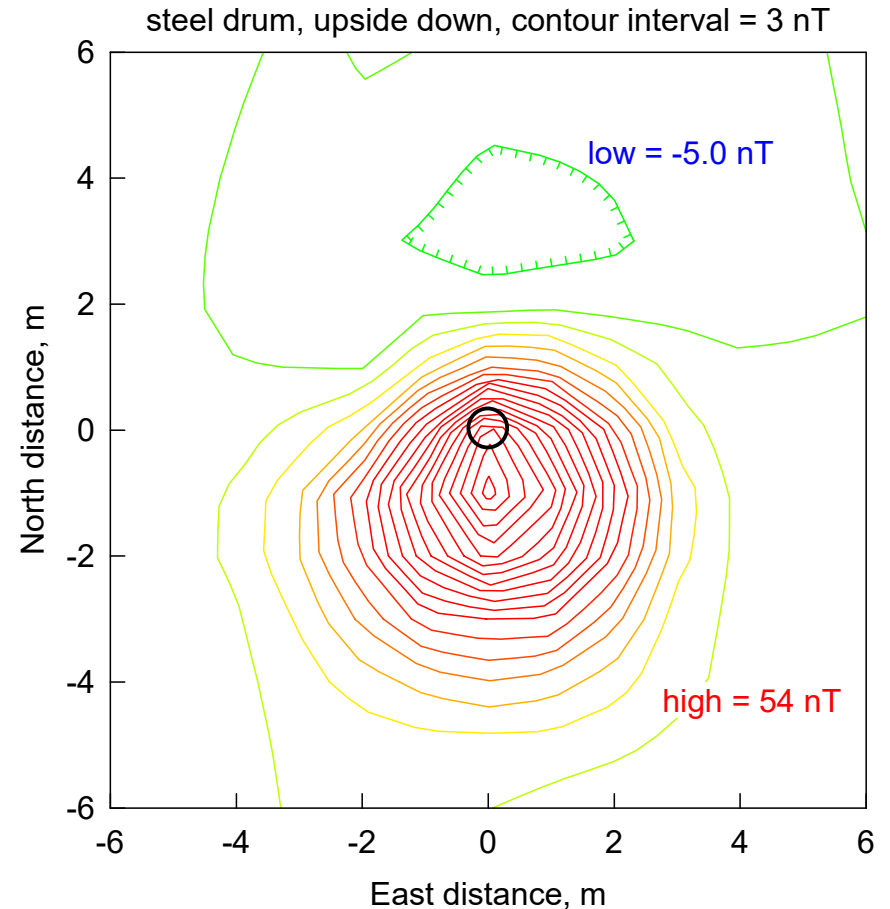
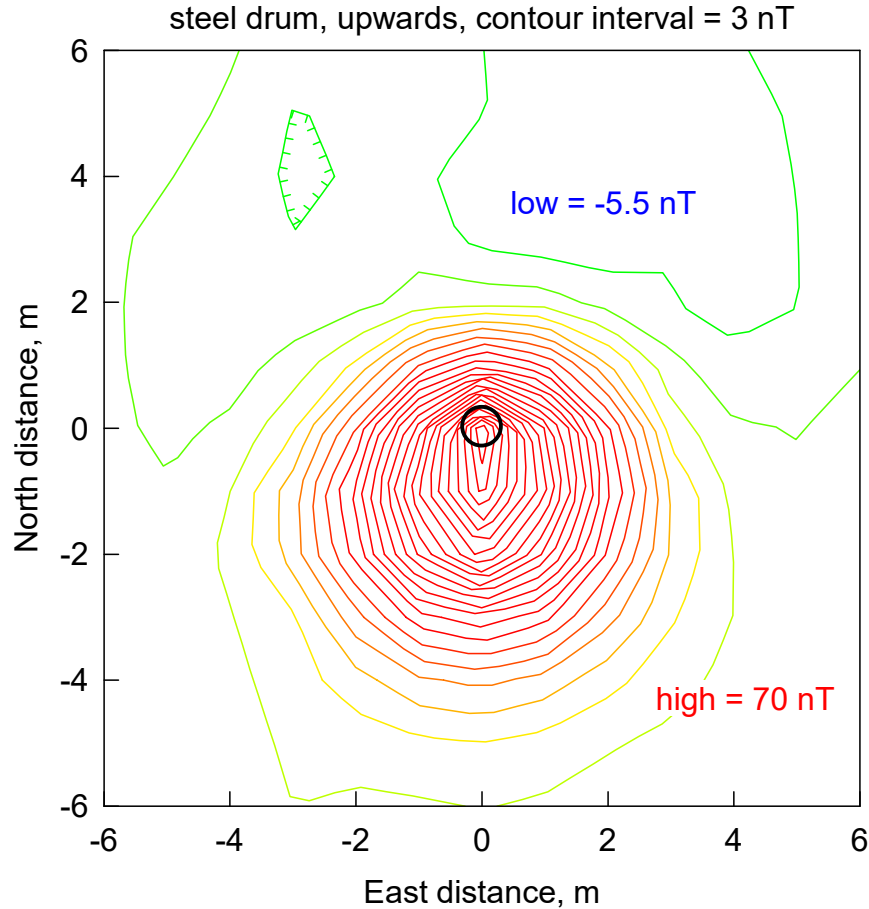


Figure 48: Two magnetic maps of a steel drum. On the left, the drum is oriented upwards (it can be opened at the top); on the right, the drum has been turned upside down, and the peak anomaly is smaller. If the drum had only induced magnetization, the two maps would be identical. If the drum had only remanent magnetization, the two maps would be quite different. The maps show that the drum has mostly induced magnetization, with a small amount of remanent magnetization. North is upwards in these maps, and the maps were measured at a height of 3 m above the middle of the drum; the drum was resting on the surface of the earth. [details](#)

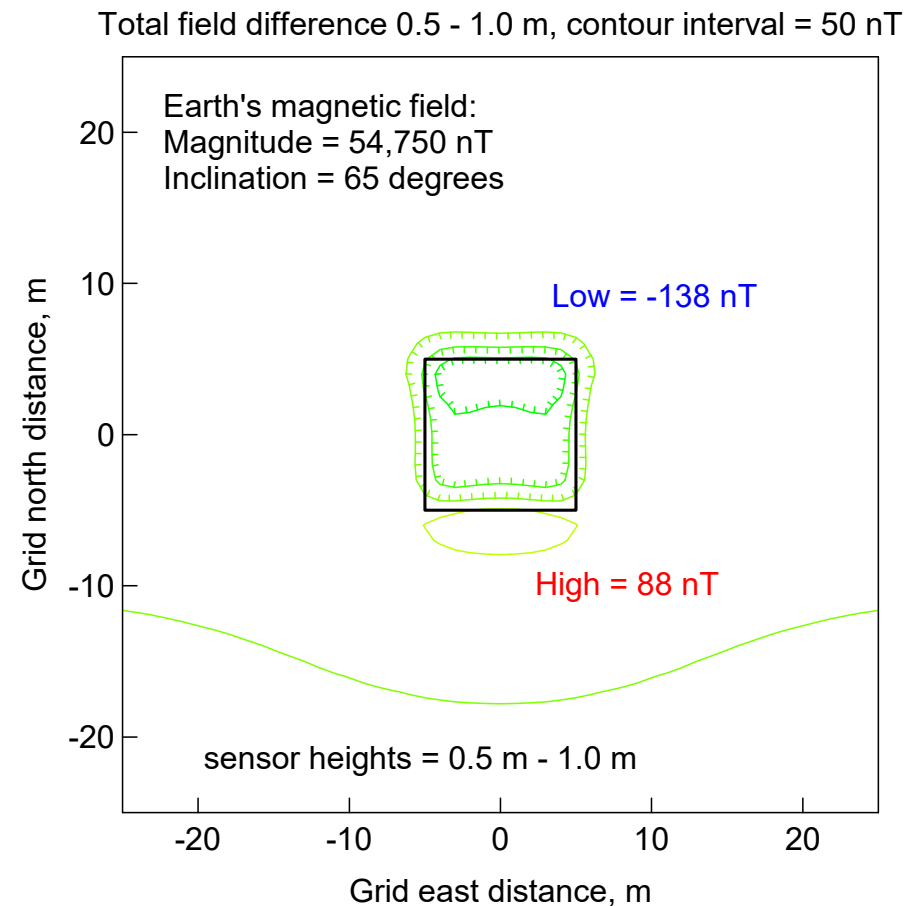
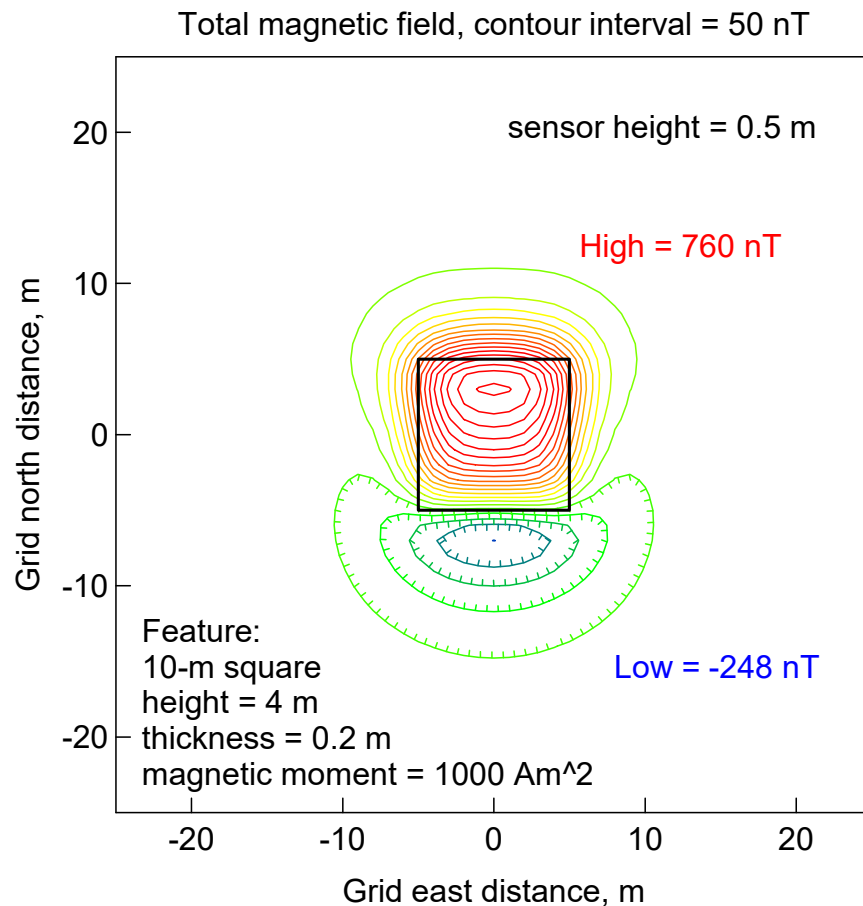



Figure 49: The anomaly of an overhead feature that is magnetic. On the left, a survey with a total-field magnetometer will find a major magnetic high below the feature (black square). Unlike a buried feature, the magnetic high is north of the low. However, for a differential magnetometer, with sensors at heights of 0.5 m and 1.0 m, the magnetic low will be to the north.

[details](#)

Total magnetic field:
sensor height = 2 feet (0.6 m)
measurement spacing = 2.5 by 5 ft

colored contour lines: interval = 20 nT
black contour lines: interval = 2 nT

magnetic N 

Magnetic map, Fort Nonsense, Pennsylvania, USA, showing four pipes with red (high) and blue (low)

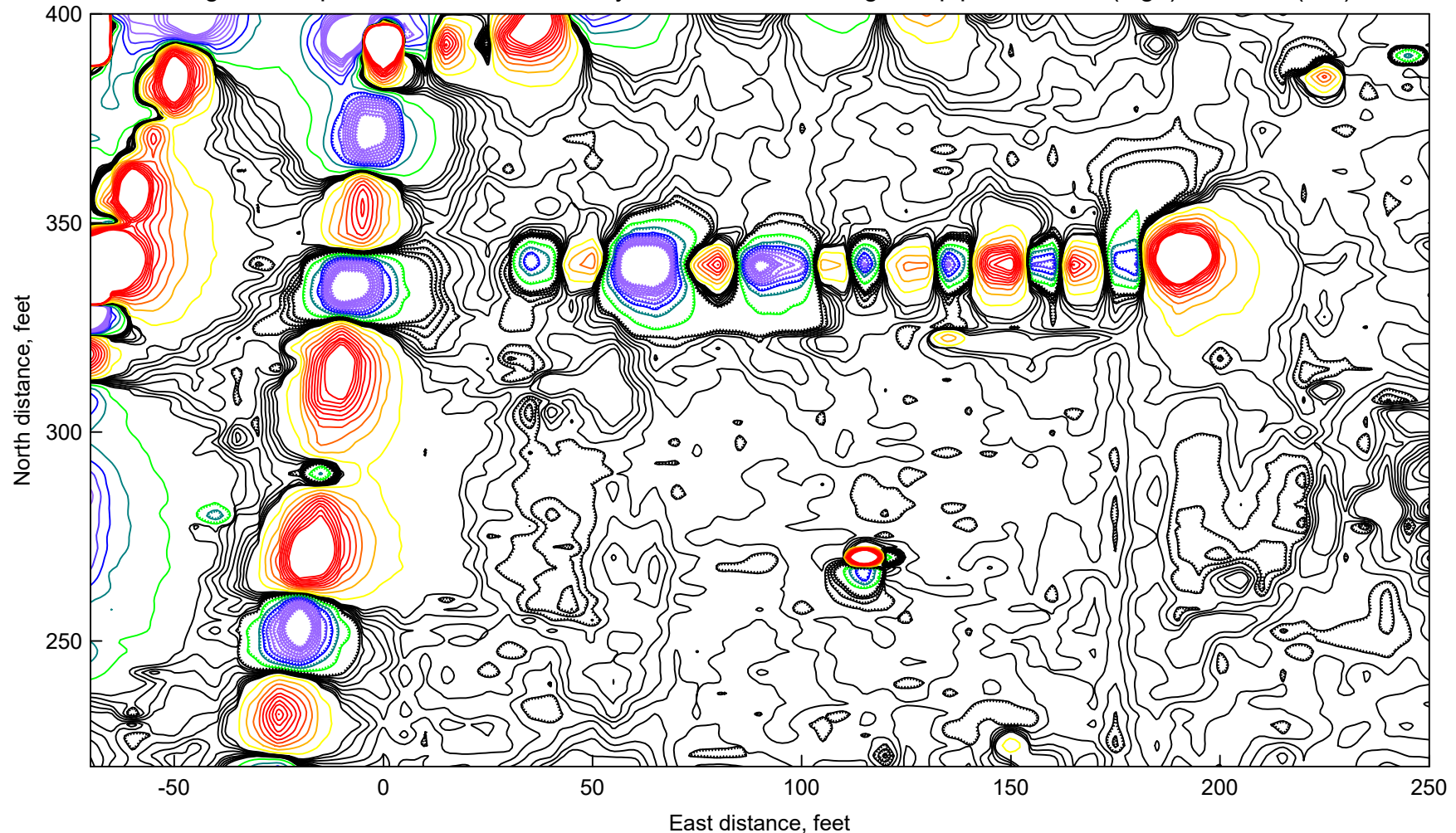


Figure 50: Four iron pipes that are underground in this area. Each pipe is detected by the magnetic survey as a "string of beads" with magnetic highs (in red) usually alternating with lows (blue). These pipes have little or no importance for archaeology. The black contour lines are drawn at intervals of 2 nT between -8 and +8 nT, and these reveal a possible road and other earthworks. [details](#)

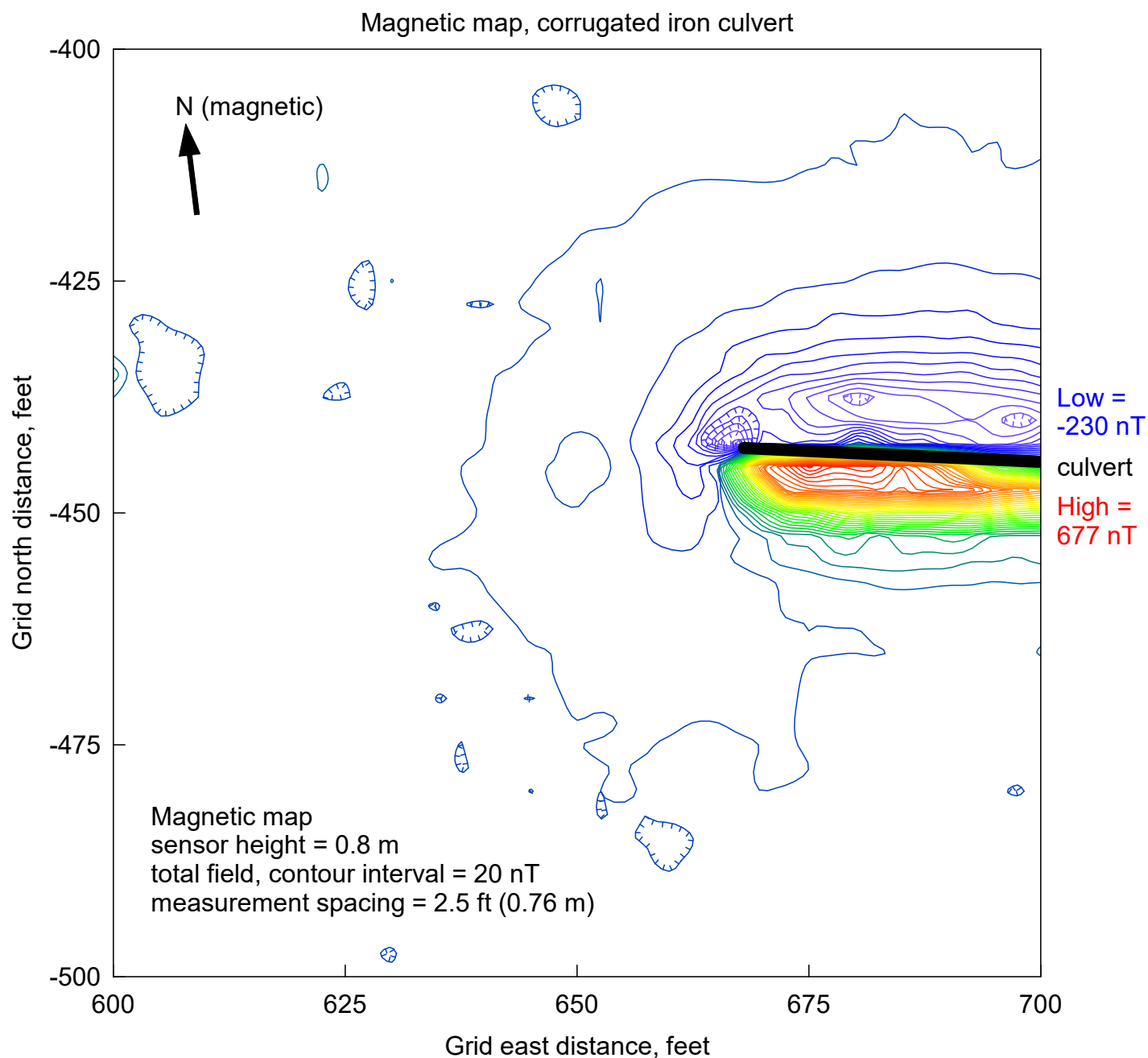


Figure 51: The magnetic map of a large-diameter pipe. The anomaly is smooth and linear, and without evidence of junctions between short segments of pipes that have been joined. This pipe has a diameter of roughly 0.25 m; it is located with a broad black line between the magnetic high and low. [details](#)

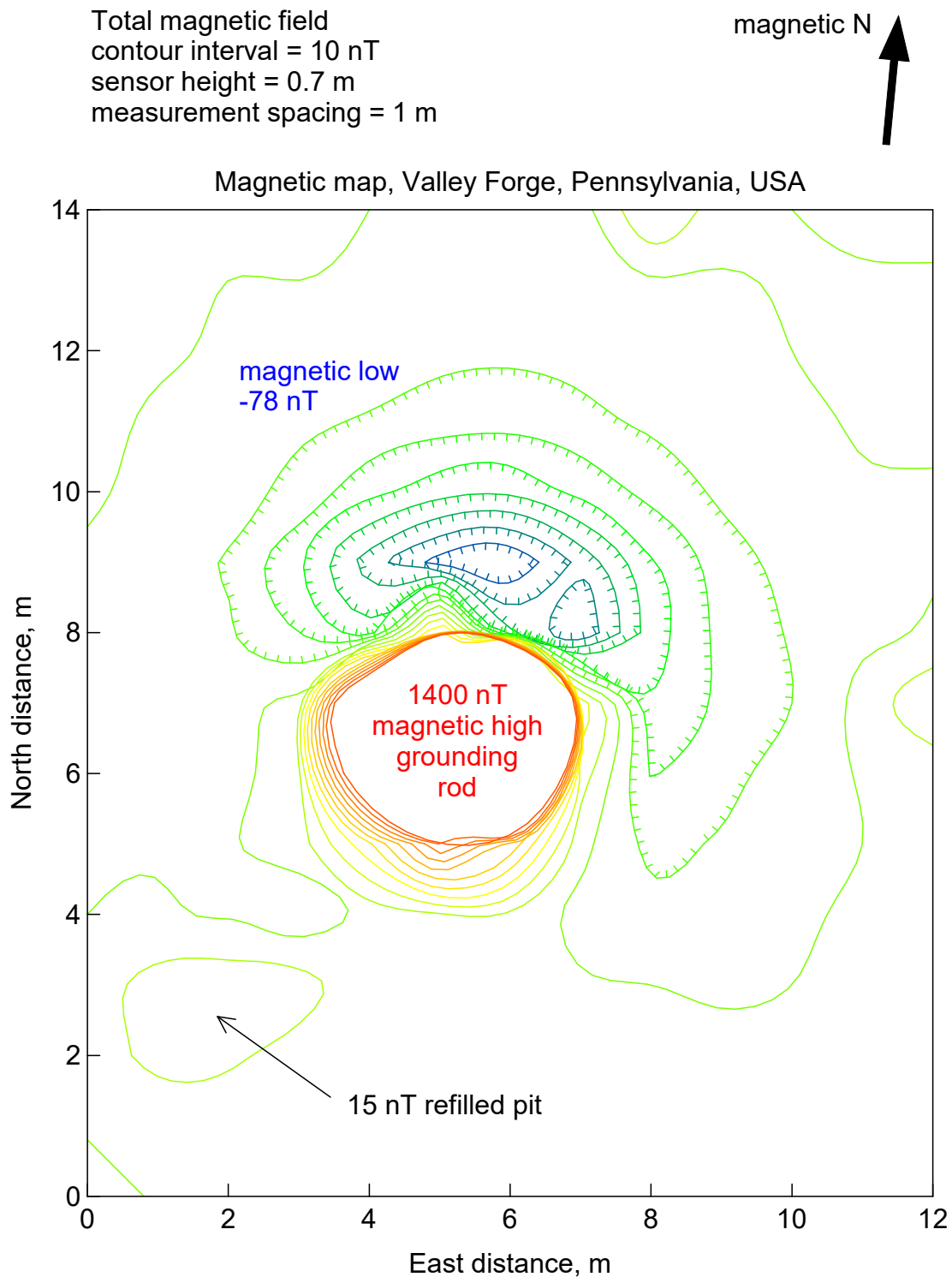


Figure 52: A strong magnetic anomaly caused by a vertical grounding rod that was 1.5 m long. The contour lines are not drawn for anomalies that were greater than 100 nT. While this grounding rod is recent and unimportant, the magnetic survey also detected a fainter anomaly to the lower left whose peak was 15 nT. This was also excavated and found to be caused by a refilled pit, almost certainly from the encampment in 1777 at this site. [details](#)

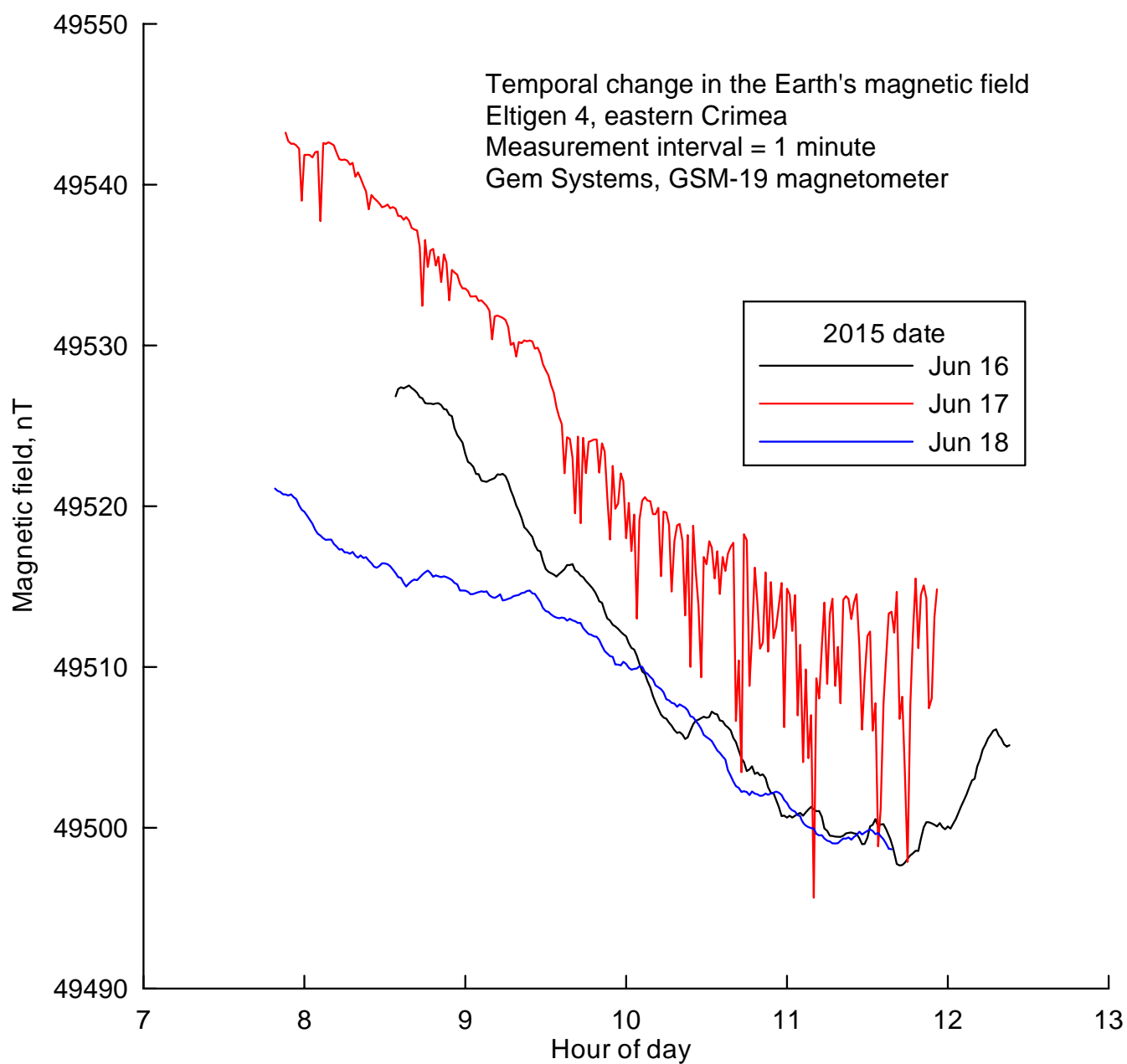


Figure 53: Abrupt drops in the magnetic field during a thunderstorm. Each of the three curves is a plot of changes in the Earth's magnetic field. A thunderstorm was nearby on one day (the 17th) but not the other two days. The broad dip near noon is normal and often found; the sharp drops in the field can create unwanted anomalies in a magnetic map. The magnetometer and its sensor were stationary for this test. [details](#)